Bidirectional coupling of a long-term integrated assessment model REMIND v3.0.0 with an hourly power sector model DIETER v1.0.2

Chen Chris Gong[1], Falko Ueckerdt[1], Robert Pietzcker[1], Adrian Odenweller[1,3], Wolf-Peter Schill[2], Martin Kittel[2], Gunnar Luderer[1,3]

[1] Potsdam Institute for Climate Impact Research (PIK), Potsdam, Germany

[2] German Institute for Economic Research (DIW Berlin), Berlin, Germany

[3] Global Energy Systems Analysis, Technische Universität Berlin, Berlin, Germany

Correspondence to: Chen Chris Gong (chen.gong@pik-potsdam.de)

Abstract. Integrated assessment models (IAMs) are a central tool for the quantitative analysis of climate change mitigation strategies. However, due to their global, cross-sectoral and centennial scope, IAMs cannot explicitly represent the temporal and spatial details required to properly analyze the key role of variable renewable electricity (VRE) for decarbonizing the power sector and enabling emission reductions through end-use electrification. In contrast, power sector models (PSMs) can incorporate high spatio-temporal resolutions, but tend to have narrower sectoral and geographic scopes and shorter time horizons. To overcome these limitations, here we present a novel methodology: an iterative and fully automated soft-coupling framework that combines the strengths of a long-term IAM and a detailed PSM. The key innovation is that the framework uses the market values of power generations as well as the capture prices of demand flexibilities in the PSM as price signals that change the capacity and power mix of the IAM. Hence, both models make endogenous investment decisions, leading to a joint solution. We apply the method to Germany in a proof-of-concept study using the IAM REMIND v3.0.0 and the PSM DIETER v1.0.2, and confirm the theoretical prediction of almost-full convergence both in terms of decision variables and (shadow) prices. At the end of the iterative process, the absolute model difference between the generation shares of any generator type for any year is <5% for a simple configuration (no storage, no flexible demand) under a "proof-of-concept" baseline scenario, and 6-7% for a more realistic and detailed configuration (with storage and flexible demand). For the simple configuration, we mathematically show that this coupling scheme corresponds uniquely to an iterative mapping of the Lagrangians of two power sector optimization problems of different time resolutions, which can lead to a comprehensive model convergence of both decision variables and (shadow) prices. The remaining differences in the two models can be explained by a slight mismatch between the standing capacities in the real-world and optimal modeling solutions purely based on cost competition. Since our approach is based on fundamental economic principles, it is applicable also to other IAM-PSM pairs.

1 Introduction

Thanks to decade-long policy support in many regions of the world and technological learning, the costs of both wind power and solar photovoltaics have plummeted (IEA, 2021; Lazard, 2021). These types of variable electricity generation are now highly cost competitive against other alternatives, such that their deployment is increasingly driven by market forces instead of climate policies. Among the newly added renewable generations in 2020, nearly two thirds were cheaper than the cheapest new fossil fuel (IRENA, 2020). Due to both cost declines and pressing concerns over climate change, investing in these clean and abundant resources has become a crucial part of national and regional strategies to decarbonize the power sector (The White House, 2021; Cherp et al., 2021; National long-term strategies, 2022; Rechsteiner, 2021; ICCSD Tsinghua University, 2022).

Given this dramatic development in the power sector over the past two decades, a universal consensus has emerged among energy transition scholars and policy makers: emissions in the power sector are relatively "easy-to-abate" (Luderer et al., 2018; Azevedo et al., 2021; Clarke et al., 2022). Compared with other primarily non-electrified end-use sectors such as buildings, transport and industry, the technologies required to transform the power sector are low-cost, mature and readily available. This trend has in recent years led to a second emerging consensus: the power sector will be the fundamental basis of a future low-cost, efficient and climate-neutral energy system (Brown et al., 2018b; Ram et al., 2018; Ramsebner et al., 2021; Luderer et al., 2022a). In addition to direct electrification, which requires end-use transformations of currently non-electrified demand, emerging technological developments in hydrogen and e-fuels produced from renewable electricity have also contributed to the broadening of potential technology portfolios for the "hard-to-abate" sectors, such as high temperature heat and chemical productions (Parra et al., 2019; Bhaskar et al., 2020; Griffiths et al., 2021). Together, direct and indirect electrification support a broad concept of "sector coupling", which facilitates decarbonization by powering end-use demand with variable renewable energy sources (Ramsebner et al., 2021).

Due to the pivotal role of electrification and sector coupling in mitigation scenarios, there is an increasing demand on the scope and level of detail of energy-economy models used to guide the energy transition and climate policies. The models would ideally encompass a global, multi-decadal and multi-sectoral scope, such that the scenarios are relevant for international and regional climate policies, while simultaneously incorporating a high level of spatio-temporal detail. The latter is important to account for the specifics of variable renewable electricity generation as well as its physical and economic interplay with the electrification of energy demand (Li and Pye, 2018; Brunner et al., 2020; Prol and Schill, 2020; Böttger and Härtel, 2022; Ruhnau, 2022). This need for improved modeling methods or frameworks, which has to overcome the trade-off between scope and detail, is a substantial methodological challenge. It entails realizing two main objectives:

Objective 1) Accurately model the power sector transformation over long time horizons in terms of investment and dispatch, especially at high shares of variable renewable energy (VRE) sources. Long-term pathways for the following power sector quantities and prices should accurately incorporate short-term hourly details:

   a)   capacity and generation mix of the power sector,

   b)   market values (annual average revenues per power generation unit) for variable and dispatchable plants,

   c)   capacity factors of the dispatchable plants and the curtailment rates of variable renewables,

   d)   storage capacity and dispatch.

Objective 2) Accurately model direct electrification of end-use sectors as well as indirect electrification technologies such as green hydrogen production, where existing and emerging sources of power demand can be in-part flexibilized.

1.1 Current modeling approaches and limitations

Current energy system models broadly fall into two distinct categories, carried out by two research communities with little institutional overlap: integrated assessment models (IAMs) and power sector models (PSMs), each with its own strengths and weaknesses. IAMs are comprehensive models of global scale and span multiple decades, linking macroeconomics, energy systems, land-use and environmental impacts (Stehfest et al., 2014; Calvin et al., 2017; Huppmann et al., 2019; Baumstark et al., 2021; Keppo et al., 2021; Guivarch et al., 2022), therefore providing an "integrated assessment" of multiple factors (Rotmans and van Asselt, 2001). IAMs substantially shape the IPCC assessments on long-term climate mitigation scenarios, and play an important role in policy making (Rogelj et al., 2018; UNEP, 2019; NGFS, 2020; P.R. Shukla et al., 2022). In comparison to IAMs, PSMs typically have narrower spatial and sectoral scopes and shorter time horizons, but provide higher resolutions and increased technological detail (Palzer and Henning, 2014; Zerrahn and Schill, 2017; Brown et al., 2018a; Ram et al., 2018; Sepulveda et al.,

76   2018; Blanford and Weissbart, 2019; Böttger and Härtel, 2022; Ringkjøb et al. 2018; Prina et al. 2020). (Also see Supplemental

77   Material S5 for a comparison of model specifications of a few selected PSMs). This allow PSMs to more accurately model the

78   power sector under high VRE shares (Bistline, 2021; Chang et al., 2021). Note that we use the term "power sector model" here to

79   represent all general smaller-scope models than IAMs (usually by geographical or time horizon measures), even though many of

80   them have sector-coupling aspects and do not only contain the traditional power sector.

81

82   IAMs and PSMs are therefore limited by a lack of spatio-temporal detail and a lack of scope, respectively. IAMs usually have a

83   temporal resolution no shorter than a year (Keppo et al., 2021) and therefore include simplified representations of hourly power

84   sector variability, which mimic the real-world dynamics to varying degrees of success (Pietzcker et al., 2017). In general, a lack

85   of high temporal resolutions can lead to difficulties when estimating the optimal level of variable renewable generation, often

86   either over- or underestimating the market value of solar or wind generation, the challenges of variable renewable integration,

87   the peak hourly residual demand, and the need for energy storage and baseload (Pina et al., 2011; Haydt et al., 2011; Ludig et

88   al., 2011; Kannan and Turton, 2013; Welsch et al., 2014; Luderer et al., 2017; Pietzcker et al., 2017; Bistline, 2021). While

89   approximate methods such as parameterization via residual load duration curves (RLDCs) are able to capture the supply-side

90   dynamics of VREs, they remain methodologically limited for representing the flexible demand-side dynamics (Ueckerdt et al.,

91   2015; Ueckerdt et al., 2017; Creutzig et al., 2017). Besides limited temporal resolutions, IAMs also usually have coarse spatial

92   resolutions, which can lead to an under- or overestimation of transmission grid bottlenecks, geographical variability of wind and

93   solar resources, and of the flexibility requirements to balance supply and demand (Aryanpur et al., 2021; Frysztacki et al., 2021;

94   Martínez-Gordón et al., 2021). PSMs, on the other hand, usually lack the global and sectoral scope required for addressing

95   global climate mitigation, in part because of limited availability of detailed data, and due to computational challenges.

96   Furthermore, PSMs with a short-term horizon may lack the vintage tracking of standing capacities, capacity evolution over time,

97   as well as long-term perfect foresight, which can help policy makers and companies to look ahead beyond the short-term

98   business cycles, to invest early and to actively drive technical progress. In contrast, in IAMs such as REMIND, proactive early

99   investment is a built-in feature, because the optimization is done from a long-term social planner's perspective. In IAMs,

100 investing early in the technological learning phase results in lower costs of energy expenditure later, avoiding the severity of

101 punishment to economic growth later in time in the form of lower consumption, which raises the welfare which the model

102 optimizes.

1.2 Iterative coupling for full model convergence

104 IAMs and PSMs differ in scope and resolution across three main modeling dimensions: temporal, spatial and technological. A

105 soft-coupling approach can tap into these complementarities and combine their strengths, at potentially only a moderate increase

106 in computational cost. The main challenge of the soft-coupling approach is to show that the two models can converge under

107 coupling, which leads to a joint equilibrium that maximizes regional interannual intertemporal welfare in the IAM and

108 minimizes total power system costs in the PSM. Ideally, the converged model offers the "best of both worlds": it has both the

109 broad scope required to assess global long-term energy transitions, as well as the technical resolution required to capture the

110 interplay between VREs, storage and newly electrified demand on a much shorter time scale.

111 Approaches aiming to bridge the "temporal resolution gap" between long-term energy system models and hourly PSMs have

112 been proposed in the past (Deane et al., 2012; Sullivan et al., 2013; Alimou et al., 2020; Brinkerink et al., 2020; Seljom et al.,

113 2020; Guo et al., 2022; Younis et al., 2022; Brinkerink et al., 2022; Mowers et al., 2023). While these achieved some aspects of

114 Objective (1) with adequate results, none attempted to incorporate and achieve Objective (2). In addition, there is a

methodological gap in the previous attempts to a full harmonization of the multiscale models. By a full harmonization, we mean a comprehensive coupling of the power sector dynamics, and an eventual model convergence in capacities, generation, and prices. In only a few previous studies, price information has been fed back into the long-term models from the short-term models: in one study only partial price information has been exchanged (Seljom et al., 2020); in another study some subset of price information is exchanged but they are not fully endogenized (instead they are parametrized), the exchange is also one directional (Mowers et al., 2023). Without a feedback mechanism through prices, the investment in the coupled model will very likely be sub-optimal due to two effects: 1) because of the misalignment in prices in the two models, there is a mismatch in investment incentives, resulting in a mismatch for optimal capacities if both models are completely endogenous; 2) in all previous studies, the capacities are fixed in the PSM and only the long-term model is allowed to invest in new capacities. This implementation can further propagate and sustain the price mismatch due to (1) via nontrivial shadow prices from these capacity bounds, and create in turn price distortions in the PSM that can be passed on to the IAM. Therefore, the methodological gap in previous work prevented a comprehensive convergence of the coupled models of both quantities and prices. As we show later in this study, without a comprehensive coupling of price information, no system-wide convergence can be achieved. However, with price coupling as our method proposes, we could achieve all aspects of Objective (1), as well as Objective (2) for one type of flexible demand with adequate numerical results, and therefore represents a first step to bridge the previous methodological gap.

Compared to previous studies, our approach features three main innovations: 1), the coupling is achieved by linking market values, and not hard fixing quantities, allowing both models to invest "as endogenously as possible"; 2), the market values of all power sector technologies are coupled, not just the electricity price of the system or the market value of a particular technology, allowing models to achieve close to full convergence; 3) under idealized coupling assumptions and for a simplified "proof-of-concept" model without storage, we can mathematically derive the necessary conditions under which comprehensive model convergence can be reached, which puts multiscale coupling on firm theoretical footing. Our coupling approach is bi-directional, iterative and fully automated.

One should note that our methodology bears certain mathematical similarities to Benders Decomposition from the discipline of Operation Research (Conejo et al., 2006), which is used in long-term energy system model PRIMES to obtain hourly detail (E3Mlab, 2018). There are however, crucial differences. For example, the optimization in our work is carried out iteratively outside solver time, whereas the Benders Decomposition is carried out iteratively during solver time. In addition, our approach can function even when the objective function is convex, whereas the Benders Decomposition cannot, allowing our approach to be applied in more general cases. Mathematically, the subproblems in Benders Decomposition have fixed capacities obtained from master problems, therefore are not endogenous, but the shadow prices of these constraints are iteratively passed to the master problems, ensuring mathematical convergence. The exact ways our methodology is connected to Benders Decomposition or other similar methods are yet to be fully explored.

To showcase such a framework and its ability to achieve iterative convergence, we couple the PSM DIETER, which has an hourly resolution (8760 hours in a year) and the IAM REMIND for a single-region Germany. Germany is a well-suited case study for exploring high VRE shares in the power sector. The country is expected to meet stringent climate targets despite the country's high level of residential and industrial power demand, relatively small geographical size and lack of solar endowment during winter seasons. Nevertheless, the German government has set very ambitious targets for the expansion and use of variable renewable energy sources (Schill et al., 2022). A viable zero-carbon power mix in Germany must include an adequate amount of storage and transmission for the renewable generation, as well as "clean firm generation" such as geothermal, biomass or gas with carbon capture and storage (CCS) (Sepulveda et al., 2018).

2 Models

The models used in this study are well-documented open source models (REMIND is an open source model but requires proprietary input data to run). A side-by-side comparison of the scope, resolution and other specifications of the two models can be found in Appendix A. The coupling scope can be found in Appendix B. Details on model input data can be found in Supplemental Material S-1.

2.1 IAM: REMIND

REMIND (REgional Model of INvestments and Development) is a process-based IAM, which describes complex global energy-economy-climate interactions (Baumstark et al., 2021). REMIND has been frequently used in long-term planning of decarbonization scenarios, most notably in the IPCC (IPCC, 2014; Rogelj et al., 2018; P.R. Shukla et al., 2022). The REMIND model links different modules, which describe the global economy, the energy, land and climate systems, with a relatively detailed representation of the energy sector compared to non-process-based IAMs. The model is formulated as an interannual intertemporal optimization problem. Due to the computational complexity of nonlinear optimization, the model simulates a time span from 2005 to 2100 with a temporal resolution of either 5 years (between 2005 to 2060) or 10 years (between 2070 to 2100). The years in REMIND are representative years of the surrounding 5 or 10-year period, e.g. year "2030" represents the 5-year period 2028 to 2032. Spatially, the model represents the world composed of aggregated global regions (Fig. B1). For each region, using a nested constant elasticity of substitution (CES) production function, the model maximizes interannual intertemporal welfare as a function of labor, capital, and energy use (Baumstark et al., 2021). The macro-economic projections of REMIND come from various established global socio-economic scenarios jointly used by social scientists and economists – the so-called Shared Socioeconomic Pathways (SSPs) (Bauer et al., 2017).

By default, REMIND runs in a regionally decentralized iterative "Nash mode", where all regions are run in parallel and the interannual intertemporal welfare is maximized for each region for each internal "Nash" iteration. Trade flows between the regions are determined between the Nash iterations. During the Nash algorithm, REMIND regions share partial information between each other, which are trade variables in primary energy products and goods. The Nash algorithm is said to converge, when all markets are cleared and no region has the incentive to change their behavior regarding their trade decisions, i.e. no resources can be reallocated to make one region better off without making at least one region worse off. A successfully converged run of stand-alone REMIND under "Nash mode" usually consists of 30 to 70 iterations of single-region models in parallel. Each parallel single-region model usually takes 3-6 minutes to solve. A typical REMIND run in the Nash mode lasts 2.5-6 hours depending on the level of sectoral details included. The latest version REMIND (v3.0.0) is published as an open-source version on github (Release REMIND v3.0.0 · remindmodel/remind, 2022). REMIND is implemented as a nonlinear programming (NLP) mathematical optimization problem. In REMIND, the nonlinearity consists of the welfare function, the CES production functions, adjustment costs, technological learning, the extraction cost functions, the bioenergy supply function and nonlinear constraints, among others.

2.2 PSM: DIETER

DIETER (Dispatch and Investment Evaluation Tool with Endogenous Renewables) is an open-source power sector model developed for Germany and Europe. In a long-run equilibrium setting (i.e. a competitive benchmark), the model minimizes overall system costs of the power sector for one year. DIETER determines the least-cost investment and hourly dispatch of various power generation, storage, and demand-side flexibility technologies. In previous literature, different versions of the

192   model have been used to explore scenarios with high VRE shares, where storage (Zerrahn et al., 2018; Zerrahn and Schill, 2017;

193   Schill and Zerrahn, 2018), hydrogen (Stöckl et al., 2021), power-to-heat (Schill and Zerrahn, 2020), or solar prosumage (Say et

194   al., 2020; Günther et al., 2021) are evaluated with a high degree of technological detail. DIETER recently also contributed to

195   model comparison exercises that focused on power sector flexibility for VRE integration and sector coupling (Gils et al., 2022b,

196   a; van Ouwerkerk et al., 2022).

197   As a first step to building a model coupling infrastructure, we implemented an earlier and simpler version of DIETER (v1.0.2),

198   which is purely based on the General Algebraic Modeling System (GAMS). It has limited features on ramping constraints,

199   flexible demand, and storage. The model minimizes total investment and dispatch cost of a power system for a single region,

200   considering all consecutive hours of one full year. The technology portfolio contains conventional generators such as coal and

201   gas power plants, nuclear power, as well as renewable sources such as hydroelectric power, solar PV and wind turbines.

202   Endogenous storage investment and dispatch, as well as demand flexibilizations are offered as additional features that can be

203   turned on or off. DIETER, like many PSMs, is a linear program (LP). A typical stand-alone run (with essential features) lasts

204   from several seconds to several minutes for a single region. See Zerrahn and Schill, 2017 for a detailed documentation of the

205   initial model, which was implemented purely in GAMS. Later, DIETER's GAMS core was embedded in a Python wrapper for

206   enhanced scenario analysis and post-processing, but the model can still be run in a GAMS-only mode (Gaete-Morales et al.,

207   2021).

208   **3 A novel coupling approach**

209   It is central to our approach that the price-based variables, such as the market values of electricity generation, are exchanged

210   between the models. This approach ensures full convergence – including both quantity convergence as well as price

211   convergence in the market equilibrium. Here, we first introduce the intuition behind this approach, then conduct a deep dive into

212   the economic theory behind energy system modeling.

213   Economic concepts such as market values or capture prices (Böttger and Härtel, 2022), as key variables in our coupling,

214   translate the physical characteristics of variable power generation or flexible consumption into economic ones. For example,

215   generation technologies differ with respect to physical features and constraints – solar and wind generation depends on current

216   weather conditions as well as diurnal and seasonal patterns, whereas this is less the case for dispatchable power plants such as

217   coal, gas, biomass, nuclear or storage (López Prol and Schill, 2021). One consequence of this is that, for example, prices in

218   hours where PV does not produce will be essentially set by other, and usually more expensive forms of generation. In cost-

219   minimizing PSMs, the shadow prices of the energy balance are interpreted as wholesale market prices (Brown and Reichenberg,

220   2021; López Prol and Schill, 2021). Therefore in general, hourly-resolution PSMs are well equipped to translate such physical

221   constraints of generation into (wholesale) power market price time series. By providing such prices generated by PSMs (among

222   other variables of the power sector dynamics) to IAMs, the latter can be indirectly informed about power market dynamics

223   happening on much shorter time scales, even if they lack hourly resolutions. Over iterations, the prices from PSMs act as "price

224   signals" to induce investment decision changes in IAMs, which can in turn provide feedback to the PSMs until the two models

225   converge.

226   One innovation of our method is that the prices used for the model coupling can be symmetrically applied on the power supply

227   side as well as the demand side. On the supply side, the coupling method mainly utilizes the concept of market value (i.e. annual

228   average revenue per energy unit of a generator) in a competitive market at equilibrium. Generally speaking, market values of

229   generation usually convey the degree of variability intrinsic to a given source of power supply, and reflect the generator's ability

230   to meet an inflexible hourly demand, especially given lower cost of variable generation compared to dispatchable technologies.

Mirroring the concept of the market value, on the demand side, there is the concept of the "capture price" of electricity demand, which conveys the degree of demand-side flexibility. Note that there may be multiple terminologies for demand-side electricity prices, we use "capture price" to be consistent with one of the literatures on this topic. The capture price is the average electricity price that a flexible demand technology pays over a year. For example, flexible demand technologies such as heat pumps, electrolyzers or electric vehicles (EVs) can take advantage of electricity at hours when the generation is cheap to obtain a lower "capture price", whereas inflexible demand has to pay a higher price on average. Price information given from a PSM to an IAM from both the supply and demand sides can change the IAM's inherent investment and dispatch decisions of power generation as well as inflexible and flexible demand-side technologies.

For an intuitive understanding of our innovative coupling scheme, we take the supply-side as an example, and use a toy model to visualize the approach of coupling via market values. The market values of electricity generating technologies have been studied in depth (Sensfuß, 2007; Sensfuß et al., 2008; Hirth, 2013; Mills and Wiser, 2015; Hildmann et al., 2015; Koutstaal and va. Hout, 2017; Figueiredo and Silva, 2018; Hirth, 2018; Brown and Reichenberg, 2021). The general idea of the coupling is illustrated in Fig. 1 for a simplified case of only two types of generators – dispatchable gas turbines and solar photovoltaics with variable output. Note that we assume the system is at a solar share of > 50% and no storage, such that the solar market value is below average electricity price, and that of gas generation is above. Before the coupling, for a general IAM with coarse temporal resolution and without any VRE integration cost parameterizations, there is no differentiation between the market values of gas and solar generators – they are both equal to the electricity price. Thus, there is no differentiated revenue for one MWh generated by variable sources and dispatchable sources. The lack of market value differentiation is a direct consequence of the limited temporal resolution in IAMs, which cannot represent hourly dynamics. However, through a market-value-based coupling, the IAM can be informed by the PSM via a price "markup". The annual price markup is defined as the difference between the market value of a specific technology and the annual average revenue that all generators together earn for one unit of generation (i.e. the annual average electricity price that a user pays). Under our soft-coupling approach, the markups from the PSM act as price-signals that change the composition of the energy mix in the next iteration of the IAM. Since in this simple example with a lot of PV and no storage, the gas generator is "more valuable" to the system, as it can generate electricity in times of scarcity (night), and thus it will receive a positive markup. When this positive price incentive is transferred from the PSM to the IAM, it increases the optimal level of investment into gas generation in the next IAM iteration. At the same time, solar generation receives a negative price incentive, reducing the optimal level of investments in the next iteration. Ultimately, the higher market value of gas turbines is due to: 1) its higher cost compared to solar (when gas is at <50% market share), 2) its ability to set prices in hours of low solar output and inflexible electricity demand. As we later show through mathematical theory of model convergence, other information besides markups also needs to be transferred such as capacity factors (annual

261   average utilization rates of the generators).
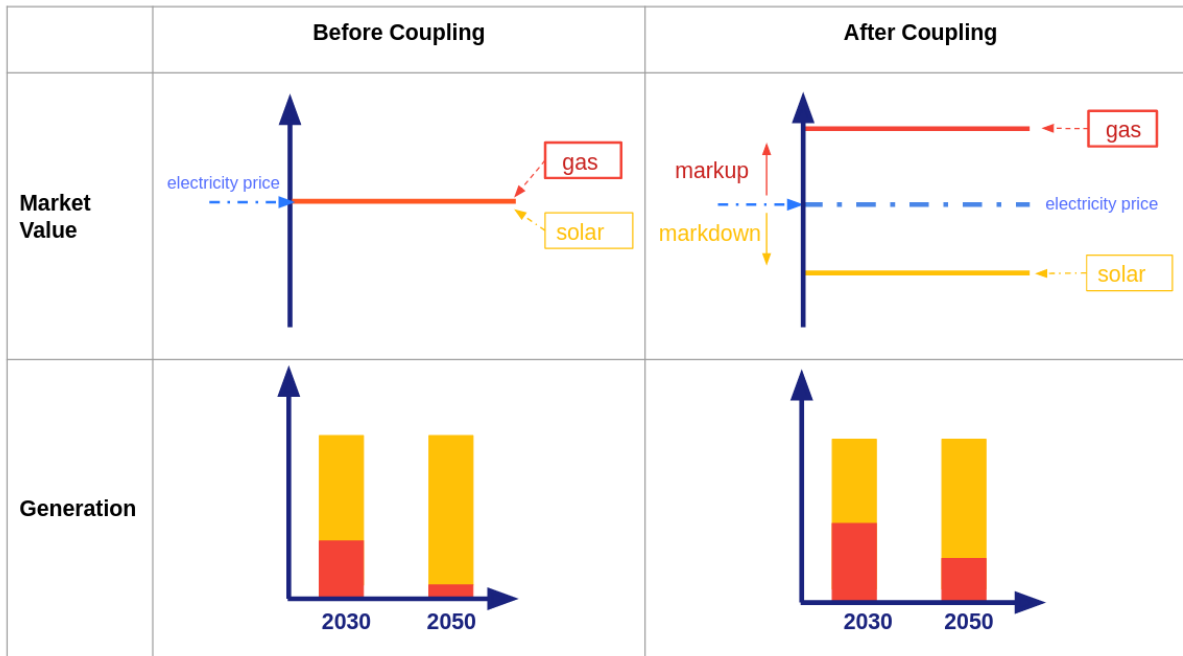
262
263   **Figure 1: Schematic illustration of the coupling approach for a simple power system in an IAM with coarse temporal**
264   **resolution, consisting of only gas and solar generators (no storage). Left column: before coupling; right column: after**
265   **coupling. Top row: endogenous prices (electricity price, market values of solar and gas generators); bottom row:**
266   **endogenous quantities (generation mix). The markups (as part of a larger set of interfaced variables) are the differences**
267   **between market values and electricity prices, and are given by the PSM of high temporal resolution as price signals to**
268   **the IAM. Usually, it is called a "markup" when the market value is higher than the annual average electricity price, and**
269   **"markdown" if it is the other way around. For simplicity, in the rest of the text we only refer to "markup" and**
270   **"markdown" collectively as "markup", regardless of whether the market value is higher or lower than the average**
271   **electricity price.**

272
273   There are several advantages to this new coupling approach centered on linking prices. First, instead of simply prescribing
274   quantities such as yearly generation and capacities, the approach allows endogenous investment decisions to be made by both
275   models as they converge towards a joint solution. This gives maximal freedom to the coupled models, while minimizing
276   unnecessary distortions from one model to the other when some necessary quantities are being prescribed. Second, our coupling
277   scheme provides an elegant treatment of both supply- and demand-side technologies using the concept of "market values" on the
278   one hand and "capture prices" on the other. Third, from a theoretical point of view, transferring the market values of all the
279   generation types in a system alongside mappings of other relevant system parameters can lead to a convergence of the solutions
280   of the two models under idealized coupling circumstances. It can be rigorously shown that our method contains an exhaustive
281   list of interfacing parameters and variables for full model convergence of both quantities and prices. To the authors' best
282   knowledge, the last point has not been explored or shown in any previous work.
283   In certain IAMs, VRE integration cost parameterization has been implemented to mimic the economic consequences of
284   variability of VRE, especially when the models have lower temporal resolution. Such VRE integration costs are contained in the
285   uncoupled default REMIND power sector modeling. However, the exact parameterization always depends on a particular set of
286   technological costs and parameters which might be subject to changes (Pietzcker et al., 2017), and the parametrization often

needs to be carried out anew under new assumptions and scenarios. In contrast, the model coupling approach is more general, and no such bespoke parametrization is needed.

Inspired by the theoretical framework based on the Karush–Kuhn–Tucker (KKT) conditions for power sector optimization problems (Brown and Reichenberg, 2021), we develop the theoretical basis for the coupling method in this section, which we use for validating convergence in numerical coupling in later sections. In Section 3.1, we analytically formulate the fundamental economic theory of the coupling approach. We first introduce the power sector formulations in the two uncoupled models (Sect. 3.1). Then we carry out a derivation of the convergence conditions and criteria, where we map the Lagrangians of the two power-sector problems at different time resolutions, and derive the equilibrium condition for the coupled models (Sect. 3.2). In Sect. 3.3, we introduce the iterative coupling interface which contains all the previously derived convergence conditions. For REMIND information being passed on to DIETER (Sect. 3.3.1), and DIETER information being passed on to REMIND (Sect. 3.3.2), we list and define the variables and parameters being exchanged at the interface, as well as additional constraints and implementations which serve to improve the coupling.

A complete list of mathematical symbols and list of abbreviations can be found in the appendices.

In the following sections, we first formulate the two uncoupled models, then move onto discussing coupled models. The theoretical tools we develop here are the foundation to the numerical implementation of coupling, and serve to validate and assess the model convergence in the result sections.

3.1 Descriptions of uncoupled models

REMIND and DIETER are both optimization models. REMIND maximizes interannual global welfare from 2005 to 2150, whereas DIETER minimizes the power sector system cost for a single year and a single region. For a given REMIND "Nash" iteration (see Sect. 2.1), the single-region economy is in long-term equilibrium after the optimization problem is solved. Since given fixed national income, lower energy system costs mean higher consumption which leads to increased welfare (see Appendix C for details), maximizing welfare can be assumed to correspond to minimizing energy system costs, a part of which is power sector costs. Therefore, to reduce the complexity of our analysis, we formulate an uncoupled REMIND model based solely on the power sector cost minimization and not the total welfare maximization. For stand-alone REMIND, the multi-year power system cost for a single region equals the sum of all variable and fixed costs of generation,

$$Z = \sum_{y,s} (c_{y,s} P_{y,s} + o_{y,s} G_{y,s}), \tag{1}$$

where c represents the fixed cost for capacity, o represents the variable cost of running power generation, P denotes endogenous capacity, and G denotes endogenous generation (defined as including curtailment in REMIND). P and G are the decision variables of the problem. The sum in the objective function is over time index y and power generating technology type s. The REMIND time index y stands for one representative year, which represents 5 or 10 years centered around it. So even though the time step is 5 to 10 years, the time resolution is one year. For example, "y=2020" represents the years 2018-2022.Capital letters (both Latin and Greek) denote independent decision variables of the optimization problem. We classify an endogenous decision variable as independent if it is not uniquely determined by one or more other decision variables, and has no binding constraints applied to itself that is not already accounted for by the constraints on the decision variable(s) it depends on. Note that for simplicity, we treat all costs in REMIND in this formulation as if they are exogenous. In reality, REMIND has endogenous fixed costs due to technological learning as well as endogenous interest rate. Some types of variable costs such as fuel costs are also endogenous, which are determined based on primary energy balance equations for oil, gas and biomass. CO_2 prices can also be endogenous under emission constraints.

325 Under the simplifying assumptions made for the derivation in this paper, the only independent decision variables are capacities,

326 generations and curtailments. Small letters denote either exogenously given parameters or endogenous shadow prices.

327 For stand-alone DIETER which has a year-long time horizon, the power system cost is:

$$\underline{Z} = \sum_s \underline{c}_s \underline{P}_s + \sum_h \left[\underline{o}_s \left(\underline{G}_{h,s} + \underline{\Gamma}_{h,vre} \right) \right], \tag{2}$$

329 where $\underline{G}_{h,s}$ is the endogenous hourly power generation (excluding curtailment, note that this is different from the generation

330 variable definition in REMIND), h is the hourly index in a year from 1 to 8760, s is the index for the power generating

331 technology in DIETER. $\underline{\Gamma}$ is hourly curtailment, only applicable in the case of variable renewables vre ($vre \subset s$). Technology

332 type s can be subdivided into two subsets: vre and dis ("dispatchables"). For simplicity, we abbreviate the index subscript from

333 $s|s = vre$ to vre and $s|s = dis$ to dis. Here in order to differentiate from REMIND notations, we use underscore $\_$ to denote

334 DIETER parameters and variables. Note that for simplicity, in the derivation we treat the technology types in both models as

335 being identical, although in fact the technologies in the two models are not one-to-one mapped (Fig. B2). During the coupling

336 all interface parameters and optimal decision variables need to be upscaled or downscaled when transferred from one model to

337 the other.

338 The cost minimization of total power sector cost Z and $\underline{Z}$ under constraints yields the optimal values of the decision variables,

339 denoted as ($P_{y,s}^*$, $G_{y,s}^*$), and ($\underline{P}_s^*$, $\underline{G}_{h,s}^*$, $\underline{\Gamma}_{h,s}^*$).

340 Without coupling and under a baseline scenario, there are several constraints for each model. In the following equations we

341 denote the shadow price (i.e. the Lagrangian multiplier) of a constraint by the symbol following $\perp$. We use small greek letters to

342 denote endogenous shadow prices, and small Latin and Greek letters to denote exogenous parameters. The major constraints are

343 as follows ("c" stands for "constraint"):

344 c1) Constraint on generation for meeting demand, a.k.a. "supply-demand balance equation", or "balance equation" in short:

345 REMIND (annual): $\quad d_y = \sum_s G_{y,s} (1 - \alpha_{y,s}) \quad \perp \lambda_y$,

346 DIETER (hourly): $\quad \underline{d}_h = \sum_s \underline{G}_{h,s} \quad\quad\quad \perp \underline{\lambda}_h$,

347 where d_y denotes annual REMIND power demand, and $\underline{d}_h$ denotes DIETER hourly demand. The shadow prices (Lagrange

348 multipliers) λ_y and $\underline{\lambda}_h$ represent the annual and hourly electricity prices in REMIND and DIETER, respectively, and are

349 equal to the marginal cost of one additional unit of electricity generation. $\alpha_{y,s}$ is the annual VRE curtailment ratio in

350 REMIND. Note that technically speaking, REMIND electricity demand d_y is determined endogenously, partially via

351 competition with other energy carriers at the final energy consumption level, such as the competition between electricity and

352 gaseous carriers such as natural gas or hydrogen in household heating. But because here we have reduced REMIND to only

353 intra-power sector dynamics for the purpose of mathematical analysis, we treat demand as exogenous.

354 c2) Constraint on maximum capacity by the available annual potential ψ_s in a region:

355 REMIND: $\quad P_{y,s} \leq \psi_s \quad \perp \omega_{y,s}$,

356 DIETER: $\quad \underline{P}_s \leq \underline{\psi}_s \quad \perp \underline{\omega}_s$.

357 Note that the resource constraint in REMIND is only relevant for wind, solar and hydro, and is assumed to be constant over

358 the model horizon. Biomass availability is not modeled via a regional potential constraint. Instead the availability of biomass

359 is priced in through the soft-coupling to the land-use model MAgPIE via a supply curve.

360 c3) Constraint on generation being non-negative:

361 REMIND: $\quad -G_{y,s} \leq 0 \quad \perp \xi_{y,s}$,

362 DIETER: $\quad -\underline{G}_{h,s} \leq 0 \quad \perp \underline{\xi}_{h,s}$.

Note that there are several other similar constraints on other positive variables such as capacities and curtailment. In practice, during the derivation they behave similarly to this positive generation constraint, therefore for simplicity, we do not include them in the derivation.

c4) Constraint on maximum generation from capacity:

REMIND: $\qquad\qquad\qquad G_{y,s} = \phi_{y,s}P_{y,s} * 8760 \qquad\qquad \perp \mu_{y,s}$,

DIETER: (variable renewables) $\underline{G}_{h,vre} + \underline{\Gamma}_{h,vre} = \underline{\phi}_{h,vre}\underline{P}_{vre} \qquad \perp \underline{\mu}_{h,vre}$

$\qquad\qquad$ (dispatchables) $\qquad \underline{G}_{h,dis} \leq \underline{P}_{dis} \qquad\qquad\qquad \perp \underline{\mu}_{h,dis}$,

where $\phi_{y,s}$ is the exogenous annual average capacity factor of the power plant s in REMIND in year y, and $\underline{\phi}_{h,vre}$ is the exogenously given hourly theoretical capacity factor (i.e. before curtailment) of VRE in DIETER. Note that strictly speaking, curtailments in the uncoupled REMIND and DIETER are endogenous decision variables but are not independent variables. However, here we use capital letter to denote hourly curtailment in DIETER as an independent decision variable to account for curtailment costs and other curtailment constraints that can arise from a more general formulation of the model.

c5) "Historical" constraints on capacities in REMIND. This makes REMIND a so-called "brown-field model", i.e. a model accounting for the standing capacities in the real-world. Past capacities ($y < 2020$) are hard-fixed, i.e. the variable capacities are fixed to certain numeric values. Current capacities ($y = 2020$) are "soft-fixed", i.e. the variable capacities are fixed to a corridor around certain standing numeric values: the lower bounds guarantee the already planned capacities, and the upper bounds reflect the finite physical capabilities of scaling up, defined by 5% above the 2020 real-world data. For simplicity, we use only one constraint for both past and current capacities,

$P_{y,s} \geq p_{y,s} \qquad \perp \sigma_{y,s}$ for $y \leq 2020$,

where $p_{y,s}$ represents the standing capacities of technology s at time y in REMIND in the past and present years.

c6) Near-term upscaling constraint on VRE capacity expansion, represented by an upper bound on near-term capacity addition in model period $(y - \Delta y, y)$, $\Delta P_{y,s} := P_{y,s} - P_{y-\Delta y,s}$, where Δy is the REMIND model time step:

$\Delta P_{y,s} \leq q_{y,s} \qquad \perp \gamma_{y,s}$ for $y = 2025$,

where $q_{y,s}$ is equal to twice the added capacity during the 2010-2020 period (only applied to Germany in default REMIND).

Note that constraints (c5) and (c6) introduce interannual intertemporality into the power sector of REMIND. This additional interannual intertemporality determines that the model equilibrium can only be strictly satisfied across the sum of all model periods and not for a single period. Another source of intertemporality in REMIND is due to the adjustment cost, which we ignore in the main text of this study since it introduces non-linearity in the power sector and also plays a relatively small role in the overall dynamics.

Note that regarding the simplification of REMIND above, to the authors' best knowledge, there is no theoretical or empirical concept that addresses the validity of drawing equivalence between welfare maximization and energy system cost minimization in IAMs. Naively, given GDP is unchanged, decreasing energy system cost raises consumption and therefore welfare. However, this is only valid under the assumption that energy is a substitute (and not a complement) to capital and labor, i.e. one usually cannot raise economic output (GDP) simply by spending more on higher energy expenditure (while satisfying the same level of energy demand). Nevertheless, this is likely a necessary condition and not a sufficient one for proving the equivalence. More theoretical research will be needed to draw a precise and rigorous equivalence. However, in practice, we see that during our numerical calculation the model is well behaved according to this reduced theory, which means that the parameters in the models are in a regime where such an assumption is valid, at least in the case of IAM REMIND.

3.2 Economic theory of model convergence

In the last section we have discussed the stand-alone uncoupled power sector formulations in REMIND and DIETER. In this section we discuss the coupled models and its convergence. Under simplified assumptions, we first derive the mapping between the models which are necessary for a convergence (Sect. 3.2.1-2), then we derive theoretical relations which are later used to validate the numerical results of the coupled run (Sect. 3.2.3).

3.2.1 Derivation of convergence conditions

Our aim is to develop a method under which comprehensive convergence can be reached for soft-coupled multiscale models. We achieve this by deriving a mapping of the two problems, such that their decision variables have identical optimal solutions and the endogenous shadow prices are also equal across the models. The convergence conditions of the coupled REMIND-DIETER model for the power sector are the result of such a mapping. Below, we first define what is meant by a "comprehensive model convergence", and then sketch the workflow of the derivation of a coupling framework which would result in a comprehensive model convergence of both decision variables and shadow prices. The detailed derivation is in Appendix D. Here, we derive the conditions under which the endogenous decision variables are identical at each model's optimum, i.e. $P_{y,s}^* = \underline{P}_{y,s}^*$, and $G_{y,s}^*(1 - \alpha_{y,s}^*) = \sum_h \underline{G}_{y,h,s}^*$ (or equivalently pre-curtailment generation $G_{y,s}^*$ and $\sum_h \left(\underline{G}_{y,h,s}^* + \underline{\Gamma}_{y,h,s}^* \right)$. A convergence of the solutions of these two sets of annual decision variables for each technology s and for each year y, along with the convergence of shadow prices gives rise to "comprehensive model convergence". We show below that this can only be achieved if there is a harmonization at the level of the KKT Lagrangians of the two problems, following the methods first developed by Karush, Kuhn and Tucker (Karush, 1939; Kuhn and Tucker, 1951).

Our coupling approach fundamentally relies on mapping the parameterization of the Lagrangians for both optimization problems. It is trivial to show that as long as the KKT Lagrangians are identical with respect to the decision variables, the solutions of the problem are identical. For example, if an optimization problem A has Lagrangian L_1 = a_1*x+b_1*y and another problem B has Lagrangian L_2 = a_2*x+b_2*y, where x and y are decision variables of the optimization problems. Then if we let a_1 = a_2, b_1 = b_2, the two problems are identical, and they must have identical optimal solutions for the decision variables x* and y*. This is the basic logic behind the Lagrangian-based method. The challenge in the case of REMIND and DIETER is to show that when a decision variable representing the same physical quantity, for example, the annual power generation from a technology is defined with low resolution in one problem, and is defined with high resolution in another, that there is nevertheless a viable mapping between the two Lagrangians. In this case, the parameterization of the Lagrangian is not only limited to exogenous parameters of the model, but also includes endogenous shadow prices and endogenous decision variables from the other model. Due to the endogenous nature of the latter two, the parametrization in the current-iteration model A must come from the solved results from the last iteration from model B, and vice versa. Fig. 2 illustrates the workflow of the analytical derivation of the convergence conditions.
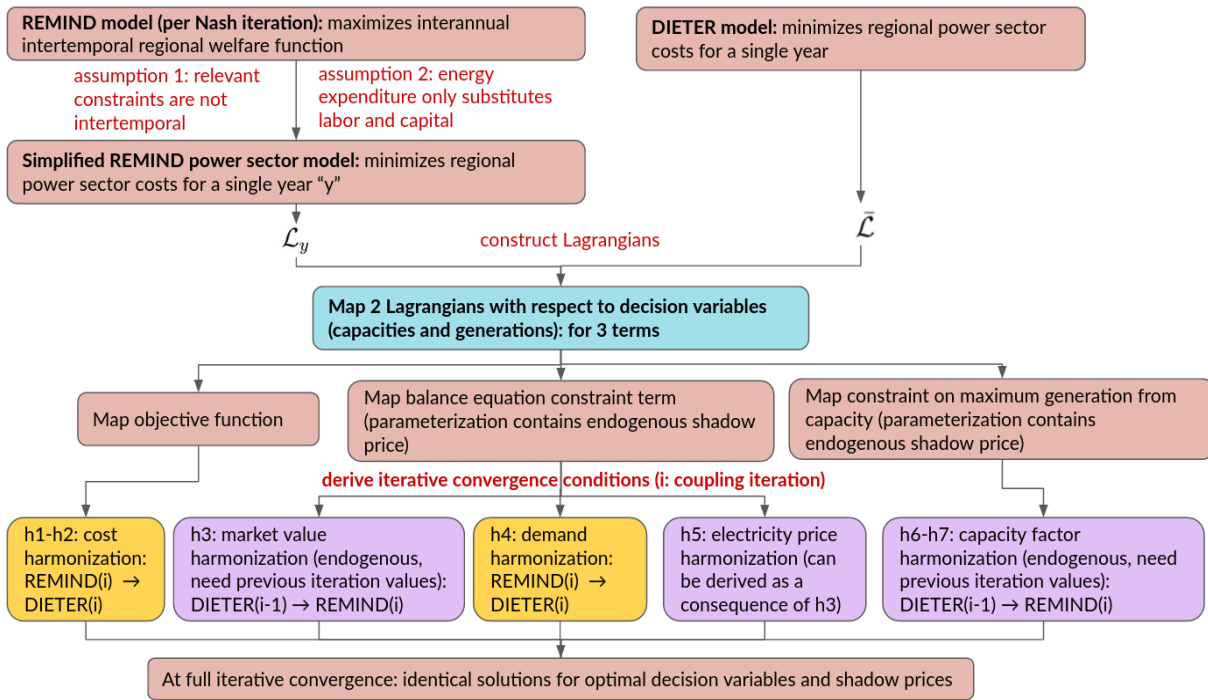
Figure 2: The schematics of the Lagrangian-based derivation procedure for a simplified version of REMIND-DIETER iterative convergence. After simplifying assumptions, we can construct the Lagrangians of the reduced REMIND model and the full DIETER model for a single year (Eqs. (3)-(4)). Comparing and mapping terms in the Lagrangians (a key step in bold), we discover that iterative exchange of a broad range of information is needed for a fully harmonized parameterization of the Lagrangians. Under the harmonization specified in the seven convergence conditions (color coded for directions of information flow), the coupled models can give rise to identical optimal solutions of the models' respective (annual aggregated) decision variables, and hence a full quantity convergence. The necessary shadow price convergence is shown in the detailed derivation of the harmonization conditions (h1-h7) in Appendix D.

The analytical derivation workflow, as shown in Fig. 2, is described in detail as follows. First, we apply simplifying assumptions to reduce the complexity of the uncoupled models (before the key step in blue in Fig. 2). Assumptions have to be made to justify reducing the scope of the REMIND model, such that for the purpose of the analysis, it is on equal footing as DIETER. We achieve this by reducing the global REMIND model to single-sector (the power sector), single-year, and single-region. To reduce the REMIND model from a macroeconomic-energy model to a power-sector-only model, we make similar assumptions as before when formulating the uncoupled REMIND power sector (see Sect. 3.1). To reduce the REMIND model further to a single year, we assume that the models only contain constraints in the power sector that are not intertemporal, i.e. ignoring the brown-field and near-term constraints for now. Since for each iteration of the REMIND model under "Nash mode", inter-regional trading happens between the iterations, the single-iteration optimization model is already for a single region, and therefore does not require simplification. After these simplifying steps, in this part of the derivation, we can treat REMIND's power sector as "separate" from the rest of the model, and treat the dynamics of a single year in REMIND as independent from the dynamics of other years. Later, the numerical results of the convergence can confirm to a large degree the validity of these assumptions, especially in the green-field temporal ranges, i.e. where the intertemporal brown-field constraints have little influence on the dynamics. Note that with the inclusion of these intertemporal constraints in the derivation, the mapping becomes more complicated, especially for the near-term range, i.e. before 2035. So in practice, this derivation of the coupling

457 interface is only an approximation to what is needed for a full convergence of DIETER and REMIND, since it deliberately
458 ignores such constraints. See also Sec. 6.1.

459 After the necessary simplification assumptions, we construct the Lagrangians for the simplified model REMIND and for
460 DIETER (after the blue block in Fig. 2) (Gan et al., 2013). For a single-year reduced REMIND power sector model, the
461 Lagrangian is:

462
$$\mathcal{L}_y = \underbrace{\sum_s \left(c_{y,s}P_{y,s} + o_{y,s}G_{y,s}\right)}_{\text{REMIND objective function}} + \underbrace{\lambda_y \left[d_y - \sum_s G_{y,s}(1 - \alpha_{y,s})\right]}_{\text{annual electricity balance equation constraint}} + \underbrace{\sum_s \mu_{y,s}\left(G_{y,s} - 8760 * \phi_{y,s}P_{y,s}\right)}_{\text{maximum generation from capacity constraint}} . \tag{3}$$

463 We would like to map it to the single-year DIETER Lagrangian $\underline{\mathcal{L}}$:

464
$$\underline{\mathcal{L}} = \underbrace{\sum_s \left[\underline{c_s}\underline{P_s} + \underline{o_s}\sum_h \left(\underline{G_{h,s}} + \underline{\Gamma_{h,vre}}\right)\right]}_{\text{DIETER objective function}} + \underbrace{\sum_h \underline{\lambda_h}\left(\underline{d_h} - \sum_s \underline{G_{h,s}}\right)}_{\text{hourly electricity balance equation constraint}} + \underbrace{\sum_{h,dis} \underline{\mu_{h,dis}}\left(\underline{G_{h,dis}} - \underline{P_{dis}}\right)}_{\text{maximum dispatchable generation from capacity constraint}}$$

465
$$+ \underbrace{\sum_{h,vre} \underline{\mu_{h,vre}}\left(\underline{G_{h,vre}} + \underline{\Gamma_{h,vre}} - \underline{\phi_{h,vre}}\underline{P_{vre}}\right)}_{\text{maximum renewable generation from capacity and weather constraint}} . \tag{4}$$

466 The algebraic derivation of mapping the two Lagrangians term-by-term is presented in Appendix D. From this algebraic
467 mapping, we can derive seven harmonization conditions (h1-h7) required for a full convergence. Conditions (h1-h7) are the
468 subsequent basis for most of the information exchanged at the coupling interface. Among them, conditions (h3, h5-7) (purple
469 blocks in Fig. 2) indicate conditions which contain endogenous information that must come from the previous iteration of
470 DIETER that is passed on to REMIND, such as markup and capacity factors. Conditions (h1-2, h4) (yellow blocks) indicate
471 conditions which contain information that come from the previous iteration of REMIND and are passed on to DIETER. For
472 schematics of the coupled iterations, see Appendix E.

473 This Lagrangian-mapping-based derivation can theoretically show that our approach (in its most simple form) necessarily leads
474 to model convergence, and has the advantage of being mathematically straight-forward and rigorous. The necessary information
475 from the power sector dynamics is all contained in the list of conditions derived from such a mapping. If the coupling contains
476 less information, a convergence is not possible; at the same time, for a model convergence, one does not need to pass on any
477 additional information beyond what is contained in this list of conditions. The list of information derived here is therefore
478 complete and exhaustive for a coupled convergence.

479 **3.2.2 List of convergence conditions**

480 The convergence conditions (h1-h7), which are derived in detail in Appendix D following the procedure in Sect. 3.2.1, are
481 summarized here:

482   **h1**) annual fixed costs are harmonized: $c_{y,s} = \underline{c_{y,s}}$,

483   **h2**) annual variable costs are harmonized: $o_{y,s} = \underline{o_{y,s}}$.

484   **h3**) annual average market values for each generation type s are harmonized via markups from DIETER. We let $\underline{\eta_{y,s}}(i-1)$
485   denote the markup for technology s in year y in the last iteration DIETER, i.e. the difference between market value and
486   annual average price of electricity:

487
$$\underline{\eta_{y,s}} = \underbrace{\frac{\sum_s \underline{\lambda_{y,h}}\underline{G_{y,h,s}}}{\sum_h \underline{G_{y,h,s}}}}_{\text{Market value}_s} - \underbrace{\frac{\sum_h \underline{\lambda_{y,h}}\underline{d_{y,h}}}{\sum_h \underline{d_{y,h}}}}_{\text{Annual average electricity price}_s} . \tag{5}$$

488   This is the heart of our coupling approach, using markups as the "price signals". Intuitively, the markups represent the
489   market value differences between REMIND and DIETER. The harmonization of market values is implemented by

490   iteratively adjusting the market value for each generator type in REMIND to be the same as that in DIETER. As long as

491   the market values (or per-unit-generation revenues) and costs are harmonized, the economic structures of the power

492   market are identical and the models can converge.

493   Using markup Eq. (5), we modify the original objective function Z in the coupled version of REMIND by subtracting the

494   product of markups and generations summed over all technologies and all years:

$$Z' = Z - \sum_{y,s} \underline{\eta}_{y,s}(i-1)G_{y,s}\left(1 - \alpha_{y,s}\right), \tag{6}$$

496   where Z' is the modified REMIND objective function in the coupled version, i is the iteration index of the iterative soft-

497   coupling.

498   **h4)** annual power demands are harmonized: $\sum_h \underline{d}_{y,h} = d_y$,

499   **h5)** annual average prices of electricity are harmonized:

$$\lambda_y = \frac{\sum_h \underline{\lambda}_{y,h}(i-1)\underline{d}_{y,h}(i-1)}{\sum_h \underline{d}_{y,h}(i-1)}, \tag{7}$$

501   where $(i-1)$ indicates that the endogenous results are from the last iteration. This is shown in Appendix D to be a direct

502   consequence of (h3) and (h4).

503   **h6)** annual average capacity factor for each generation type s are harmonized:

$$\phi_{y,s} = \sum_h \underline{\phi}_{y,h,s}(i-1)\,/8760, \tag{8}$$

505   where $\underline{\phi}_{y,h,s}(i-1) = \frac{G_{y,h,s}(i-1)}{\underline{P}_{y,s}(i-1)}$ is the hourly capacity factor in DIETER, determined by endogenous hourly generation

506   and annual capacities in the last iteration.

507   **h7)** annual curtailment are harmonized:

$$G_{y,vre}\alpha_{y,vre} = \sum_h \underline{\Gamma}_{y,h,vre}(i-1). \tag{9}$$

509 In mapping the Lagrangians (Eqs. (3-4)), except the objective function, the rest of the parametrization contains endogenous

510 shadow prices and endogenous quantities. Since endogenous values can only be known ex post, this imposes a strict requirement

511 on the coupling that it must be iterative, with the endogenous part of the parameterization coming from previous iteration

512 optimization results – usually from the other model. The mapping of the endogenous information requires careful argument in

513 each case (i.e. the derivation of (h3)-(h7)). In the case of the balance equation constraint Lagrangian term (corresponding to

514 (c1)), the shadow prices of the constraint in current-iteration REMIND model are exogenously corrected by a set of technology-

515 specific "markups" (see Sect. 3.1 introduction), such that the new "corrected" market value in REMIND is manipulated to

516 match the market value of the previous iteration of DIETER. This is the heart of our coupling approach, using markups as the

517 "price signals". In the case of the constraint on maximum generation from capacity (corresponding to (c4)), the endogenous

518 shadow prices in the current iteration REMIND can be shown to be automatically mapped to the those in the previous iteration

519 of DIETER, given that the annual average capacity factors in the constraints are harmonized (h6-h7).

520 In actual implementation, most of the above mappings are modified for numerical stability (Sect. 3.3.2, Appendix H).

521 **3.2.3 Theoretical tools for validating convergence**

522 Here we first state the convergence criteria, which are mathematical relations which are being satisfied under model

523 convergence. Then we also discuss equilibrium conditions of the coupled models which alongside the convergence criteria can

524 be used to check numeric results to validate and assess the convergence outcome.

525 Under a theoretical full convergence of the coupled model,

526   v1) annual average electricity prices,

527   v2) capacities,

528   v3) (post- or pre-curtailment) generations,

529 all should be identical at the end of the coupling in both models. These are the most important criteria by which we validate full

530 model convergence. Technically, electricity price convergence (v1) (i.e. convergence condition (h5)) can be derived from (h3)-

531 (h4). Nevertheless, we check this ex post, together with quantity convergence (v2-v3). In actual coupled model runs, following

532 only the convergence conditions (h1-h7), the convergence criteria (v1-v3) might not be exactly fulfilled. Therefore in practice,

533 in order to validate the degree of numerical convergence, the alignment between REMIND and DIETER generation shares is set

534 to be within a few percentage points before coupled runs terminate.

535 Besides using convergence criteria (v1-v3), we also use a type of equilibrium condition – the so-called "zero-profit rules"

536 (ZPRs) to validate the numerical model convergence. ZPRs are mathematical relations which state that under market

537 equilibrium, prices are equal to the costs for electricity. This is not always the case, especially in the situation where there are

538 extra constraints in the model which distort this equality. ZPRs contain model parameters and decision variables at market

539 equilibrium, and they can be derived from the KKT conditions of the model (Appendix F). ZPRs are therefore reliable tools in

540 ascertaining the sources of market values or the price of electricity of the power sector, because according to the ZPRs, one can

541 always decompose the prices into the cost components, i.e. so-called levelized costs of electricity (LCOE). The decomposition

542 of prices into cost components is important, because the prices of electricity in the power market are overdetermined by the

543 energy mix, so it is possible that two different power mixes correspond to the same electricity price. In numerical results, a

544 slight mismatch of energy mix at the end of the coupling is unavoidable, so alongside comparing the prices, it is often helpful to

545 compare the makeup of the LCOE across the models, such that they also appear harmonized at the end of the iterative

546 convergence. Overall, ZPRs is a helpful tool for visualizing and understanding the power market dynamics, both from the point

547 of view of each generator type as well as from the point of view of the entire electricity system. It is worth noting, that the zero-

548 profit rules, which are mathematical conditions derived from an idealized modeling of the power sector as fully competitive, are

549 only an approximation to the real-world markets, where firm profits exist. ZPRs in its technical definition simply means that at

550 model equilibrium, cost equals revenue. Given that the profits are defined as the difference between revenue and cost, the profits

551 are zero in this situation. The name "zero-profit rule" therefore should not be overinterpreted beyond their technical contents,

552 and one should be aware of their theoretical origin and assumptions under which they are valid.

553 The ZPRs of the coupled model can be derived based on: 1), the uncoupled models; 2), the modification made to the model due

554 to the coupling interface (h1-h7); 3), any additional modifications made to the model during our numerical implementation. In

555 the last category, for a complete numerical implementation of the coupling, we add one additional capacity constraint (c7) and

556 (c8) for each model. The first capacity constraint (c7) is created in REMIND to circumvent the issue of extremely high markup

557 from peaker gas plants in the scarcity hour of the year in the DIETER model, which otherwise causes instability during the

558 iterative coupling. The second constraint (c8) is a simple brown-field constraint implemented in DIETER to address the fact that

559 DIETER is a green-field model, which is otherwise ignorant about standing-capacities in the real world. For simplicity, (c7) and

560 (c8) are not included in the convergence condition derivations in Sect. 3.2.1. The derivation of the ZPRs outlined by the above

561 three steps have been carried out in: Appendix F (uncoupled models), Appendix G (coupled REMIND only including coupling

562 interface, coupled DIETER including constraint (c8)), and Appendix H (coupled REMIND, including constraint (c7)).

563 In summary, the ZPRs for both coupled models are as follows:

564   a) Coupled REMIND:

i) Technology-specific ZPR:

$$\underbrace{\frac{\sum_y\left(c_{y,s}P_{y,s}+o_{y,s}G_{y,s}\right)}{\sum_y G_{y,s}}}_{\text{Pre-curtailment LCOE}_s}+\underbrace{\frac{\sum_y\left(c_{y,s}P_{y,s}+o_{y,s}G_{y,s}\right)\alpha_{y,s}}{\sum_y G_{y,s}\left(1-\alpha_{y,s}\right)}}_{\text{Curtailment LCOE}_s}$$

$$=-\underbrace{\frac{\sum_y\left(\omega_{y,s}-\sigma_{y,s}+\gamma_{y,s}+\nu_{y,s}\right)P_{y,s}}{\sum_y G_{y,s}\left(1-\alpha_{y,s}\right)}}_{\text{Capacity shadow price}'_s}+\underbrace{\frac{\sum_y\left(\lambda_y+\underline{\eta}'_{y,s}\right)G_{y,s}\left(1-\alpha_{y,s}\right)}{\sum_y G_{y,s}\left(1-\alpha_{y,s}\right)}}_{\text{Market value}'_s}\qquad(10)$$

ii) System ZPR:

$$\underbrace{\frac{\sum_{y,s}\left(c_{y,s}P_{y,s}+o_{y,s}G_{y,s}\right)}{\sum_{y,s}G_{y,s}}}_{\text{Pre-curtailment LCOE}_{system}}+\underbrace{\frac{\sum_{y,s}\left(c_{y,s}P_{y,s}+o_{y,s}G_{y,s}\right)\alpha_{y,s}}{\sum_{y,s}G_{y,s}\left(1-\alpha_{y,s}\right)}}_{\text{Curtailment cost}_{system}}$$

$$=-\underbrace{\frac{\sum_{y,s}\left(\omega_{y,s}-\sigma_{y,s}+\gamma_{y,s}+\nu_{y,s}\right)P_{y,s}}{\sum_{y,s}G_{y,s}\left(1-\alpha_{y,s}\right)}}_{\text{Capacity shadow price}'_{system}}+\underbrace{\frac{\sum_{y,s}\left(\lambda_y+\underline{\eta}'_{y,s}\right)G_{y,s}\left(1-\alpha_{y,s}\right)}{\sum_{y,s}G_{y,s}\left(1-\alpha_{y,s}\right)}}_{\text{Electricity price}'_{system}}\qquad(11)$$

b) Coupled DIETER:

i) Technology-specific ZPR:

$$\underbrace{\frac{\underline{c}_s\underline{P}_s+\underline{o}_s\sum_h\left(\underline{G}_{h,s}+\underline{\Gamma}_{h,vre}\right)}{\sum_h\underline{G}_{h,s}}}_{\text{LCOE}_s}=-\underbrace{\frac{\left(\omega_s+\underline{\varsigma}_s\right)\underline{P}_s}{\sum_h\underline{G}_{h,s}}}_{\text{Capacity shadow price}'_s}+\underbrace{\frac{\sum_h\lambda_h\underline{G}_{h,s}}{\sum_h\underline{G}_{h,s}}}_{\text{Market value}_s}.\qquad(12)$$

ii) System ZPR:

$$\underbrace{\frac{\sum_s\left[\underline{c}_s\underline{P}_s+\underline{o}_s\sum_h\left(\underline{G}_{h,s}+\underline{\Gamma}_{h,vre}\right)\right]}{\sum_{h,s}\underline{G}_{h,s}}}_{\text{LCOE}_{system}}=-\underbrace{\frac{\sum_s\left(\omega_s+\underline{\varsigma}_s\right)\underline{P}_s}{\sum_{h,s}\underline{G}_{h,s}}}_{\text{Capacity shadow price}'_{system}}+\underbrace{\frac{\sum_h\lambda_h\underline{d}_h}{\sum_h\underline{d}_h}}_{\text{Annual average electricity price}_{system}}.\qquad(13)$$

"Prime" sign indicates the term has been modified from the uncoupled versions due to implementation in the coupling. ν and ς are capacity shadow prices introduced from the additional constraints (c7-c8) (Appendix G-H). It is worth noting that constraints (c7-c8) introduced due to coupling can impact the Lagrangians of the two models which we used to derive convergence conditions and criteria. However, in actual coupled runs, evidently there is only a moderate distortion due to these extra constraints. Condition (c8) even helps with convergence, because it puts most of the brown-field and near-term constraints which REMIND sees also into DIETER (see Sect. 6.1).

Due to the fact that several sources of shadow prices cannot be incorporated during the derivation for convergence (Sect. 3.2.1), in numerical experiments of coupled run it is appropriate to compare the following two types of prices across the two models for price convergence:

1) Electricity price convergence, not including any capacity shadow prices;

2) Sum of electricity prices and all respective capacity shadow prices converge.

Under the simplified analysis of convergence (discounting brown-field constraints, scarcity prices, etc), price convergence in 1) is predicted by theory (see also convergence condition (h5)). However, it is only under the most idealized situation. Convergence in 2) on the other hand includes all the prices, which should match if LCOEs match across the system. We use the first type to check price convergence over iteration, and use the second type only in the context of checking the system ZPRs across the models because of the theoretical relations between full prices and LCOEs.

3.3 Implementation via interface: exchange of variables

In this section we list parameters and endogenous variables that are exchanged between REMIND and DIETER. This already satisfies most convergence conditions, while the remaining condition (h5) is checked in Sect. 4 as part of the convergence criteria (v1-v3). An overview of the model coupling and the flow of information under convergence conditions is shown in Fig. 3.
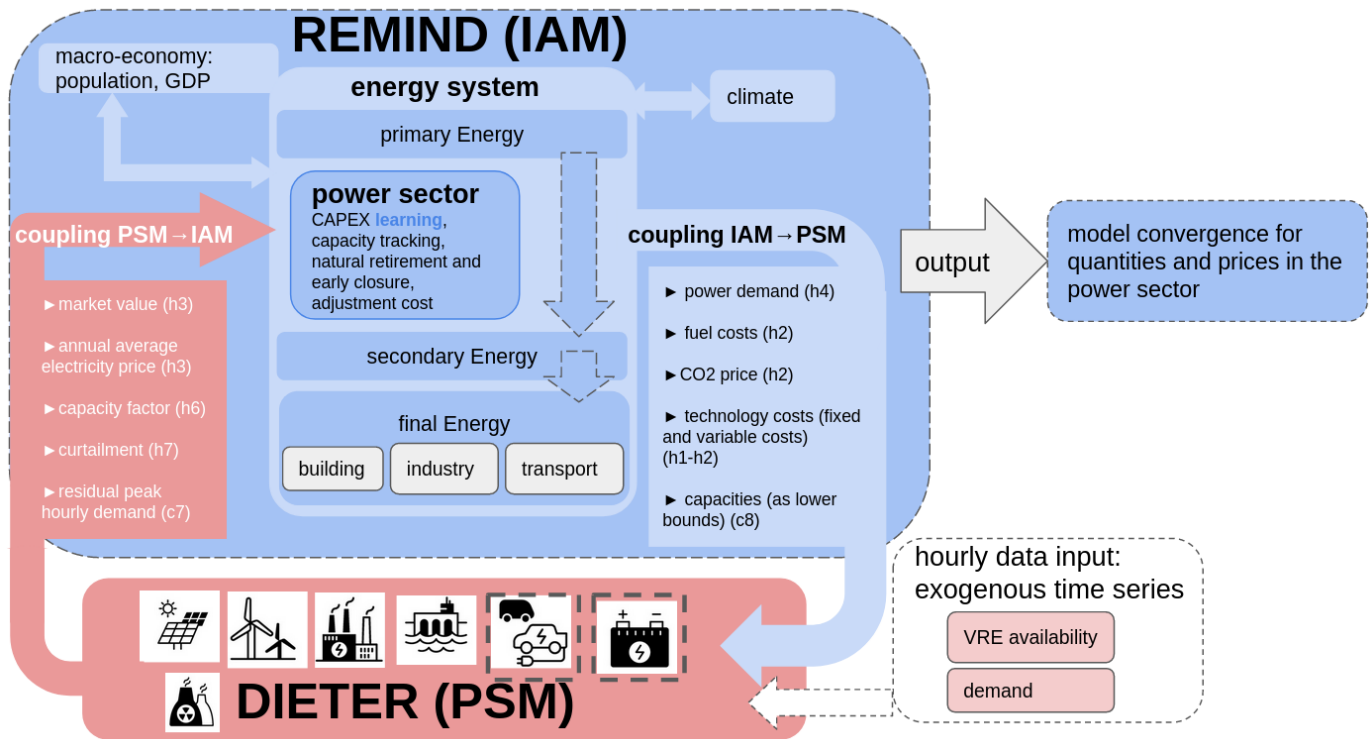
Figure 3: The schematics of the REMIND-DIETER iterative soft-coupling. The power sector module of IAM REMIND, which is between the layer of primary to secondary energy transformation, is hard-coupled with other modules inside REMIND such as macro-economy, industry and transport. In PSM DIETER, the power market with generators of various types is modeled with hourly resolution, with options for storage and flexible demand. The information exchanged between the models (block arrows) are determined via the convergence conditions (h1-h7) derived before (Sect. 3.2.1). In order to improve performance and facilitate convergence, additional constraints (c7) and (c8) are included in the coupling interface. The coupling interface for REMIND → DIETER is programmed as a part of modified DIETER code, and vice versa. Both interfaces are written in GAMS. For a single-region, the scheduling of coupled iterations is illustrated in Fig. E1 in Appendix E. 16 DIETER optimization problems are solved for each representative year of REMIND in parallel, scheduled after each internal REMIND "Nash" iteration (see Sect. 2.1 for a description of the iterative "Nash" algorithm).

During the coupling, the following exchanges of parameters and variables take place iteratively in both directions via the interface.

3.3.1 REMIND to DIETER

The following information flow from REMIND to DIETER.
1. Technology fixed costs (convergence condition (h1)):

a. Annualized capital investment cost: It is calculated from endogenously determined overnight investment cost, plant lifetime, and the endogenously determined interest rate. The overnight investment cost is determined from floor cost, learning rate and the endogenous global accumulated deployment. Note that investment costs decrease according to endogenous learning rate. Interest rate is about 5% on average but is endogenous and time dependent in REMIND;

b. Annualized operation and maintenance (O&M) fixed costs (OMF): They are a fixed share of the capital costs;

c. Adjustment cost: It is technology-specific and is proportional to the capital investment cost. See Appendix I for its implementation.

2. Technology variable costs (convergence condition (h2)):

a. Primary energy fuel costs: They are endogenously determined as the shadow prices of the primary fuel balance equations in REMIND. Import prices, domestic prices of extraction, amount of regional reserve, and the amount of fuel demand can all influence the fuel cost. The relevant fuel costs include coal, gas, biomass and uranium. The fuel costs can have interannual intertemporal oscillatory components which can cause instability during iteration if coupled directly. We mitigate this by conducting a linear fit to the time series before passing them to DIETER;

b. Conversion efficiency of each generation technology;

c. O&M variable costs (OMV);

d. CO_2 emission cost: Exogenous or endogenous CO_2 price from REMIND multiplied by the carbon content of a type of fossil fuel and divided by the conversion efficiency of a generation technology gives the CO_2 cost of 1MWh of generation. Note that in REMIND, biomass is considered to contain zero carbon emission when combusted.;

e. Grid cost: In REMIND the stylized grid capacity equation is proportional to the amount of pre-curtailment VRE generation. So effectively the grid cost is a variable cost. Note that in future work, grid costs can be modeled in more detail either in DIETER or in another PSM. Here, we use the parameterized grid costs which are implemented in default REMIND as an approximation to the necessary grid cost.

3. Power demand (convergence condition (h4)). REMIND informs DIETER of the total power demand d_y of a representative year y. In the next iteration of DIETER, the exogenous time series for the hourly demand from a historical year (2019) is scaled up to demand of the last iteration REMIND, $d_y(i-1)$, such that the annual total power demand in DIETER is equal to that of REMIND for each coupled year: $\underline{d}_h = \underline{d}_{2019,h} * \frac{d_y(i-1)}{\sum_h \underline{d}_{2019,h}}$.

4. Pre-investment capacities $P_{y-\Delta y/2,s}/(1-ER)$ as an additional brown-field constraint (see constraint (c8) in Appendix G). ER is the endogenous early retirement rate in REMIND.

5. Total regional renewable resources for wind, solar and hydro (constraint (c2)), such that DIETER capacities are constrained by the same total available resources as in REMIND.

6. Annual average theoretical capacity factors of VREs and hydroelectric in REMIND (convergence condition (h6)). We note the pre-curtailment utilization rates of VRE capacity as "theoretical capacity factors", as these can be achieved in theory if there is no curtailment. They are usually determined by meteorological factors such as wind and solar potential, as well as the efficiency of the turbines or solar photovoltaic modules. In contrast, the post-curtailment utilization rate of VRE are "real capacity factors", as these are the real utilization rates after optimal endogenous dispatch. The time series of theoretical utilization rate of VRE generations of one historical year in DIETER are scaled up such that the annual average theoretical capacity factors in DIETER equals the exogenous parameters in REMIND:

$$\underline{\phi}_{h,vre}(y) = min\left(0.99, \underline{\phi}_{h,vre}(y=2019) * \frac{\phi_{vre}}{\sum_h \underline{\phi}_{h,vre}(y=2019)}\right).$$

In DIETER, to be realistic, the rescaled hourly capacity factor for solar and wind has an upper bound at 99%. The slight mismatch of the capacity factors due to this additional upper bound is negligible

3.3.2 DIETER to REMIND

The following information is passed from last-iteration DIETER to REMIND:

1. Market values $\underline{MV}'_{y,s}$ and the annual average electricity price $\underline{J}'_y$ (convergence condition (h3)), where $\underline{MV}'_{y,s}$ is the annual average market value without the surplus scarcity hour price, and $\underline{J}'_y$ is the annual average electricity price without the surplus scarcity hour price.

2. Peak hourly residual power demand $\underline{d}_{residual}$ as a fraction of total annual demand $\sum_h \underline{d}_h$ (constraint (c7)). This produces the peak residual demand in REMIND $d_{residual,y}$ that is proportional to the last-iteration DIETER peak to total demand ratio $\frac{d_{residual}(y,i-1)}{\sum_h \underline{d}_h(y,i-1)}$, and the in-iteration total annual demand $d_y(i)$:

$$d_{residual,y}(i) = \frac{d_{residual}(y,i-1)}{\sum_h \underline{d}_h(y,i-1)} * d_y(i) ,$$

where $\underline{d}_{residual}$ was defined in Appendix H (Eq. (H1)).

3. Annual capacity factors of dispatchable plants $\underline{\phi}_{dis} = \frac{\sum_h \underline{G}_{h,dis}}{P_{dis}* 8760}$ (convergence condition (h6)).

4. Annual solar and wind curtailment ratio: curtailment as a fraction to total annual post-curtailment generation $\frac{\sum_h \underline{\Gamma}_{h,vre}}{\sum_h \underline{G}_{h,vre}}$ (convergence condition (h7)).

For the information flowing from DIETER to REMIND, we use an innovative method of multiplicative "prefactors", which can stabilize the coupling and increase the speed towards model convergence. The prefactors are automatic linear stabilizers of the current-iteration variables in REMIND. They depend on current-iteration endogenous variables in REMIND, and are multiplied usually with the last-iteration endogenous DIETER results that are exogenously passed to REMIND. This allows some degree of endogeneity in these exchanged variables, and their values can be adjusted according to the updated dynamics in the current REMIND iteration, such as interregional trading or price elasticity of demand, under which the exogenous last-iteration DIETER optimality can be used as an approximate starting point but do not necessarily hold exactly.

The prefactors usually depend on the differences between generation shares in the two models: e.g. the prefactor for markup is a linear function of the difference between the current-iteration REMIND endogenous generation share and last-iteration DIETER generation share. We illustrate the mechanism of prefactors using markup for solar as an example: A lower market value for solar is consistent with a higher solar share, according to the well-known self-cannibalization effect of decreasing VRE market value as the VRE share increases (Hirth, 2018). Therefore, we can introduce an automatic stabilization measure through a negative feedback loop: If the REMIND endogenous share is larger than in the last DIETER iteration, in which case the in-iteration market value should be lower than the last-iteration DIETER market value, the multiplicative prefactor for market value should be so constructed such that it is smaller than one. This lowers the market value for solar, and decreases the in-iteration REMIND markup $\eta_{y,s}(i)$, hence preventing over-incentivizing the solar generation using the old market value based on the last-iteration energy mix. Overall, this produces a stabilizing effect on the system by making the markup as a price signal responsive to endogenous quantity change. We use prefactors ubiquitously when passing variables from DIETER to REMIND, such that during the iteration REMIND can adjust more smoothly and easily. We discuss the implementation of these prefactors in detail in Appendix H.2.

4 Numerical convergence under "proof-of-concept" baseline scenario

In this section, we check the convergence behavior for prices and quantities (capacity and generation) in coupled model runs using the convergence validation criteria from the last section. Comparing the numerical results with the theoretical prediction, we can validate that REMIND-DIETER soft-coupling indeed produces almost full convergence.

Throughout this section, we only use one scenario – a "proof-of-concept" baseline scenario. Under the "proof-of-concept" scenario of the coupled run, we disable storage (i.e. batteries and hydrogen) and flexible demand (i.e. electrolyzers) in both models, as this allows us to use the theoretically derived convergence criteria from Sect. 3, which would become overly complex in a model with storage and flexible demand. The coupled run is under a baseline scenario, i.e. there is no additional climate policy implementation. Since this is a configuration created only for comparing to the theoretical prediction, it is not meant to be a policy-relevant configuration. In more policy-relevant coupled runs, we turn on storage and flexible demand (see Sect. 5). For schematics and computational runtimes of the coupled iterations, see Appendix E.

For the coupled runs, we define a baseline scenario for single-region Germany under SSP2 assumptions, corresponding to the "middle-of-the-road" scenario (for a definition of the SSPs, see Koch and Leimbach, 2022). Specifically, this means that REMIND runs for all global regions in parallel, but DIETER only runs for Germany. Only information in the German power sector is exchanged for the two models. We use a low CO_2 price to represent "no additional policy", which is 30$/$tCO_2$ in 2020 and 37$/$tCO_2$ for years beyond 2020. According to the 2011 Nuclear Energy Act of Germany, remaining nuclear capacities are set to early retire in REMIND within the time period until 2022. We assume hydroelectric generation in Germany to come from run-of-the-river. In DIETER, we cap dispatchable generation's annual capacity factors at 80% for non-nuclear power plants, and 85% for nuclear power plants, so the dispatch results are in line with real-world power sectors. This constraint only adjusts the capacity factor constraint (c4), which would pose no additional distortion to our mathematical analysis.

Due to the particular implementation of offshore wind in REMIND, DIETER wind offshore capacities are fixed to that of REMIND to avoid too much distortion. Since in our scenarios, offshore wind capacity in Germany is relatively small compared to other generators, this fixing presents only a minor distortion to the coupling. Hydroelectric generation in REMIND is assumed to have an average annual capacity factor of around 25%. This capacity factor is implemented as a bound in DIETER. For simplicity, instead of a time series profile for hydroelectric generation, we allow the hourly capacity factor to be no higher than 90%, meaning hydro is close to being dispatchable in all our scenarios. In the German context, hydro usually means run-of-the-river, which has a variable output. Nevertheless, we find the 90% maximum hourly capacity factor a reasonable assumption to make, since in our runs we do not yet consider pumped hydro as a technology in this study, so a more dispatchable quality of hydro can be assumed. Results presented in this section belong to the same coupled run under the "proof-of-concept" scenario.

4.1 Electricity price convergence

According to theoretical convergence criteria (under simplifying assumptions, Sect. 3.2.1-3), at numerical convergence, the electricity price of REMIND should be equal to the price of DIETER. However, REMIND is interannual intertemporal, whereas DIETER is only year-long, so we compare the differences over time, as well as the interannual average of the price differences (Fig. 4).

Figure 4: Annual average electricity price convergence behavior of a coupled run for Germany under a "proof-of-concept" baseline scenario. (a): the difference between the annual electricity price time series of REMIND and the annual average electricity price time series in DIETER as a function of coupled iteration. (b): the interannual average of the differences in (a) as a share of REMIND price. Due to the interannual intertemporal nature of REMIND, in (a) the price difference can appear to have oscillatory components, obscuring the visual assessment of convergence. As a result, we show the trend of price convergence over iterations more clearly in panel (b) by taking the temporal average of the price differences. The REMIND price in both plots is a running average of three neighboring time periods to visually smooth out oscillations.

In Fig. 4a, the price difference oscillates from period to period. As the coupling starts, the REMIND price is much higher than DIETER, especially in the earlier years. After around the 10th iteration, the difference in early years starts to reverse: DIETER's price becomes higher than REMIND. Around 2040-2060, REMIND has a higher average price than DIETER, due to the VRE market values being higher than their LCOE. This is discussed later in Sect. 4.3.2.

In Fig. 4b, we calculate the difference between two time series – the time-averaged power prices in the two models. We observe the difference between them decreases over the iterations, showing a clear converging trend, and stabilizes at around 3% of the REMIND price. There are two observations regarding the price convergence of the coupled run. First, the convergence happens rather quickly within 10 iterations. Second, the converged value of the price difference is not exactly 0, but slightly above 0, at a few percent of the full price (a few $/MWh). Under ideal convergence conditions, according to (v1), the two prices should be equal at full convergence for every coupled year. However, in practice, the average prices do not perfectly match, as there are several sources of distortions from capacity shadow prices. The capacity shadow prices come from many sources in both models: extra constraints such as (c7-c8) which are not part of the analysis leading to (v1), constraints that are in REMIND but not in DIETER (c5-c6), and exogenous wind offshore capacity in DIETER. Some of these capacity shadow prices in both models can be more or less consistent with each other (such as standing capacity constraint in DIETER and brown-field

749   constraints in REMIND), but others are not and can distort two models in different ways, causing some degrees of misalignment

750   in prices. As discussed before, prices can be overdetermined by the energy mix (Sect. 3.2.3). Therefore, some of the capacity

751   shadow prices – even though not aligned between the two models – can nevertheless cancel each other (especially averaged over

752   time), potentially causing the price differences to be moderate. To examine exactly how well the prices at the end of the

753   coupling match, we need to check the cost decomposition of prices. This is discussed later in Sect. 4.3.

754   Also note that Fig. 4b presents a time-averaged price comparison, and on average the difference between the prices in the two

755   models is small at the end of the coupling. However, when one compares the maximal deviation for any single year at the end of

756   the coupling, it can be as high as 10$/MWh, e.g. around 2050 (Fig. 4a). This is much larger than the 3% averaged deviation in

757   Fig. 4b. However, compared to default REMIND prices (which we cannot show due to limited space), we are fairly confident

758   that the oscillation of coupled REMIND results from internal dynamics that are also visible in the default uncoupled version. So

759   a time-averaged treatment is adequate in displaying total price convergence here.

760   **4.2 Quantity convergence**

761   Besides price convergence, the capacity and generation decision variables must also converge within a certain tolerance at the

762   end of the coupling. This is reflected in the generation mix (Fig. 5) and the capacity mix (Fig. 6) at the end of the coupled run.

763   Due to the existence of several sources of mismatch between the two models already mentioned in the last section, which is

764   already manifested in the mismatch in electricity prices of the two models, a certain degree of mismatch in quantities is also to

765   be expected. Nevertheless, the agreement between the two endogenous sets of decision variables is satisfactory. For this coupled

766   run, the differences of the generation share of any single technology between the two models are smaller than 4.4% for each

767   year until 2100. Figure (5b) highlights some subtle model differences in generation. For example, after 2040, REMIND favors

768   solar and coal, whereas DIETER tends to have more combined cycle gas turbines (CCGT) and wind onshore. Due to the low

769   capacity factor of OCGT and solar compared to the capacity factors of the other generators, the capacity mix differences

770   between models are amplified for these two technologies (Fig. 6). But overall, the generation mixes and the capacity portfolios

771   at the end of coupled run are generally similar.

772
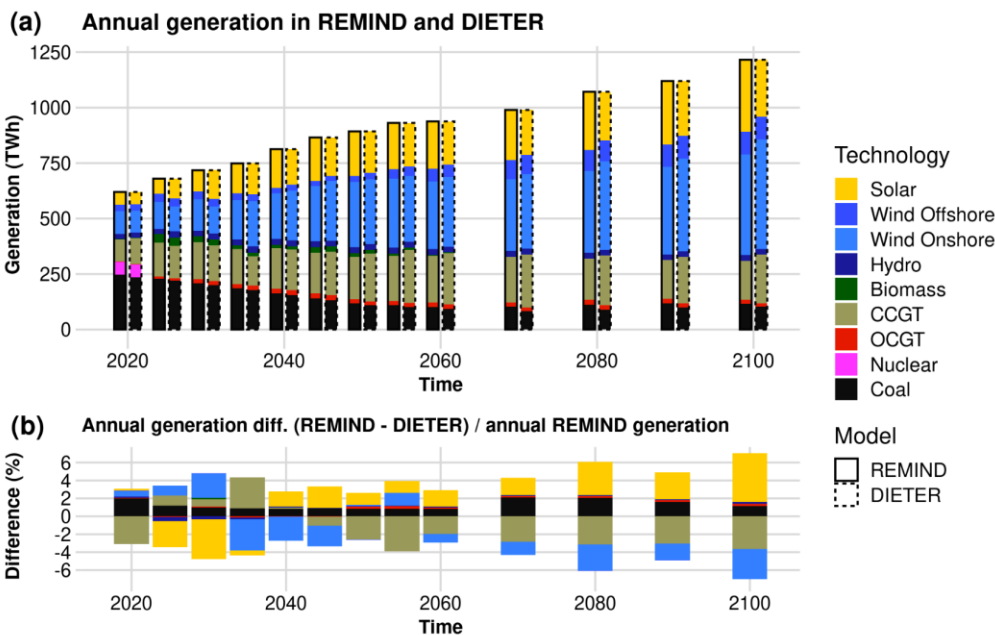
Figure 5: Annual electricity generation convergence at the final iteration of a coupled run for Germany under the "proof-of-concept" baseline scenario. (a) Side-by-side comparison of the two generation portfolios at the end of the coupled run. (b) The difference between the generation mix in the two models as a share of total REMIND generation.
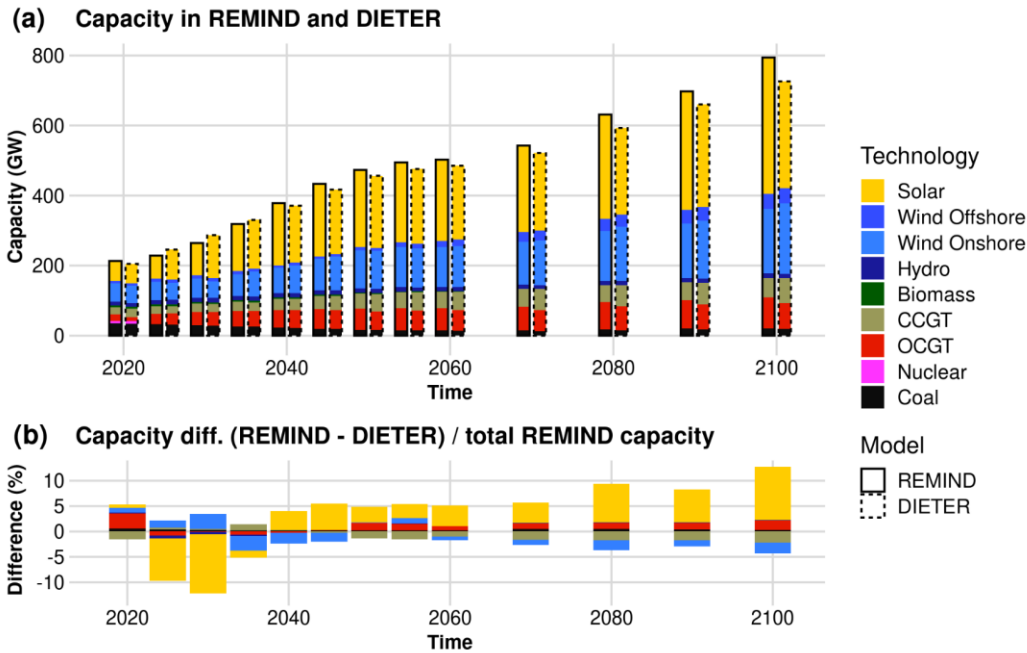
Figure 6: Capacity convergence at the final iteration of a coupled run for Germany under the "proof-of-concept" baseline scenario. (a) Side-by-side comparison of the two models' capacity mix at the end of the coupled run. (b) The capacity difference between the two models as a share of total REMIND capacity.

For periods that are policy relevant in the short- to medium-term (i.e. before 2070), the convergence for quantities is generally slightly worse in the near-term, i.e. in the 2020s and 2030s, likely due to the capacity bounds mismatch in the near-term (such as the capacity bounds (c5-c6) in REMIND not being completely replicated by standing capacity constraint (c8) in DIETER). If DIETER does not contain identical bounds as REMIND, then its endogenous decision will have more of a green-field rationale than REMIND does, the latter of which is more constrained in the near-term. In case an improvement of near-term convergence is desired, these bounds could be implemented more carefully, and more technology-specific. Due to the limited scope, we only apply a generic standing capacity constraint (c8) in DIETER to represent the basket of various constraints. The convergence of quantities is also not perfect in the green-field periods, such as after 2040, where both models are less constrained by near-term dynamics. The reason for this is likely due to the fact that in DIETER, hydroelectric generation is not economically competitive against other cheaper forms of generation such as solar and wind. But in REMIND it is economically competitive, likely due to the long life-time of the plants. Semi-exogenous wind offshore capacitates in both models could also play a role. This is discussed in more detail in Section 6.1.

4.3 Zero-profit rules for the coupled model

As our analytical discussion showed before in Sect. 3.2.3, model equilibria in the form of ZPRs are useful in validating convergence in a more detailed way by decomposing prices into cost components as well as any perturbation from capacity shadow prices. In this section, we first compare the system LCOE, price and capacity shadow prices of the two models for ZPRs on the system level, then we show the technology-specific ZPRs. Using this validating step, we can visually ascertain that the

798 cost components and prices/market values in the two models are remarkably similar on the system level as well as on the

799 technological level, demonstrating that the underlying principle behind the coupled convergence holds to a good degree.

800 **4.3.1 System-level zero-profit rule**

801 At the convergence of the soft-coupled model, we expect ZPRs to be satisfied for the two systems individually (Eq. (11) for

802 REMIND and Eq. (13) for DIETER), i.e. each price times series also matches the LCOE time series to a good degree, barring

803 distortions from the capacity shadow prices. This is to say, under full convergence, the time series of system LCOE, and the sum

804 of the time series of the electricity prices and time series for capacity shadow prices for both models should overlap one another

805 within numerical tolerance. The costs and prices at the last iteration of the coupled run are summarized in Fig. 7. The electricity

806 prices derived from the shadow prices of the balance equations are shown in dark grey: (a), REMIND electricity price λ_y, (b)

807 DIETER annual average electricity price $\underline{J}_y = \frac{\sum_h \underline{\lambda}_{y,h} \underline{d}_{y,h}}{\sum_h \underline{d}_{y,h}}$. Adding all the sources of capacity shadow prices, we obtain the blue

808 lines: (a) REMIND capacity constraints (c5-c7), (b) DIETER capacity constraint (c8). All capacity shadow prices have been

809 converted to per energy unit via capacity factors. (Note: Fig. 4 shows the difference between the black lines, without considering

810 the capacity shadow prices. See Sect. 3.2.3.)

811 From Fig. 7, we can conclude that the ZPR for DIETER is satisfied to very good accuracy for every year (the blue line – the

812 sum of electricity price and capacity shadow price has exactly the same value as the sum of LCOE bars). For REMIND, the ZPR

813 is satisfied year-on-year to a lesser degree, but on average to a good degree given the interannual fluctuations. The prices in

814 coupled REMIND become very erratic for the early years (2020-2025), likely due to the interaction between the historical or

815 near-term bounds in REMIND and the exchanged information from DIETER for those years. The LCOEs component structures

816 match well across the models for most years, which serves as additional visual support on price convergence shown in Fig. 4,

817 i.e. the cost structures behind the prices are harmonized as well at the end of coupling. The origins of the differences between

818 LCOEs and prices, as well as the degree with which capacity shadow prices account for them, can be found when one examines

819 the LCOE and market values of specific technologies, which are analyzed next.

820

821
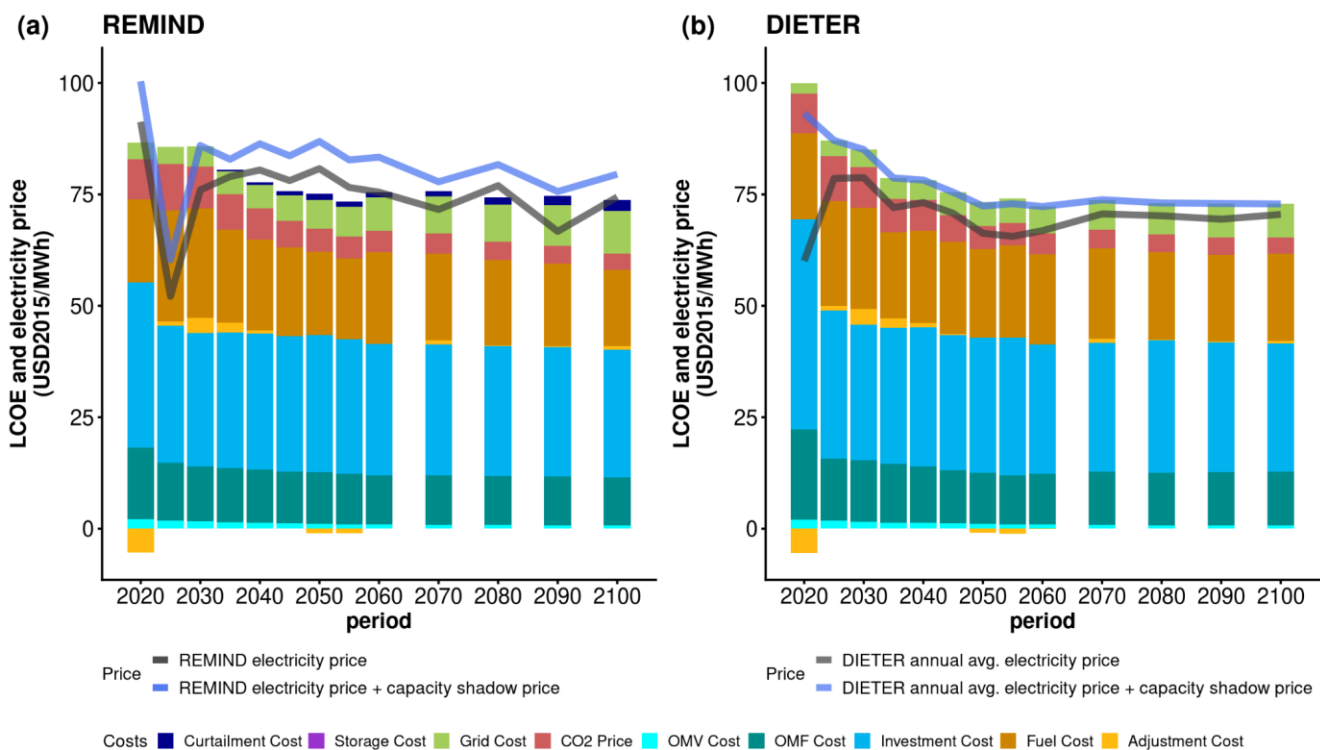
Figure 7: Cost components of the system LCOEs (bars), electricity prices (grey lines) and the sum of electricity prices and capacity shadow prices for (a) REMIND and (b) DIETER under "proof-of-concept" baseline scenario. Visually the ZPRs for both models are satisfied within numerical tolerance. The intertemporal structure of the LCOE breakdown is very similar for most of the coupled periods. For DIETER, a small remaining difference exists between the price (grey line) and the LCOE (bars), which can be entirely explained by the capacity shadow price due to the standing capacity constraint. The REMIND price time series is a rolling average of 3 time periods. The large negative adjustment costs in 2020 are due to coal and nuclear phase-out.

4.3.2 Technology-specific zero-profit rule

After validating ZPRs on the system level, we further dive into each technology and check the ZPRs for each technology in both models at the last iteration of the coupled run (Fig. 8).

832
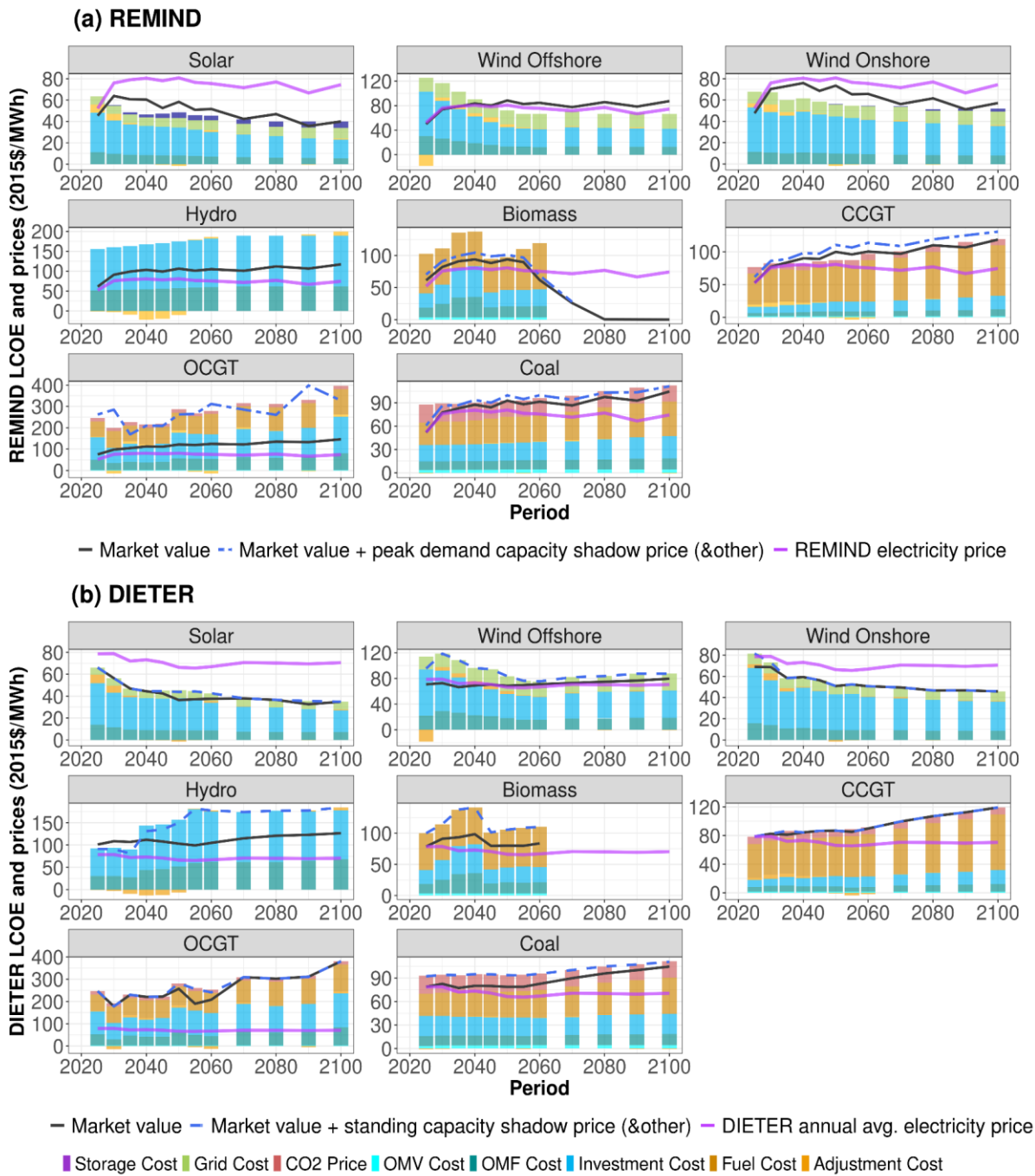
833 **Figure 8: Technology-specific costs and market values for (a) REMIND and (b) DIETER under "proof-of-concept"**

834 **scenario. Cost components of the technology LCOE are plotted in stacked bars. Market values are shown in solid black**

835 **lines. The sum of market values and all sources of capacity shadow prices are shown in dashed lines: for DIETER (two-**

836 **dash blue lines), they contain mostly the standing capacity shadow price, and to a small extent the capacity shadow**

837 **prices of the resource constraint; for REMIND (dashed blue lines), they contain mostly the peak demand capacity**

838 **shadow price, and small capacity shadow prices due to brown-field and resource constraints. Electricity prices are**

839 **shown in purple solid lines as references. Due to large positive shadow prices in 2020 due to fixings to the historical**

840 **capacities, only periods beyond 2020 are shown. REMIND market values and capacity shadow prices are a rolling**

841 **average of 3 time periods.**

842

843   In Fig. 8(b), DIETER LCOE and market values for the eight types of generators are shown. As expected from the ZPR, the

844   LCOE always matches the sum of the market value and capacity shadow prices for each technology, and for each year (Eq.

845   (12)). The difference between the dashed and solid lines are largely the generation capacity shadow prices. It is worth noting

846   that at the end of convergence, the sizes of the shadow prices are in general small for the main generator types, e.g. solar, wind

847   onshore, CCGT and OCGT. This indicates the fact that for these technologies for most periods, the optimal DIETER generation

848   mix is close to that of a green-field model. That is, DIETER hardly faces any exogenous constraints (except resource constraints

849   that are aligned with those of REMIND) and can make fully endogenous investment and dispatch decisions based on cost

850   information alone. On the whole, DIETER at the coupled convergence experiences only a small amount of distortion from the

851   brown-field model REMIND, especially concerning the "model suboptimal" real-world standing capacities from biomass, hydro

852   and coal.

853   In Fig. 8(a), we show the REMIND LCOE and market values for the same generation technologies. Due to the intertemporal

854   nature of REMIND, the sum of market value and capacity shadow price for each technology, and for each year matches the

855   LCOE generally slightly less well than DIETER. This means for REMIND the ZPR (Eq. (10)) for each generator type is also

856   satisfied to a good degree for main generator types, e.g. solar, wind onshore, coal, CCGT and OCGT. The mismatch in biomass

857   and hydro might come from the shadow price from historical capacities.

858   Since the differences between market values and costs are accounted for by capacity shadow price to a large degree, it is worth

859   interpreting physically the sources of these "hidden" costs/revenues. For REMIND, the capacity shadow prices consist of those

860   in (c2), (c5), (c6), as well as the "peak residual demand constraint" from DIETER (c7). Constraint (c7) is created to circumvent

861   high markups especially from peaker gas plants (Appendix H.1). Because peaker gas plants generate power mostly only at hours

862   with high prices (especially scarcity hour price), and therefore have very high market values compared to annual average

863   electricity price. The high market values of OCGT – usually more than 5 times the average annual electricity prices – acts as a

864   large incentive in the next iteration REMIND, and leads to overinvestment in capacities. Over iterations, this causes oscillations

865   in the quantities and prices in the coupled model and prevents model convergence. To circumvent the issue of high markup, we

866   implement (c7) as an equivalent peak residual demand constraint. As can be shown mathematically (Appendix H), (c7)

867   generates essentially the scarcity hour price, and it is very easy to validate this for OCGT in Fig. 8(a). The capacity shadow

868   price derived from this peak residual demand constraint, when translated to energy terms and added to the market value,

869   correctly recovers the LCOE for OCGT, recovering the original ZPR (Appendix H.1.2). This indicates that under multiscale

870   model coupling, an extra constraint is an effective way to circumvent potential issues of numerical divergence due to the large

871   impact from short-term dynamics, such as the large market value of peaker gas plants.

872   For DIETER, the two sources of capacity shadow price are the total renewable potential limit (constraint (c2) in Sect. 3.1), and

873   the standing capacity constraint from REMIND (constraint (c8) in Sect. 3.2.3). For the first type, the resulting capacity shadow

874   price is a hidden "positive cost" from the perspective of the power user. Since endogenously DIETER would like to invest more,

875   but is limited by the natural resources available. An example for this first type is hydroelectric power between 2020 and 2035,

876   due to the limited resource (run-of-the-river) in Germany. It is worth noting that from the generator's perspective, the capacity

877   shadow price from resource constraint can be interpreted as an extra resource rent. The second type of capacity constraint

878   originates from the standing capacity, the latter is received by DIETER from REMIND as a lower bound. This constraint usually

879   results in a hidden "negative cost" from the perspective of a power user, i.e. a part of the cost (LCOE) does not get passed on to

880   the electricity price, so the users get part of the capacity "for free". (This can also be interpreted as subsidies for generators to

881   sustain these unprofitable capacities.) This is because based on greenfield cost optimization, DIETER endogenously would

882   invest less in certain technologies. However, since the standing capacities account for the existing generation assets in the real

883 world, which can be model suboptimal, the overall costs are above a greenfield equilibrium and above the prices the user pays.

884 We find examples of such a capacity shadow price manifested in biomass, coal and hydroelectric, all of which are part of the

885 existing German power capacity mix, but evidently not all of them for any given period are "green-field optimal" based on pure

886 cost consideration in DIETER. Interestingly, after 2035, the sign of the capacity shadow price for hydroelectric generators

887 reverses. This is likely due to the continuous decline of the VRE costs after 2035 tips the power sector into a regime where

888 hydroelectric becomes less economically competitive in DIETER, at least compared to REMIND. As a result, the standing

889 constraint from REMIND starts to be binding on the capacity from below, relieving the resource constraint binding from above.

890 For DIETER, the capacity shadow price from standing capacities also indicates the degree of disagreement between DIETER

891 and REMIND. For most future years, REMIND standing capacity constraints are not binding in DIETER for solar, wind

892 onshore, CCGT and OCGT, indicating good agreement between the models. The small amount of shadow prices near 2060 for

893 OCGT and solar in Fig. 8(b) are likely due to the time step size change in REMIND which causes a small jump in the interest

894 rates near these years.

895 Lastly, in Fig. 4 before we observe a slightly higher average electricity price in REMIND than in DIETER, especially in the

896 intermediate years. This could be due to fixed offshore wind capacities, which are never economical to be invested

897 endogenously in the parameterization used here. This generates a high capacity shadow price until around 2045-2060, visible in

898 both DIETER and REMIND.

5 Scenario results under baseline and policy scenarios

900 In this section, we present baseline and policy scenario results for Germany, using a more realistic configuration of the coupled

901 model with electricity storage and flexible electrolyzer demand for green hydrogen production which is then used outside the

902 power sector (e.g. in industry or heavy trucks). We show results for a baseline scenario and a net-zero by 2045 climate policy

903 scenario. Note that due to REMIND's global scope, under the net-zero scenario we also assume a larger climate policy

904 background of 1.5C goal for end-of-century temperature rise globally (corresponding to a 500Gt of CO_2 emission budget until

905 2100), and a larger regional goal of EU-wide net-zero emission. Both scenarios consider nuclear phaseout law in Germany.

906 In Sect. 5.1, we present long-term power sector development. In Sect. 5.2, we present short-term power sector hourly dispatch

907 and price results. In the following, we broadly describe how these additional features are implemented:

908 1. Storage: We use a simple storage implementation where DIETER makes endogenous investment into two kinds of storage

909 technologies:

910 1) lithium-ion utility-scale batteries;

911 2) onsite green hydrogen production via flexible electrolyzers, storage and combustion for power production.

912 The principle of the coupling remains mostly unchanged. REMIND receives the price markups from generation technologies

913 as in the case before without storage. However, for simplicity, the capacities of storage are not part of endogenous

914 investment in REMIND. In REMIND, the energy loss due to storage conversion efficiency is taken as a fraction of total

915 demand from DIETER as a parameter, and stabilized with a prefactor for each type of renewable generation (similar to the

916 case of curtailment rate in Sect. 3.3.2, 4). Our battery cost development is given in Supplemental Material S1-2.

917 The reason we only allow DIETER to endogenously invest in storage technologies, is that the additional intertemporal

918 optimization offered in REMIND is relatively less important than that for the investment of generation technologies. In

919 REMIND, intertemporality mainly accounts for two aspects in the real-world: 1) implementing adjustment cost and 2)

920 tracking of standing capacity. The adjustment costs simulate system inertia to rapid capacity addition or removal. In the case

921 of battery and other storage technologies, the ramp up of deployment faces relatively fewer inertia compared to wind and

922   solar. Compared to generation technologies such as wind and solar, the storage technologies tend to have lower total

923   capacities, meaning their ramp up rate is usually lower. Also, their deployment is mostly constrained by their higher cost.

924   For utility storage technologies, they are mostly not yet deployed at scale, which means there is very little existing capacity,

925   the investment for storage in REMIND is mostly green-field, rendering it unnecessary to give DIETER a standing capacity

926   of them.

927 2. Flexible demand: As a simple representation of flexible demand, we choose to implement a common Power-to-Gas (PtG)

928   technology, namely the so-called "green hydrogen" electrolysis. We split the total power demand required to produce green

929   hydrogen from REMIND from the total power demand $d_y(i-1)$ (Sect. 3.3.1, 3) – both demands are endogenous in

930   REMIND. We implement the electrolysis demand as completely flexible in DIETER, i.e. there is no ramping cost or

931   constraint. Thereby flexibilizing part of endogenous total power demand $d_y(i-1)$ in REMIND. As a result, the cost

932   minimization in DIETER automatically allocates the flexible demand to hours where electricity costs are low due to the

933   existence of low-cost VRE. The economic value of flexible demand can be quantified by the capture price. The annual

934   capture price of demand-side technology s_d is the annual average price of the hours when the flexible demand consumes

935   electricity, weighted by the hourly flexible power demand by electrolyzers: $\underline{CP}_{s_d} = \frac{\sum_{h,s_d} \underline{d}_{h,s_d} \underline{\lambda}_h}{\sum_{h,s_d} \underline{d}_{h,s_d}}$.

936 This concept is equivalent to the market value for a variable or dispatchable generator, but here for a flexible or inflexible

937 demand source. Similar to before, we implement a stabilization measure using a prefactor (Appendix H.2, 5).

938 **5.1. Long-term development**

939 This section presents scenario results of the coupled model with a long-term view on capacity and generation, using either the

940 proof-of-concept scenario or more realistic configurations.

941 **5.1.1 Baseline scenario**

942
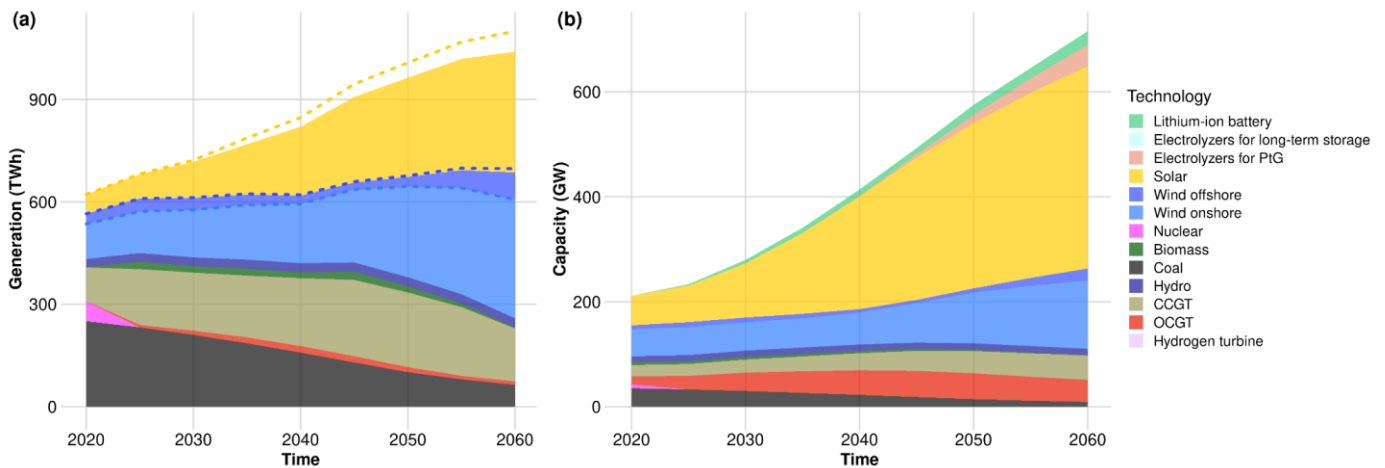
943 **Figure 9: DIETER-REMIND converged results of the long-term (a) generation and (b) capacity expansion for**

944 **Germany's power sector in the baseline scenario, assuming a constant 37$/tCO2 CO2 price. Dashed lines represent**

945 **generation before storage loss and curtailment. Storage generation is not visualized in (a).**

946

947 In Fig. 9(a), under baseline scenario, and with available storage and flexible demand, we observe a more than 35% increase of

948 the total power demand from 2020 to 2045, and more than 65% by 2080. This is due to an increase in end-use electrification.

949 The increased electrification comes from a moderate growth in electricity use in the building sector and a more significant

growth in EV fleet. In the building sector, the final energy share of electricity is projected to increase from 28% in 2020 to 39% in 2045. The final energy share of electricity in the transport sector is 22% by 2045, up from 2% in 2020. Note that even under no additional climate policies, based on only the increase in EVs shares in new-cars sales in many world markets today, we expect higher power usage from EVs in the future. Within the energy mix, we see a slow decline in coal generation over time, which is replaced by CCGT generation and a significant increase of VRE. VRE share reaches above 50% by 2045, but slightly less than half of the energy mix still contains coal and gas power. In terms of capacity expansion (Fig. 9(b)), due to both lower generation cost and higher power demand, solar capacity expands by almost 5 times from today until 2045. However, the moderate VRE shares mean that the requirement on battery capacity is not high, namely only 12GW of batteries by 2045. Due to the low CO2 price, long-term electricity storage through hydrogen does not appear to be economically competitive and is not invested under the baseline.

By comparing the above baseline scenario (with storage and flexible demand) (Fig. 9) with the "proof-of-concept" baseline scenario (without storage or flexible demand) before (Fig. 5 and 6), it is clear that while battery storage and partial demand flexibility play a role after 2040 in increasing the VRE share in Fig. 9, in the near term, the scenarios with and without available storage and demand flexibility look very similar under no additional climate policies. However, due to technological learning effect, even absent additional CO2 price policy, the energy mix here has a relatively high VRE share (>60%) after 2050 compared to the basic case without storage and demand-side flexibilization. However, due to the low CO2 price there is still a significant share of dispatchable technologies such as CCGT and OCGT, which is more economical than the implementation of long-term power storage via electrolysis and hydrogen turbines.

5.1.2 Net-zero policy scenario
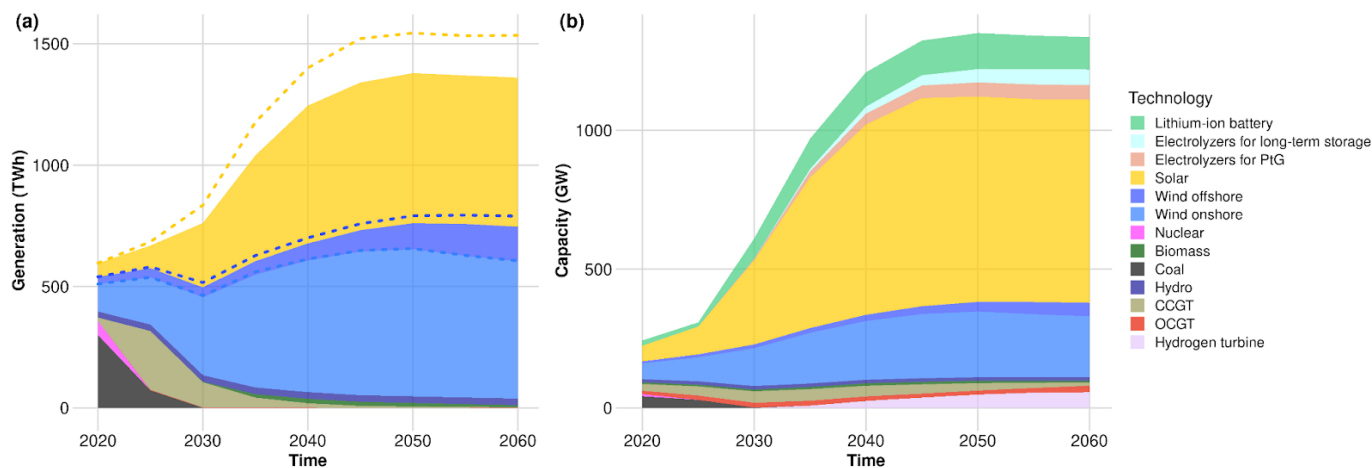
Figure 10: DIETER-REMIND results of the long-term generation and capacity expansion for Germany's power sector in the "net-zero 2045" scenario. CO2 price is endogenously determined based on the climate goal. It is 115$/tCO2 for 2030, 292$/tCO2 for 2035, 464$/tCO2 for 2040, and 636$/tCO2 for 2045. Dashed lines represent pre-curtailment generation. Storage generation is not visualized in (a).

In Fig. 10, under stringent climate policy (economic-wide carbon neutrality in 2045), with available storage and partially flexibilized demand (for hydrogen production used in other sectors), the total power demand more than doubles, and the power mix is dramatically transformed. Compared to both the baseline case without storage and demand-side flexibilization (Fig. 5 and 6) and the baseline scenario with storage and flexible demand (Fig. 9), a very high VRE share in the generation mix is reached

already by 2040 (>94%). This is mostly due to an earlier investment in VRE to drive down the cost, combined with the increased deployment of both short- and long-term storage and flexibilization of part of the demand. Capacities for storage increase significantly: lithium-ion batteries from 18GW in 2020 to 125GW in 2045, and 37 GW of hydrogen electrolysis and hydrogen turbine capacity (with ~40TWh of H2 storage capacity). Despite high storage capacities, due to high VRE share, curtailment and storage loss still increases quite significantly with time, especially for solar PV. But note that in a coupled run where interregional transmission expansion is possible connecting Germany and the rest of Europe, this loss can be reduced (see Sec. 6.3). In terms of capacity expansion (Fig. 10(b)), gas power plants are mostly replaced, as hydrogen turbines fill the role of peaking dispatchable plants that guarantee supply for peak demand hours. The CCGT gas turbines are equipped with CCS.

Under the stringent climate policy scenario, dramatic changes in the end-use sectors will be underway in the form of direct electrification and substitution of fossil gas with hydrogen. In the building sector, the final energy share of electricity is projected to increase from 28% in 2020 to 66% in 2045. In transport, the final energy share of electricity is 56% by 2045. In the industry sector, the share of electricity increases from 25% to 63%. By 2045 there is also a notable increase in the use of green hydrogen produced from 45GW flexible electrolyzers (at about 42% average annual capacity factor), amounting to 0.5EJ (3.5 million tons) per year in the final energy, which is primarily used in industry. For a comparison with other published Germany net-zero scenarios results, see Supplemental material S4.

5.2. Short-term dispatch

In this section, results of hourly resolution are shown and discussed for a selected model year. We use established methods such as residual load duration curves (RLDCs) to visualize the hourly dispatch result, as well as show the hourly generation and dispatch time series for some typical days in summer and winter.

5.2.1 Residual load duration curve model comparison

RLDCs can be used to visualize the dispatch of energy system models. Each subsequent curve is calculated by subtracting the generation of a technology from the hourly residual demand curve, and then sorting the remaining demand in descending order. On the left-side of RLDC graphs one can easily check the amount of residual demand not met by variable wind and solar production. The top-most line in RLDC graph is the load duration curve for inflexible demand (excluding the demand from flexible electrolysis for hydrogen production used in other sectors).

In a baseline configuration without flexibilized demand or storage, despite lacking the explicit hourly dispatch, via bidirectional soft-linkage, REMIND could achieve a final dispatch result that replicates DIETER to a satisfactory degree (Fig. 11). This is a combined effect of a convergence of capacities (Sect. 4.2) and full-load hours at the end of the coupled run. In the peak residual demand hour (the leftmost point in the RLDC), the DIETER-coupled REMIND accounts for the requirement of dispatchable capacities via the constraint (c7), and the composition of the mix is replicated from DIETER and correctly guarantees that the peak hourly demand is met.
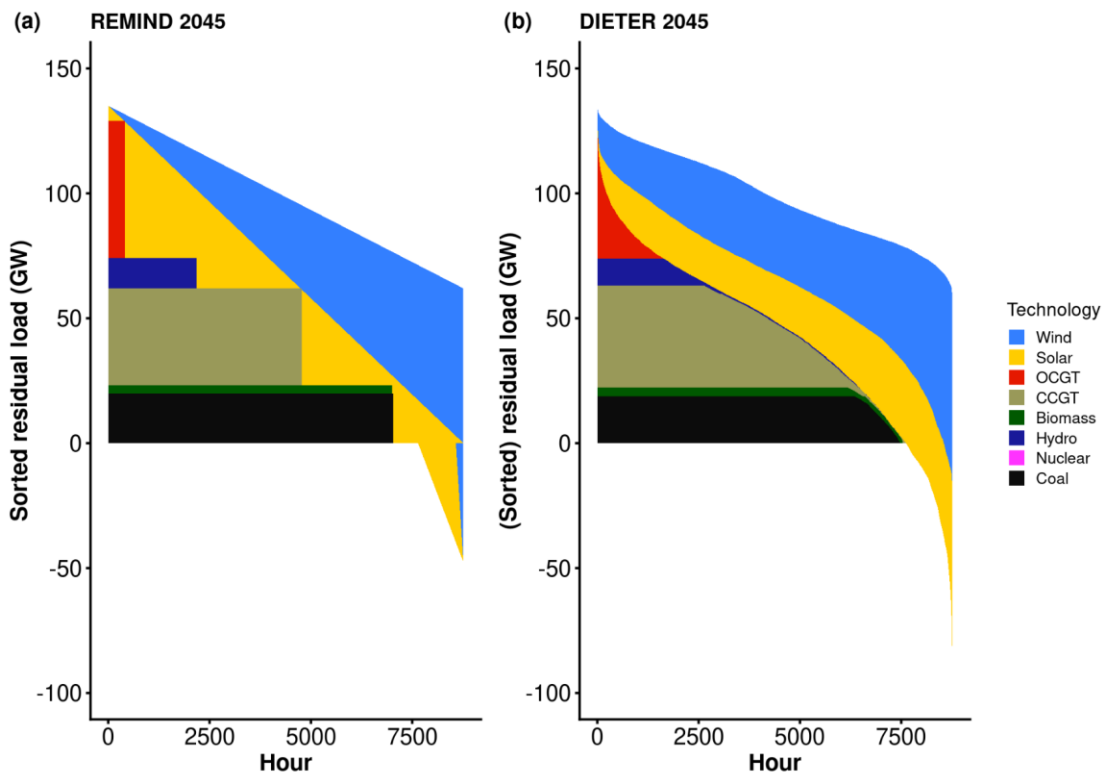
Figure 11: Side-by-side RLDC comparison between (a) REMIND and (b) DIETER for the simple configuration under the baseline scenario without storage or flexible demand. The DIETER RLDC (panel (b)) is constructed by subtracting hourly generation from hourly load and sorting, with dispatchable generation technologies plotted in order of their annual average capacity factors. VREs are arranged such that the generation with higher curtailment rate (i.e., solar, in this case) is on the inside of the graph. To construct the REMIND RLDC (panel (a)), the dispatchable generations are sorted by their capacity factors and stacked from the bottom. The rectangles depicting dispatchable generation are made up by the width equal to the full-load-hour and the height equal to the capacity. The top-most lines on either side are load-duration curves (sorted hourly demand, which is entirely inflexible under this setup). For the purpose of better visualizations, solar and wind RLDCs are tilted at an angle for REMIND and plotted in the same order as the DIETER RLDC. For simplicity, in REMIND wind and solar RLDC share the same top pivot point in peak residual demand hour.

In net-zero policy with storage and flexible electrolysis demand, comparing dispatch results under both scenarios (Fig. 11 and 12) for model year 2045, it can be observed that under a stringent emission constraint, the system allocates a significant amount of short-term storage to replace the dispatchable generation such as coal and CCGT. Long-term storage such as hydrogen electrolysis combined with hydrogen turbines further reduce the capacity factor of remaining OCGT and CCGT. Besides storage, there is also a significant amount of deployment of flexible electrolysis demand for producing hydrogen (PtG), which is not used in the power sector, but in industry or heavy-duty transport. The use of PtG technologies leverages cheap variable wind and solar energy to achieve the goal of sector coupling. By way of storage and PtG, a significant share of the curtailment can be utilized (more than 70%), either by shifting the supply to times of low VRE production via storage, or by producing hydrogen using surpluses which can be used in other sectors.
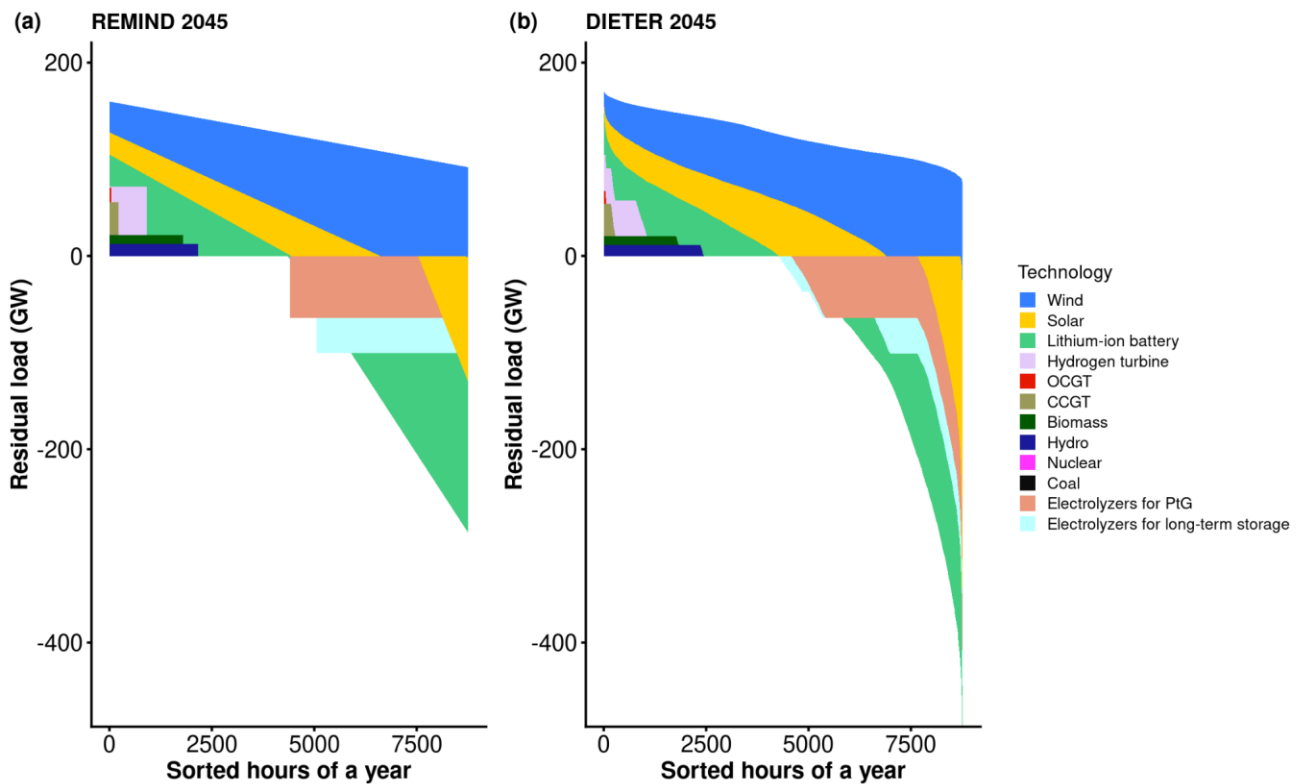
Figure 12: Side-by-side comparison between (a) REMIND and (b) DIETER RLDCs for net-zero by 2045 scenario with storage and flexibilized demand for Germany. The storage loading and discharging in DIETER RLDC (panel (b)) is constructed by subtracting hourly loading or discharging from hourly inflexible load and sorting. The REMIND RLDC (panel (a)) is constructed similar to Fig. 11. The top-most lines on either side are load-duration curves for inflexible demand. For better visual comparison, in REMIND solar RLDC starts at 80% of the peak residual demand.

5.2.2 Hourly dispatch and power consumptions for typical days in summer and winter

To more directly inspect the results of the hourly dispatch under various scenarios, we visualize the hourly generation and demand for typical days. Due to the climate in Germany, solar potential is particularly low during winter months. Therefore it is important to observe the periods in both summer and winter.

From the optimal hourly dispatch results of typical days from the coupled model, we observe that compared to baseline (Fig. 13a-b), in 2045 for a net-zero year (Fig. 13c-d), there is a significant amount of surplus solar generation in the summer during the day, and some amount of surplus wind generation in the winter during nights and days. Under a net-zero scenario, the generation from fossil fuel plants in the baseline is replaced by battery dispatch (especially in summer) and hydrogen turbines (especially in winter), and the peaker plants, which under baseline are turned on in the summer evening, are partially replaced by solar over-capacity and batteries. A significant share of renewable surplus energy is used for the production of green hydrogen – hydrogen made from zero-carbon electricity. Due to the complete flexibility of electrolyzers, the capture price of hydrogen production is only around ⅓ of the average price of electricity (Supplemental Material S2 and Fig. S1 in Supplemental Material).

In winter, hydrogen turbines serve as a baseload for the few days when wind generation is insufficient to meet the demand. To ensure supply during longer winter periods of "renewable droughts" with little wind and solar output, e.g., over a 2-3-day period (hour 540-600 in Fig. 13d), long-term duration storage with hydrogen electrolysis and hydrogen turbines, as well as some dispatchable generation (such as CCGT with CCS and integrated biomass gasification combined cycle) play a major role.

(a) Summer (baseline w/o storage or demand flexibility)

(b) Winter (baseline w/o storage or demand flexibility)

(c) Summer (net-zero w/ storage and demand flexibility)

(d) Winter (net-zero w/ storage and demand flexibility)

Wind onshore curtailment	Solar curtailment	Wind offshore curtailment
Solar	Wind onshore	Wind offshore
Lithium-ion battery	Electrolyzers for long-term storage	Wind
OCGT	Biomass	CCGT
Coal	Hydro	Nuclear
Hydrogen turbine	Electrolyzers for PtG	Electricity demand

1056

Figure 13: Comparison of hourly generation (positive) and consumption/storage loading (negative) for a few consecutive typical days in two seasons in Germany in 2045. (a) Summer, under "proof-of-concept" baseline scenario, no storage or flexible demand; (b) Winter, under "proof-of-concept" baseline scenario, no storage or flexible demand; (c) Summer,

net-zero scenario, with storage and flexible demand; (d) Winter, net-zero scenario, with storage and flexible demand.
Due to the fact that modern electrolyzers are very flexible, no ramping costs are applied to them in the models, and
therefore some switching behavior between PtG electrolyzers turning on and off can be seen, but it is a minor artifact.

6 Discussion

In this section, we discuss the reasons for remaining differences between the coupled models, as well as the assumptions and
limitations of the soft-coupling.

6.1 Remaining discrepancies

In all our test runs, at the end of the coupling, it is always the case that the two models cannot be perfectly harmonized, and
there is a slight residual difference in the convergence results (Section 4). The reason is two-fold.

The first reason is "legacy mismatch", i.e. a mismatch in brown-field standing capacity constraints in the two models. The
coupling method we develop here is mostly based on price information for achieving convergence. Therefore, capacity
constraints that are present in the standalone long-term model but not in the standalone hourly dispatch model need to be
transferred. These standing capacities are hard to evaluate purely based on economic terms, as they are ultimately a result of
real-world actions and policies, which might not align with the simplified economic incentives in techno-economic energy
models. Therefore, the only way this information can be transferred from the "brown-field" model to the "green-field" model is
by implementing a lower capacity bound in the latter. However, this bound nevertheless might not capture all the shadow prices
caused by the standing capacities in REMIND. This is ultimately due to the specific generic form of the constraint we
implemented, i.e. we pass on the pre-investment capacities as a lower bound regardless of technology types. In general, hidden
"legacy revenues", which are manifested as the shadow prices of economically less competitive generators in DIETER, such as
biomass, coal, hydroelectric (solid line lower than bars in Fig. 8), provide incentives for brown-field models to deploy them over
long-term, but does not provide enough economic case for the green-field model. This results in an observed phenomenon in the
coupled run, that if these "legacy" capacities and their impact on the costs have not been fully transferred to the green-field
model, the prices of the green-field model tend to be lower than the coupled brown-field models, causing distortion to the
convergence of quantities. The effect of legacy mismatch and illustrative test run results are discussed in more detail in
Supplemental Material S3.

The second reason for the discrepancies at the end of the coupling is that there are actual mismatches in the Lagrangian
harmonization itself, which can originate from multiple sources. It could due to intertemporal constraints and dynamics (such as
adjustment costs and brown-field constraints) not linearly reducible to single-year dynamics, resulting in misalignment between
multi-period REMIND and single-year DIETER. It could be also due to slight numerical inaccuracies of the interest rate
estimate, which is not explicit in REMIND, but are derived from endogenous and intertemporal consumption. Lastly, there
could be a mismatch due to a linear fitting of REMIND endogenous time series of fuel costs (biomass, oil, coal, uranium) before
passing this information to DIETER which might a small amount of mismatch for fuel costs between REMIND and DIETER.

6.2 Limitation of the coupling methodology

There are limitations to our proposed methodology, both in terms of converging two multiscale power sector models, as well as
other potential applications of model convergence. Firstly, in terms of the problem presented here – a multiscale power sector
model coupling, the method derived here is only necessary for a full convergence, but may not be sufficient, i.e. a full
convergence is not guaranteed. A number of additional factors could prevent a full convergence. One is the "legacy mismatch"

1097   and misalignment in Lagrangian mappings mentioned above in Sect. 6.1. Another factor is the role prefactors play (Sect. 3.3.2,

1098   Appendix H.2). The prefactors help stabilize the coupling by turning exogenous values obtained from last-iteration DIETER to

1099   endogenous values in REMIND, such that they can be adjusted to be in line with the optimal mix of current iteration. However,

1100   they usually contain some small positive or negative parameters that are determined heuristically (e.g. $\underline{b}_{y,s}$ in Eq. (H13)). These

1101   heuristic parameters usually come from rough estimates based on relations between variables in the system and generation

1102   shares, e.g. how much market value of solar generation will decrease when solar generation share increases by a certain

1103   percentage. In practice, while the prefactors help stabilize the run and improve convergence speed, choosing the wrong prefactor

1104   parameters can lead to divergence or instability. Second, another limitation when it comes to modeling power market multiscale

1105   coupling, is the number of products in the market. In the formulation here, both models describe the general equilibrium of a

1106   competitive market with one type of homogenous goods, i.e. electricity. However, if we introduce heat as a by-product, such as

1107   from a combined heat and power plant, then there are two types of goods: heat and electricity. The feasibility of coupling

1108   models with more than one type of goods/market is not yet explored. Thirdly, there are multiple iterative processes that are

1109   internal to REMIND, which happen concurrent with the DIETER-REMIND coupled convergence. Among these processes,

1110   DIETER and the REMIND "Nash" algorithms (for inter-regional trading) both run between the internal REMIND "Nash"

1111   iterations, which means they are external to the REMIND single-region optimization problems and therefore are soft-linked.

1112   Nevertheless, in our runs, we observe the power sector convergence to be rather swift and smooth, and happen in parallel to

1113   other iterative processes, such as the "Nash" algorithm and the CO2 price path algorithm (for climate policy runs). However, a

1114   systematic monitoring of the multiple internal convergence processes in REMIND during the REMIND-DIETER convergence

1115   processes under other model setups and configurations is still to be more thoroughly researched.

1116   More generally, the approach developed here – the Lagrangian mapping method for converging two multiscale optimization

1117   problems – could be useful for a general modeling of market equilibrium of multiple time resolutions. In this study, the

1118   resolution in the coupled problems is specifically only meant for temporal resolution. However, mathematically speaking,

1119   coupling models of different spatial resolutions (or both temporal and spatial resolutions) should be very similar. At least in

1120   theory, the soft-coupling approach developed here should be applicable to increasing the resolution in any arbitrary

1121   independent/orthogonal dimension of the problem of finding equilibrium market dynamics. In theory, it is also possible to build

1122   a multi-layer coupled problem architecture, where at each level the low-resolution variables can be disaggregated into finer

1123   resolution along some dimensions. However, further research is needed to explore the feasibility and convergence performance

1124   of such schemes.

1125   **6.3 Limitation of coupled results**

1126   Since the nature of this study is a proof-of-concept, the scenario results presented should be primarily interpreted as such.

1127   Nevertheless, it may be useful to enumerate a list of limitation for a more accurate interpretation of the results:

1128   1)   The power-sector is only coupled for one single global region, i.e. information exchange only occurs for the variables

1129   of one region – Germany, while all other regions contain the low-resolution version of the power sector of uncoupled

1130   REMIND. The former coupled one-region result is based on a time series of VRE production today in a world of low to

1131   medium VRE share and very limited power grid expansion (in 2019). The latter results of the uncoupled regions

1132   however are parametrized based on results from detailed PSM under a more optimistic assumption of transmission

1133   build-out, which allows VRE pooling from an expanded EU-wide power grid to smooth out regional weather variations

1134   (Pietzcker et al., 2017). Note that in standalone REMIND, while by default there are no annual electricity import and

1135   export imbalances between countries and regions, transmission during the year is implicitly assumed, especially for the

EU region. Comparing the capacity and generation mixes of the coupled and uncoupled runs (Appendix J), we find that in the uncoupled case, there are slightly more solar and wind capacities and generations, and much less gas generation in the long term. EU-wide transmission expansion would pool both supply and demand variability, thus reducing the need for dispatchable capacity for meeting the peak demand.

2) Due to the scope of this study, we implemented a limited set of options on storage and sector coupling technologies in this study, and neglected the additional supply-side details for the German power market (such as the reserve market). Many potentially significant technological options consisting of pumped hydro storage, compressed-air energy storage, vehicle-to-grid, and flexible heat-pumps are not explicitly modeled.

3) Ramping costs for dispatchable generators are not considered, although the effect should be small (Schill et al., 2017).

4) In terms of power transmission and trading inside Germany, we assume a very simple "copperplate" spatial resolution, not explicitly modeling transmission bottlenecks inside the region. Currently, the grid capacity equation is parametrized to be proportional to pre-curtailment variable renewable generation, and the parametrization is rather optimistic based on PSM studies conducted in Pietzcker et al., 2017. As hinted in a recent work by Frysztacki et al., 2022, lower level of spatial detail results in an underestimation of constraints present in a real electric system, leading to an underestimation of system cost.

5) Near-term events: we have not modeled the current gas and energy crisis in Europe, which is likely to imply an overestimation of near-term gas availability in the power sector. Relatedly, we are likely to have overestimated the early retirement of coal power plants, which are capped at maximum 9% per year of current capacity early retirement rate in REMIND if it is uneconomical relative to cheaper sources of generation. We have included the COVID shock to the GDP projection.

6) Only one weather year (2019) is used for the DIETER input data. From the perspective of sufficient power supply under all weather conditions with few blackout events, this could introduce an underestimation of the need for reserve capacity, storage and demand-side flexibility.

7) Climate impact on building demand is not included in current version of REMIND or its energy demand model for building sector "EDGE-B" (Levesque et al., 2018). Climate extremes such as heat waves are not included in either model, and are not considered under different climate scenarios (e.g. baseline, net-zero) in the IAM.

8) "Perfect foresight" is assumed under REMIND's intertemporal optimization over several decades, therefore also assumed under the coupled model. There exist many discussions related to the differences between the "ideal world" depicted in IAM and energy system modeling on the one hand and "imperfect" but realistic real-world decision making and political economy on the other (Ellenbeck and Lilliestam, 2019; Geels et al., 2016; Keppo et al., 2021; Staub-Kaminski et al., 2014; Pahle et al., 2022). Considering perfect foresight models such as REMIND dominate IPCC model results, it is especially important to understand the differences between the approaches with perfect foresight and those without (the so-called "myopic models"). Such work has been carried out in studies such as Fuso Nerini et al., 2017; Sitarz et al., 2023. If myopia is introduced in the model, the climate policy exemplified by carbon prices still follows an increasing expectation for more and more stringent climate policies, but the trajectory can be less smooth, and in the near-term looks more "flat", hence inducing lock-in effects which slows the transition in the near-term. These additional lock-in effects are not modelled in our work here.

9) The resulting power mix is largely due to limited options within the available energy portfolio due to Germany's energy policy and natural resources, e.g. the political decision of nuclear and coal capacity phase-out, as well as limited hydro and offshore wind potential. In future research, we would like to apply the same method to all global regions.

6.4 Potential computational barriers under soft-coupling

Even though via soft-coupling IAM can obtain hourly resolution with only a moderate computational cost increase, it nevertheless increases the complexity of the whole problem, increasing the solver time of the IAM, especially before convergence is reached under the iteration with a PSM. With additional complexity of endogenous climate policies, computational time can be long for scenarios under climate constraint (see Appendix E). This can be potentially overcome by several measures, which can be the topics for future research:

1) Optimize for computational costs in individual models. Individual IAM and PSM are usually developed incrementally, which results over time in less overall computational efficiency. However, because individually the models are not too costly to run, there are less incentive to manage computational cost when they are run as standalone models. However, when coupled, the computational cost may become a barrier. One of the easiest ways to reduce coupled run time is to reduce run times of the individual coupled models. Because the soft-coupling takes many iterations, a small reduction in computational time in either model will multiply to give a large reduction in iteratively soft-coupled runs.

2) Other internal iterations of the IAM (if they exist) can be optimized. For example, in REMIND, most of the iterations (usually 30-50 iterations) in the coupled runs are dedicated to converging inter-regional trade between the 21 regions in the model, because DIETER iteration converges usually quite fast (5-10 iterations). By making the algorithm for the convergence of inter-regional trade faster, we can reduce total coupled iterations, therefore reducing overall computational cost. Less computational time can also be achieved, if DIETER is no longer run together with REMIND after DIETER-REMIND iteration convergence is reached, and when trade adjustment (or other internal adjustments in REMIND) is small enough to not have substantial impact on the power sector results. This is especially the case if PSM gets more complex and its computational time exceeds far more than single-iteration REMIND time (also see Appendix E for a comparison of the contributions to runtime due to REMIND internal iteration and due to PSM).

3) Limiting endogenous investments of capacities of certain technologies only in one model. For example, in the case of electricity transmission, more than one region (e.g. Germany with neighboring European countries) will need to be hard-coupled together in the PSM, which naturally increases computational cost of the PSM. But when the solutions are passed to the IAM, the regions can again be parallelized, as long as IAM does not engage in the endogenous investment of the transmission capacity. Hence the increased cost of computation due to implementing transmission is only limited to PSM. This is also the case if within Germany the spatial resolution is increased.

4) Only include essential features in PSM. Some PSMs are quite detailed and complicated for the purpose of studying specific technologies and the behavior of many agents or users. To couple to IAM, PSM should consider coarse-graining or aggregating some details, while retaining the essence of the dynamics being studied. For example, to implement smart EV charging (e.g. vehicle-to-grid), modelers of PSM should create a version for coupling which aggregates the many time series of charging and discharging of EVs to only one or two time series.

Faster solvers and faster supercomputers will also contribute to improving the computational efficiency of the coupled model.

7 Conclusion and Outlook

In this study, we develop a new method of soft-coupling an IAM with a coarse temporal resolution and a PSM with an hourly temporal resolution. Our coupling method can be shown both mathematically and in practice to produce a convergence of the two systems to a sufficient degree. This method allows the incorporation of the temporal details of variable renewable generation explicitly in large-scope IAM modeling frameworks, and increases the accuracy of power sector dynamics in long

term models. Furthermore, it allows a more explicit modeling of the power sector and sector-coupling, a vision of the energy transition where end-use demand sectors such as building, industry and transport make economic use of the generation from variable sources by

    1) directly using the power at the time of production for inflexible form of demand,

    2) shifting time of power supply via battery and other power storage technology,

    3) transforming it to another energy carrier or product ahead of time of consumption and at times of surplus wind and solar production (e.g. PtG), without conversion back to electricity.

The fully coupled framework allows a more explicit modeling of economic competition of these options under high shares of variable renewables, finding more accurate optimal paths under long-term climate scenarios towards a net-zero power sector and the wider economy globally. In future research we plan to expand the study in the direction of demand-side management and flexibilization, and later possibly in the direction of heat storage.

Coupling DIETER to the global model REMIND for the single region Germany, this study serves as a proof-of-concept. Our main innovation is two-fold: we derive convergence theoretically, and show almost full convergence numerically. Theoretically, we derive the coupling methodology by mapping the KKT Lagrangians of the simplified versions of the two models. One key aspect of the mapping consists of iterative adjustment of the market value (i.e. the annual average revenue of one energy unit of generation) or the capture price (i.e. the annual average price of one energy unit of consumption) in the low-resolution IAM such that they take on the values as those in the high-resolution PSM. By finding the set of mathematical coupling conditions necessary for an iterative convergence as defined by the convergence of both quantities and prices, we could then design the coupling interface accordingly, such that at the end of the coupling a joint optimal result can be found.

Numerically, we compare the converged results of the two models by examining the long-term power mix (both capacity and generation quantities), prices of electricity, as well as generation dispatch (via RLDC), and find good agreement between the two models at the end of coupled convergence despite some slight mismatches. For a "proof-of-concept" baseline scenario under simple configuration without storage or flexible demand, we could achieve an energy mix with 4.4% tolerance for any technology's absolute share difference in each time step. For a climate policy scenario under a more realistic configuration with storage and flexible demand, we could achieve 6-7% tolerance. The cost breakdown and prices of power generations for both models are found to be very similar at the end of the iterative process, providing additional evidence that the quantity harmonization follows the underlying principle of the price and cost harmonization. The remaining differences can be partially explained by the lack of full harmonization of the brown-field and near-term capacity constraints, as well as potential mismatches due to numerical techniques aimed at enhancing performance and stability. Using the coupling methodology, we provide scenarios for power sector transition under a stringent German climate goal. Under this scenario, we observe a least-cost pathway consisting of an almost complete transformation to a wind- and solar-based power system. The results indicate an increasing role of storage and dispatchable capacity in a deep decarb scenario, consistent with the findings of previous PSM studies, but which is now transferred to the long-term models via soft-coupling.

For future works, besides expanding the research program on sector coupling into a direction containing a broader technological portfolio, we also aim to apply this framework to other world regions of interest in the REMIND model. Another important aspect would be to represent the variability-smoothing effect of transmission grids by using the same coupling framework to couple REMIND to other power sector models with more explicit modeling of transmission bottlenecks and expansion for two or more regions.

1252 **Appendices**

1253 **Appendix A: Comparison of model scope and specification**
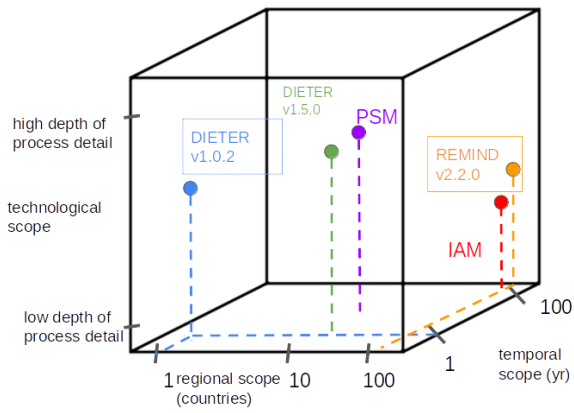
1254
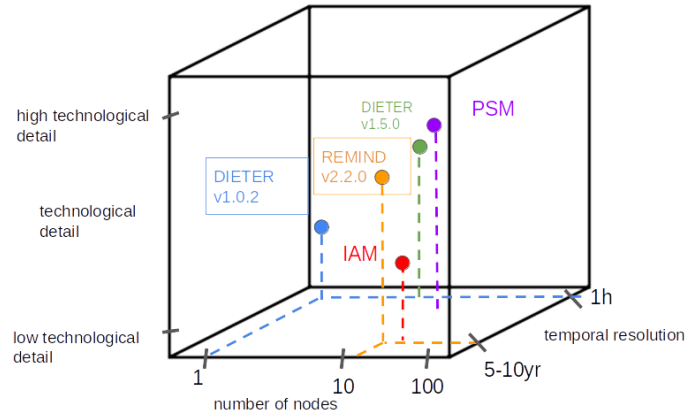
1255 (a) Model scope   (b) Model resolution

1256 **Figure A1: Comparison of resolution and scope for REMIND and a typical IAM, as well as two versions of DIETER**

1257 **(v1.0.2 is used in this study) and a typical PSM.**

Model name and version	REMIND v3.0.0 (dev)	DIETER v1.0.2
	model type	IAM	PSM
Scope and resolution	spatial scope	entire globe	single region (Germany)
	intertemporal scope of "perfect foresight"	2005-2100 (in actual model it is 2005-2150)	any year-long period
	temporal resolution	5- or 10-year time-step	hourly (all consecutive hours)
	regional resolution	single EU region	single EU region
	sectoral scope	all energy sectors (transport, building, industry), industrial processes, air pollution, land-use sector, etc	power sector
	available climate policy options	CO2 price, early-phase nuclear and coal phase out (for Germany), EU-ETS	CO2 price
Power sector dynamics	endogenous hourly dispatch	no	yes
	differentiated market value for various technologies	no	yes
	price elasticity of demand	yes	no
	capital cost of technology	endogenous via learning curve (Leimbach et al., 2010)	exogenous
	vintage tracking of existing capital stock	yes	no
	transmission assumption	copper plate within region	copper plate within region
Model code and data specification	programming language	GAMS	GAMS
	input data openness	partially open data	fully open data (for Germany)
	source code openness	open	open
	solver	CONOPT	CPLEX

1258   **Table A1: Comparison between the coupled models REMIND and DIETER.**

1259

1260   Because IAMs usually start out with certain assumptions for the development of macroeconomic metrics such as for GDP and

1261   population, which in turn determine the corresponding energy service levels to a larger degree prior to optimizing the energy

1262   system mix to meet demand, they are also frequently referred to as "top-down" energy system models. PSMs usually start out

modeling the fine spatiotemporal detail of the real-world power systems, expanding the capacity installation of power generating plants, grid transmission and storage at minimum cost. Such models are also known as "unit commitment models" for electrical power production (Padhy, 2004). Later in model development PSMs usually expand to include other energy services such as heating and transportation which are electrified. In this way PSMs are also often referred to as "bottom-up" models. Reviews and intercomparison of IAMs have been carried out recently where various IAMs are analyzed and harmonized (Weyant, 2017; Butnar et al., 2019; Keppo et al., 2021; Wilson et al., 2021; Giarola et al., 2021).

For methodological reasons, we have to set the length of the model time horizon to be until 2150, which is longer than the valid model time horizon until 2100. This is because without the extra years after 2100, the model has much less time to utilize the capacities installed in the few decades before 2100, making it more difficult to justify the installation of new capacity economically. This is manifested in a model artifact, where in the last few model periods investment in capacities decrease in general. By extending the time horizon, this "boundary" effect is pushed further to the future, so the artifact only appears after 2100. Therefore the meaningful model results for REMIND are only between 2005-2100, even though years until 2150 are also modeled and coupled.

Reviews and intercomparison of typical scopes and resolutions of PSMs can be found in Supplemental Material S5. Comparison of more PSMs can be found in Ringkjøb et al. 2018 and Prina et al. 2020.

Both models have open published source code. Partially thanks to the PSM community's advocacy of "open models", which encompasses all steps from input data, model source code to numerical solvers (openmod - Open Energy Modelling Initiative, 2022), many research institutions also responded to their calls to openly publish their models. For example, the IAM used in this study – REMIND, has for two years opened its source code on popular hosting site GitHub.

Appendix B: Model coupling scope

While REMIND and DIETER can both model a European-wide system with spatial subdivision (see Fig. B1 for REMIND regional division), the soft-coupling currently is only applied to Germany, in line with the proof-of-concept nature of this study. The coupling is from 2020 to 2150 for every defined REMIND period. All common and available REMIND generating technologies are enabled for the coupling, as shown in Fig. B2. The information for the species of technologies in REMIND are upscaled and coupled to DIETER, whereas information from DIETER is then downscaled during the feedback loop that completes the coupled iteration.

REMIND-EU (21 regions)
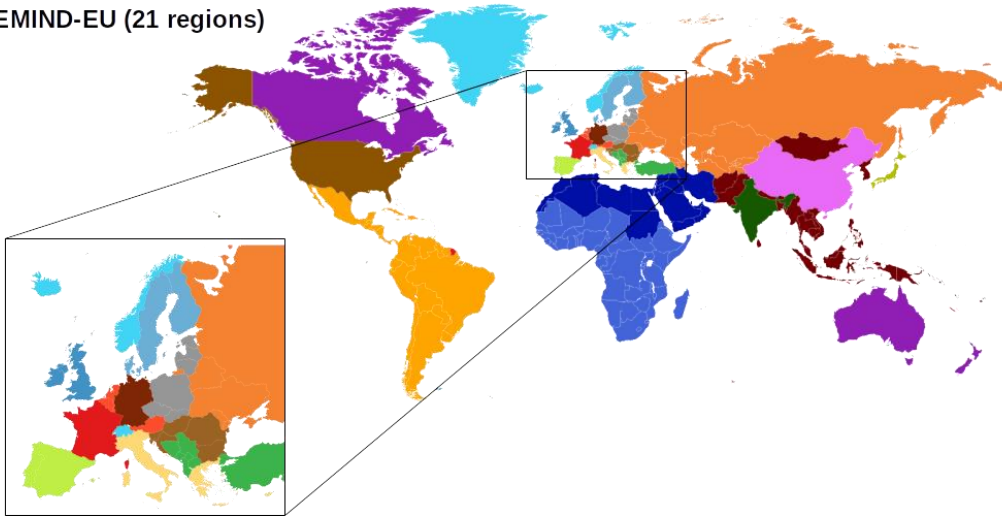
Figure B1: REMIND regional resolution used in this study (21 global regions, including detailed differentiations of EU regions). The spatial resolution of REMIND is flexible and depends on the resolution of the input data. Regional mapping is from the REMIND-EU model (Rodrigues et al., 2022).
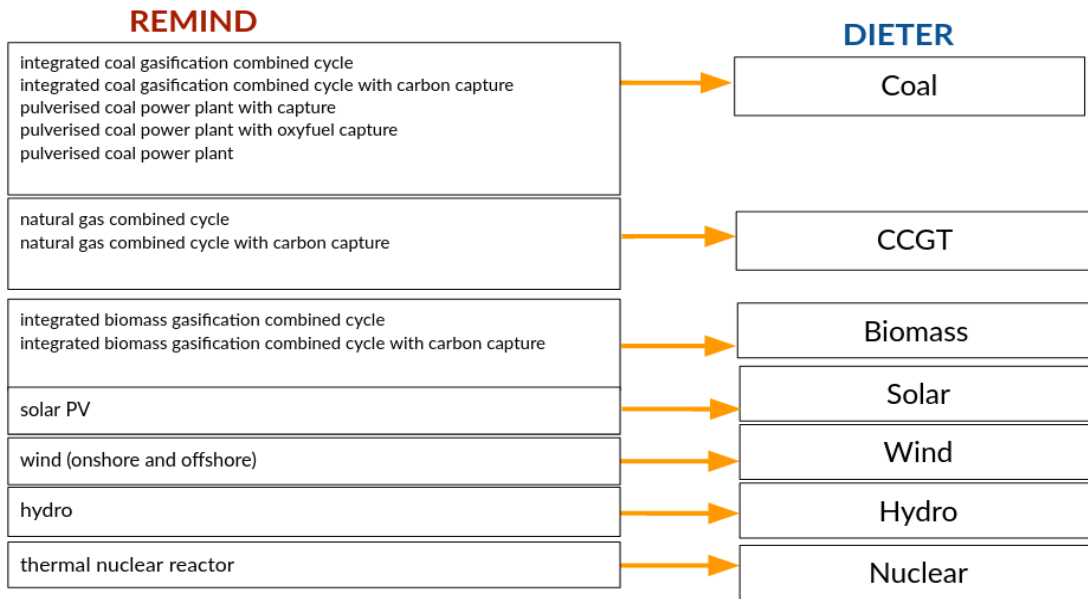
Figure B2: Mapping of coupled technologies between REMIND and DIETER.

Appendix C: REMIND's interannual intertemporal objective function for single-region

Single-region interannual intertemporal welfare is an aggregated utility, which in turn is a logarithm function of consumption. In REMIND, the total welfare of a region is maximized and is equal to

$$W_{reg} = \sum_{y=2005}^{2150} \frac{1}{(1 + \varrho_{reg})^{y-2005}} * \Delta y * V_{y,reg} * ln\left(\frac{\chi_{y,reg}}{\Gamma_{y,reg}}\right),$$

where regional consumption is $\chi_{y,reg}$ at model time y, and the weight of the consumption determined by the pure rate of time preference ϱ_{reg} and population $V_{y,reg}$. The consumption $\chi_{y,reg}$ at time y is in turn equal to the difference between regional

1303 income (gross domestic product) minus export (which is not available for consumption) and saving (i.e. investments), subtracted

1304 by the cost of the energy system (including the power sector) and other costs in the economy. For simplicity we do not discuss

1305 several other expenditures such as capital investment for energy service, other energy related expenditures such as R&D and

1306 innovation, taxes, cost of pollution and land-use change.

Appendix D: Deriving the soft-coupling convergence conditions

1307

1308 In Sect. 3.2.1, we sketch the derivation procedure and offer a short summary of the analytical results. Here we describe the

1309 derivation procedure of the coupled convergence framework in detail.

1310 Using the Lagrangian multiplier method, based on the objective functions (Eqs. (1-2)) and constraints (c1-c6) in Sect. 3.1 we

1311 can construct the KKT Lagrangians (Karush, 1939; Kuhn and Tucker, 1951; Gan et al., 2013):

1312 REMIND:

1314
$$\mathcal{L} = \underbrace{\sum_{y,s}(c_{y,s}P_{y,s} + o_{y,s}G_{y,s})}_{\text{REMIND objective function}} + \underbrace{\sum_{y}\lambda_y\left[d_y - \sum_s G_{y,s}(1-\alpha_{y,s})\right]}_{\text{annual electricity balance equation constraint}} + \underbrace{\sum_{y,s}\omega_{y,s}(P_{y,s}-\psi_s)}_{\text{resource constraint}} + \underbrace{\sum_{y,s}\xi_{y,s}(-G_{y,s})}_{\text{positive generation constraint}}$$

1315
$$+ \underbrace{\sum_{y,s}\mu_{y,s}(G_{y,s} - 8760*\phi_{y,s}P_{y,s})}_{\text{maximum generation from capacity constraint}} + \underbrace{\sum_{y\leq2020,s}\sigma_{y,s}(p_{y,s}-P_{y,s})}_{\text{standing capacity constraint}} + \underbrace{\sum_{y=2025,s}\gamma_{y,s}(P_{y,s}-P_{y-\Delta y,s}-q_{y,s})}_{\text{near-term ramp-up capacity constraint}}, \quad (D1)$$

1313 DIETER:

1316
$$\underline{\mathcal{L}} = \underbrace{\sum_s\left[\underline{c_s}\underline{P_s} + \underline{o_s}\sum_h(\underline{G_{h,s}} + \underline{\Gamma_{h,vre}})\right]}_{\text{DIETER objective function}} + \underbrace{\sum_h\underline{\lambda_h}\left(\underline{d_h} - \sum_s\underline{G_{h,s}}\right)}_{\text{hourly electricity balance equation constraint}} + \underbrace{\sum_s\underline{\omega_s}\left(\underline{P_s}-\underline{\psi_s}\right)}_{\text{resource constraint}} + \underbrace{\sum_{h,s}\underline{\xi_{h,s}}(-\underline{G_{h,s}})}_{\text{positive generation constraint}}$$

1317
$$+ \underbrace{\sum_{h,dis}\underline{\mu_{h,dis}}(\underline{G_{h,dis}} - \underline{P_{dis}})}_{\text{maximum dispatchable generation from capacity constraint}} + \underbrace{\sum_{h,vre}\underline{\mu_{h,vre}}\left(\underline{G_{h,vre}} + \underline{\Gamma_{h,vre}} - \underline{\phi}_{h,vre}\underline{P_{vre}}\right)}_{\text{maximum renewable generation from capacity and weather constraint}}. \quad (D2)$$

1318 Comparing Lagrangians $\mathcal{L}$ and $\underline{\mathcal{L}}$, there are notable similarities between the terms. But first, we can reduce the complexity by

1319 noticing that there are terms containing capacity shadow prices that are either trivial or already harmonized: resource constraint

1320 shadow prices ω are already identical for both models by design (constraint (c2) in Sect. 3.1); positive generation constraint

1321 shadow price ξ is 0 due to KKT conditions for both models (constraint (c3)). These constraint terms can be safely excluded from

1322 the subsequent mapping. We then note the important fact that REMIND Lagrangian is a sum over multiple years, whereas

1323 DIETER Lagrangian is for each year. To make a direct comparison and therefore mapping possible, we assume that the brown-

1324 field and near-term constraints are not binding. After this simplifying assumption, we realize that REMIND becomes linearly

1325 independent in terms of the temporal slices, because by now the only yet-to-be-harmonized constraints left in the standalone

1326 models are (c1) and (c4), which are both constraints for each year and do not result in temporal correlations. Note that this

1327 simplifying assumption is assumed to be valid only for the derivation in this section. Later in actual simulations, we see that

1328 these bounds generate shadow prices which are not necessarily small, impacting the degree of convergence especially in earlier

1329 years. These constraints are also temporally localized in early periods, exerting little impact on later, more "green-field" years.

1330 In fact, when including brown-field constraint into DIETER (c8), the model convergence is improved (Sec. 6.1).

1331 After the aforementioned simplifications, we can construct a single-year REMIND Lagrangian $\mathcal{L}_y$:

1332
$$\mathcal{L}_y = \underbrace{\sum_s(c_{y,s}P_{y,s} + o_{y,s}G_{y,s})}_{\text{REMIND objective function}} + \underbrace{\lambda_y\left[d_y - \sum_s G_{y,s}(1-\alpha_{y,s})\right]}_{\text{annual electricity balance equation constraint}} + \underbrace{\sum_s\mu_{y,s}(G_{y,s} - 8760*\phi_{y,s}P_{y,s})}_{\text{maximum generation from capacity constraint}}, \quad (D3)$$

1333   and map it to the single-year DIETER Lagrangian $\underline{\mathcal{L}}$:

1334
$$\underline{\mathcal{L}} = \underbrace{\sum_s \left[\underline{c}_s\underline{P}_s + \underline{o}_s\sum_h\left(\underline{G}_{h,s} + \underline{\Gamma}_{h,vre}\right)\right]}_{\text{DIETER objective function}} + \underbrace{\sum_h\underline{\lambda}_h\left(\underline{d}_h - \sum_s\underline{G}_{h,s}\right)}_{\text{hourly electricity balance equation constraint}} + \underbrace{\sum_{h,dis}\underline{\mu}_{h,dis}\left(\underline{G}_{h,dis} - \underline{P}_{dis}\right)}_{\text{maximum dispatchable generation from capacity constraint}}$$

1335
$$+ \underbrace{\sum_{h,vre}\underline{\mu}_{h,vre}\left(\underline{G}_{h,vre} + \underline{\Gamma}_{h,vre} - \underline{\phi}_{h,vre}\underline{P}_{vre}\right)}_{\text{maximum renewable generation from capacity and weather constraint}} \qquad . \qquad\qquad\qquad (D4)$$

1336   These are the same as Eqs. (3)-(4).

1337   Comparing $\mathcal{L}_y$ and $\underline{\mathcal{L}}$, we can map them by matching the following four terms in the Lagrangians individually:

1338   A)   annual total power sector costs: $Z_y = \sum_s\left(c_{y,s}P_{y,s} + o_{y,s}G_{y,s}\right)$ and $\underline{Z} = \sum_s\left[\underline{c}_{y,s}\underline{P}_{y,s} + \underline{o}_{y,s}\sum_h(\underline{G}_{y,h,s} + \underline{\Gamma}_{y,h,vre})\right]$,

1339   B)   annual revenue of usable (post-curtailment) generation for each generator s: $\lambda_yG_{y,s}\left(1 - \alpha_{y,s}\right)$ and $\sum_h\underline{\lambda}_{y,h}\underline{G}_{y,h,s}$,

1340   C)   annual payment made by the consumers: λ_yd_y and $\sum_h\underline{\lambda}_{y,h}\underline{d}_{y,h}$,

1341   D)   maximum generation from capacity constraint term for each generator s: $\mu_{y,s}\left(G_{y,s} - 8760 * \phi_{y,s}P_{y,s}\right)$ and

1342 $\sum_h\underline{\mu}_{y,h,s}\left(\underline{G}_{y,h,s} + \underline{\Gamma}_{y,h,s} - \underline{\phi}_{y,h,s}\underline{P}_{y,s}\right)$ (we write the two terms for VRE and dispatchable into one term for DIETER here

1343   for simplicity, i.e. $\underline{\Gamma}_{y,h,dis} = 0$ and $\underline{\phi}_{y,h,dis} = 1$ for dispatchables).

1344   The following conditions (h1-h7) can be derived from the harmonization of terms (A)-(D). Each term is harmonized by

1345   matching the values in front of decision variables at the aggregated levels, namely capacities and annual generations.

1346   Term A) can be mapped if:

1347   **h1)** annual fixed costs are harmonized for each generator species s: $c_{y,s} = \underline{c}_{y,s}$,

1348   **h2)** annual variable costs are harmonized for each generator species s: $o_{y,s} = \underline{o}_{y,s}$.

1349   Term B) can be mapped if:

1350   **h3)** for each generator species s, the annual average revenue per unit generation, i.e. the market value, is harmonized by

1351   exogenously manipulating the market value in REMIND to be the same as the last-iteration annual average market value in

1352   DIETER. We achieve this by adding a correction term, thereby modifying REMIND original objective function Z to Z':

1353 $Z' = Z - \sum_{y,s}\underline{\eta}_{y,s}(i - 1)G_{y,s}\left(1 - \alpha_{y,s}\right)$,

1354   where $\underline{\eta}_{y,s}(i - 1)$ is the markup for technology s in DIETER in the last iteration $i - 1$, i is the index of the iteration of the

1355   iterative soft-coupling. Z' is the modified REMIND objective function in the coupled version.

1356   The detailed derivation is as follows.

1357   Lagrangian term B for the models have the physical meanings of total annual revenue of usable (post-curtailment)

1358   generation. (Annual revenue is equal to the product of usable generation and annual market value.) We denote total annual

1359   revenue from technology s as $\Theta_{y,s}$ for REMIND and $\underline{\Theta}_{y,s}$ for DIETER. Then for REMIND the revenue (term B) is

1360 $\Theta_{y,s} = \lambda_yG_{y,s}\left(1 - \alpha_{y,s}\right)$,   (D5)

1361   and for DIETER

1362 $\underline{\Theta}_{y,s} = \sum_h\underline{\lambda}_{y,h}\underline{G}_{y,h,s}$.   (D6)

1363   To harmonize terms $\Theta_{y,s}$ and $\underline{\Theta}_{y,s}$, our goal is to create a one-to-one mapping of the values in front of the decision variable

1364   annual aggregated post-curtailment generation of technology s, which is $G_{y,s}\left(1 - \alpha_{y,s}\right)$ for REMIND and $\sum_h\underline{G}_{y,h,s}$ for

1365   DIETER, the latter is namely a direct sum of the hourly generations. However, we notice for DIETER revenue $\underline{\Theta}_{y,s}$ is a

1366   weighted sum of the hourly generation, and the direct sum cannot be separated in a straight-forward way. So first we have

1367   to rewrite $\underline{\Theta}_{y,s}$ (Eq. (D6)) by first dividing then multiplying by the aggregated annual generation:

1370 $$\underline{\Theta}_{y,s} = \frac{\sum_h \underline{\lambda}_{y,h} \underline{G}_{y,h,s}}{\sum_h \underline{G}_{y,h,s}} \sum_h \underline{G}_{y,h,s}.$$ (D7)

1368 We notice that the multiplicative term in front of the DIETER annual aggregated generation $\sum_h \underline{G}_{y,h,s}$ is $\frac{\sum_h \underline{\lambda}_{y,h} \underline{G}_{y,h,s}}{\sum_h \underline{G}_{y,h,s}}$, which

1369 is nothing other than the market value of generation technology s (see also Eq. (F24)).

1371 We now take a look at revenue $\Theta_{y,s}$ on the REMIND side, which is equal to $\lambda_y G_{y,s}(1 - \alpha_{y,s})$ (Eq. (D5)). To map (D5) to

1372 the DIETER revenue term $\underline{\Theta}_{y,s}$ (Eq. (D7)) in terms of the aggregated decision variable $G_{y,s}(1 - \alpha_{y,s})$ and $\sum_h \underline{G}_{y,h,s}$, we

1373 essentially would like the multiplicative term in front of the generation variable in $\Theta_{y,s}$, which is λ_y, to be also $\frac{\sum_h \underline{\lambda}_{y,h} \underline{G}_{y,h,s}}{\sum_h \underline{G}_{y,h,s}}$

1374 like in DIETER. This means the DIETER-corrected revenue in REMIND *should* be

1379 $$\Theta'_{y,s} = \frac{\sum_h \underline{\lambda}_{y,h} \underline{G}_{y,h,s}}{\sum_h \underline{G}_{y,h,s}} G_{y,s}(1 - \alpha_{y,s}).$$ (D8)

1375 To harmonize $\Theta_{y,s}$ and $\underline{\Theta}_{y,s}$, we can simply add a linear correction term to compensate for the difference between them.

1376 Noticing in Eq. (D5), the multiplicative term in front of the REMIND generation variable $G_{y,s}(1 - \alpha_{y,s})$ is λ_y, which can

1377 be interpreted as the REMIND market value, we realize essentially for a linear correction term, we should add the market

1378 value difference $\Delta MV_{y,s}$ between the two models

1380 $$\Delta MV_{y,s} = \underline{MV}_s - MV_s = \frac{\sum_h \underline{\lambda}_{y,h} \underline{G}_{y,h,s}}{\sum_h \underline{G}_{y,h,s}} - \lambda_y ,$$ (D9)

1381 to the multiplicative term λ_y in $\Theta_{y,s}$, so λ_y is canceled. Note that in Eq. (D9), as discussed before, the DIETER market

1382 value is dependent on technology index s, whereas the REMIND one does not.

1383 After adding the linear correction term, the modified revenue in REMIND $\Theta'_{y,s}$ after harmonization is:

1384 $$\Theta'_{y,s} = \Theta_{y,s} + \Delta MV_{y,s} G_{y,s}(1 - \alpha_{y,s}) = (\Delta MV_{y,s} + \lambda_y) G_{y,s}(1 - \alpha_{y,s}),$$ (D10)

1385 plugging in (D9),

1386 $$\Theta'_{y,s} = \left(\frac{\sum_h \underline{\lambda}_{y,h} \underline{G}_{y,h,s}}{\sum_h \underline{G}_{y,h,s}} - \lambda_y + \lambda_y \right) G_{y,s}(1 - \alpha_{y,s}) = \frac{\sum_h \underline{\lambda}_{y,h} \underline{G}_{y,h,s}}{\sum_h \underline{G}_{y,h,s}} G_{y,s}(1 - \alpha_{y,s}),$$ (D11)

1387 which is as desired in (D8).

1388 In practice, in the case of annual shadow price λ_y in REMIND, we find that the coupling behaves more stable numerically,

1389 if we use the annual average electricity price of DIETER instead of the last-iteration electricity price of REMIND λ_y in

1390 (D9). The equivalence between the two prices is expressed later in (h5). We can use this substitution, since as we show

1391 later that (h5) can be derived from market value harmonization (h3) and demand harmonization (h4). With this

1392 substitution, the correction term which we call $\eta_{y,s}$ is in fact:

1393 $$\eta_{y,s} = \underline{MV}_s - \underline{J} = \frac{\sum_h \underline{\lambda}_{y,h} \underline{G}_{y,h,s}}{\sum_h \underline{G}_{y,h,s}} - \frac{\sum_h \underline{\lambda}_{y,h} \underline{d}_{y,h}}{\sum_h \underline{d}_{y,h}},$$ (D12)

1394 where $\underline{J} = \frac{\sum_h \underline{\lambda}_{y,h} \underline{d}_{y,h}}{\sum_h \underline{d}_{y,h}}$ is the annual average electricity price in DIETER. We calculate (D12) using the last iteration

1395 DIETER solutions. Note that compared to the earlier (D9), we have simply replaced the second term REMIND annual

1396 price with DIETER annual price.

1397 It is not hard to recognize $\eta_{y,s}$ as the "markup" for technology s in DIETER, where markup as defined before is the

1398 difference between the market value of a technology $\underline{MV}_s$ and the load-weighted annual average electricity price $\underline{J}$ (see

1399 Sect. 3.1 introduction).

1400   Now we have concluded the derivation for the markup term $\underline{\eta}_{y,s}$ in (h3).

1401   Although the multiplicative terms in front of decision variables in the two models can be harmonized via the correction

1402   term (D12), we notice that it contains endogenous values, i.e. hourly generation $\underline{G}_{y,h,s}$ and hourly shadow price $\underline{\lambda}_{y,h}$ in

1403   DIETER. Since any endogenous value can only be known ex post, this means the Lagrangian mapping relies on

1404   endogenous values from the last iteration, i.e.

1405 $\underline{\eta}_{y,s}(i-1) = \underline{MV_s}(i-1) - \underline{J}(i-1) = \dfrac{\sum_h \underline{\lambda}_{y,h}(i-1)\underline{G}_{y,h,s}(i-1)}{\sum_h \underline{G}_{y,h,s}(i-1)} - \dfrac{\sum_h \underline{\lambda}_{y,h}(i-1)\underline{d}_{y,h}(i-1)}{\sum_h \underline{d}_{y,h}(i-1)}.$

1406   Now, using the markup term $\underline{\eta}_{y,s}$, we define the linear correction term for the revenue in REMIND $\Theta_{y,s}$ as

1407 $\Delta\Theta_{y,s} = \underline{\eta}_{y,s}(i-1)G_{y,s}\left(1 - \alpha_{y,s}\right).$

1408   The physical meaning of $\Delta\Theta_{y,s}$ is the revenue difference in the two models for technology s, given that the post-

1409   curtailment generations are expressed in terms of REMIND variables.

1410   The coupled REMIND has a modified objective function Z' based on a linear correction. The correction term $\Delta\Theta_{y,s}$ need to

1411   be summed over s and y and subtracted – due to the negative sign in front of term B, from the REMIND objective function

1412 Z, since the objective term as a part of the Lagrangian can be directly manipulated:

1413 $Z' = Z - M = Z - \sum\limits_{y,s}\Delta\Theta_{y,s} = Z - \sum\limits_{y,s}\underline{\eta}_{y,s}(i-1)G_{y,s}\left(1 - \alpha_{y,s}\right),$

1414   where we call the total system revenue differences M, again, these are revenues where the post-curtailment generations are

1415   expressed in terms of REMIND variables (and not DIETER variables).

1416   Now we have concluded the derivation for the convergence condition (h3).

1417   Depending on the starting point of the REMIND power system, and due to the internal iterative changes of REMIND

1418   results due to the adjustments in trade between regions during the "Nash" algorithm, coupled convergence usually can only

1419   be achieved over multiple iterations. Therefore the derived markup equation (Eq. (D12)) in general can be only expected to

1420   reflect the actual market value differences approximately in the two models. This is the reason that in the iterative

1421   algorithm after the first iteration, we add $M(i) - M(i-1)$ to the objective function Z, as the quantities and prices

1422   gradually converge between the two models. As convergence is approached, the total revenue difference between iteration

1423 $M(i) - M(i-1)$ should go to zero. This is confirmed by the numerical experiments (not shown).

1424 Term C) can be mapped if:

1425   **h4)** annual power demand in the two models are harmonized: $d_y = \sum_h \underline{d}_{y,h}$,

1426   **h5)** annual average price of electricity is mapped to each other $\lambda_y = \frac{\sum_h \underline{\lambda}_{y,h}\underline{d}_{y,h}}{\sum_h \underline{d}_{y,h}}$ (dividing term (C) by (h4)). Because

1427   electricity price is by definition equal to total annual system revenue divided by total annual demand, (h5) can be shown to

1428   hold true, given technology-specific revenues are harmonized in (h3) and demand are harmonized in (h4). (If technology-

1429   specific revenues are harmonized in (h3), then the system revenues which are technology-specific revenues summed over

1430   technologies are also harmonized.) (h5) therefore can be seen as a derived condition from (h3) and (h4).

1431 Term D) can be mapped if:

1432   **h6)** annual average capacity factors are harmonized, i.e. $\phi_{y,s}$ in REMIND is set to equal to the endogenous last-iteration

1433   DIETER result for each generation type s:

1434 $\phi_{y,s} = \sum\limits_{h}\underline{\phi}_{y,h,s} / 8760$,

1435 where $\underline{\phi}_{y,h,s} = \frac{\underline{G}_{y,h,s}}{\underline{P}_{y,s}}$ is the hourly capacity factor in DIETER. Without explicit manipulation of the shadow prices $\mu_{y,s}$ and

1436 $\underline{\mu}_{y,h,s}$, we show the following claim is true, i.e. by above capacity factor harmonization, the terms containing endogenous

1437 shadow prices will be automatically mapped. Showing this requires careful mathematical argument, which we make in

1438 detail in the case of dispatchable, and later argue the case is similar for renewable.

1439 For dispatchable generators the argument is as follows. (For simplicity we use the generic index s.)

1440 We first rewrite REMIND term D by plugging in the harmonization condition $\phi_{y,s} = \sum_h \underline{\phi}_{y,h,s} / 8760$:

1441
$$\mu_{y,s}\big(G_{y,s} - 8760 * \phi_{y,s}P_{y,s}\big) = \sum_y \mu_{y,s}\left(G_{y,s} - \sum_h \underline{\phi}_{y,h,s}P_{y,s}\right),$$

1442 and it should be mapped to the term $\sum_{y,h} \underline{\mu}_{y,h,s}\left(\underline{G}_{y,h,s} - \underline{P}_{y,s}\right)$ in DIETER.

1443 Splitting the two terms, these four terms need to be harmonized:

1444 $\mu_{y,s}G_{y,s}$ and $\sum_h \underline{\mu}_{y,h,s}\underline{G}_{y,h,s}$ (D13)

1445 $\mu_{y,s}\sum_h \underline{\phi}_{y,h,s}P_{y,s}$ and $\sum_h \underline{\mu}_{y,h,s}\underline{P}_{y,s}$ (D14)

1446 for all y, s.

1447 To show the mappings (D13)-(D14) are automatically satisfied given (h6), we first consider two simplified power sector

1448 toy problems, Q1 and Q2, with only dispatchable technologies. Both problems have identical objective functions $\tilde{Z} =$

1449 $\sum_s\big(\tilde{c}_s\tilde{P}_s + \tilde{o}_s\tilde{G}_s\big)$, and the fixed and variable cost parameters $\tilde{c}_s$ and $\tilde{o}_s$ are identical. Both problems have identical hourly

1450 balance equation constraint, but with two different kinds of maximum generation constraint, Q1 has an inequality

1451 constraint for each hour, Q2 has an aggregated annual equality constraint:

1452 Q1: $min\ Z$, s.t. $\tilde{G}_{h,s} \leq \tilde{P}_s \perp \tilde{\mu}_{h,s}$, $\tilde{d}_h = \sum_s \tilde{G}_{h,s} \perp \tilde{\lambda}_h$

1453 Q2: $min\ Z$, s.t. $\sum_h \tilde{G}_{h,s} = 8760 * \tilde{\phi}_s\tilde{P}_s \perp \tilde{\mu}'_s$, $\tilde{d}_h = \sum_s \tilde{G}_{h,s} \perp \tilde{\lambda}'_h$

1454 Then the Lagrangians are:

1455
$$\tilde{\mathcal{L}}_1 = \underbrace{\sum_s\left(\tilde{c}_s\tilde{P}_s + \tilde{o}_s\sum_h \tilde{G}_{h,s}\right)}_{\text{objective function}} + \underbrace{\sum_h \tilde{\lambda}_h\left(\tilde{d}_h - \sum_s \tilde{G}_{h,s}\right)}_{\text{hourly electricity balance equation constraint}} + \underbrace{\sum_{h,s} \tilde{\mu}_{h,s}\left(\tilde{G}_{h,s} - \tilde{P}_s\right)}_{\text{maximum generation from capacity constraint}}$$

1456
$$\tilde{\mathcal{L}}_2 = \underbrace{\sum_s\left(\tilde{c}_s\tilde{P}_s + \tilde{o}_s\sum_h \tilde{G}_{h,s}\right)}_{\text{objective function}} + \underbrace{\sum_h \tilde{\lambda}'_h\left(\tilde{d}_h - \sum_s \tilde{G}_{h,s}\right)}_{\text{hourly electricity balance equation constraint}} + \underbrace{\sum_s \tilde{\mu}'_s\left(\sum_h \tilde{G}_{h,s} - 8760\tilde{\phi}_s\tilde{P}_s\right)}_{\text{maximum generation from capacity constraint}} .$$

1457 The relevant KKT conditions:

1458 Stationarity condition for Q1:

1459 $\frac{\partial \tilde{\mathcal{L}}_1}{\partial \tilde{P}_s} = \tilde{c}_s - \sum_h \tilde{\mu}_{h,s} = 0$ (D15)

1460 Stationarity condition for Q2:

1461 $\frac{\partial \tilde{\mathcal{L}}_2}{\partial \tilde{P}_s} = \tilde{c}_s - 8760\tilde{\phi}_s\tilde{\mu}'_s = 0$ (D16)

1462 Since the fixed cost $\tilde{c}_s$ are equal for the two models, from Eqs. (D15)-(D16) we can derive the relation between the two

1463 shadow prices:

1464 $8760 * \tilde{\phi}_s\tilde{\mu}'_s = \sum_h \tilde{\mu}_{h,s}$. (D17)

1465 Note that for the toy models, the identical balance equation constraints do not contain capacity P, which is why the balance

1466 equation constraints do not influence the stationary conditions for P (Eqs. (D15)-(D16)).

1467   We now show (D14) is automatically mapped given capacity factor harmonization (h6). We first write the equality

1468   condition for the REMIND-DIETER case, analogous to the toy model result (D17),

1469 $8760 * \phi_{y,s}\mu_{y,s} = \sum_h \underline{\mu}_{y,h,s}$.   (D18)

1470   Note that we can apply the toy model case to the REMIND-DIETER coupling case in rather straight-forward way, because

1471   in the case of REMIND-DIETER, the objective function terms have been already harmonized by (h1)-(h2), and the balance

1472   equation constraint terms do not contain P, so they have no bearing on the generation-capacity constraint term, just like in

1473   the case of the toy models.

1474   Plugging (h6) $\phi_{y,s} = \sum_h \underline{\phi}_{y,h,s}(i-1)/8760$ into (D18), we have derived the equality for the parameter mapping required

1475   in (D14), i.e.,

1476 $\mu_{y,s} \sum_h \underline{\phi}_{y,h,s}(i-1) = \sum_h \underline{\mu}_{y,h,s}$.

1477   To show (D13), we first use hourly capacity factor from DIETER,

1478 $\underline{G}_{y,h,s} = \underline{\phi}_{y,h,s}\underline{P}_{y,s}$,   (D19)

1479   as well as the primal feasibility condition from REMIND $G_{y,s} = 8760 * \phi_{y,s}P_{y,s}$ (Eq. (F9)), to rewrite both sides of the

1480   mapping in (D13) in capacity terms. For REMIND, plugging in (F9),

1481 $\mu_{y,s}G_{y,s} = \mu_{y,s} * 8760 * \phi_{y,s}P_{y,s}$,   (D20)

1482   and for DIETER, plugging in (D19),

1483 $\sum_h \underline{\mu}_{y,h,s}\underline{G}_{y,h,s} = \sum_h \underline{\mu}_{y,h,s}\underline{\phi}_{y,h,s}\underline{P}_{y,s}$.   (D21)

1484   Take the complementary slackness condition of DIETER $\underline{\mu}_{h,s}(\underline{G}_{h,s} - \underline{P}_s) = 0$ (Eq. (F16)), insert (D19) on the left-hand-

1485   side, we obtain

1486 $\underline{\mu}_{h,s}(\underline{G}_{h,s} - \underline{P}_s) = \underline{\mu}_{h,s}(\underline{\phi}_{y,h,s}\underline{P}_{y,s} - \underline{P}_s) = 0$.

1487   Rearranging, we get

1488 $\underline{\mu}_{y,h,s}\underline{\phi}_{y,h,s}\underline{P}_s = \underline{\mu}_{y,h,s}\underline{P}_s$,   (D22)

1489   for each hour h.

1490   Plug (D22) and then (D18) into the right-hand-side of (D21), to obtain

1491 $\sum_h \underline{\mu}_{y,h,s}\underline{G}_{y,h,s} = \sum_h \underline{\mu}_{y,h,s}\underline{P}_{y,s} = 8760 * \phi_{y,s}\mu_{y,s}\underline{P}_{y,s}$.   (D23)

1492   Compare (D20) with (D23), they now have identical parameters in front of the capacity variable $P_{y,s}$ and $\underline{P}_{y,s}$, as desired.

1493   We concluded the proof that by exogenously setting the annual capacity factor of REMIND to that of the last iteration

1494   DIETER, we automatically harmonize the generation-capacity constraint term of the Lagrangian, in the case of

1495   dispatchable generators.

1496   **h7)** for VRE, annual curtailment rates are harmonized $G_{y,vre}\alpha_{y,vre} = \sum_h \underline{\Gamma}_{y,h,vre}$, i.e. by exogenously setting curtailment rate

1497   in REMIND $\alpha_{y,vre} = \sum_h \underline{\Gamma}_{y,h,vre}(i-1)/G_{y,vre}$, taking the endogenously determined curtailed power $\underline{\Gamma}_{y,h,vre}$ from the last

1498   iteration DIETER. This in general also harmonizes terms other than term D, as it harmonizes the definition for generation

1499   variable in DIETER which is post-curtailment and REMIND definition for generation variable which is pre-curtailment.

1500   For VREs the derivation is conceptually similar to the above case for dispatchable in (h6), since we can define a real

1501   capacity factor (post-curtailment) similar to the capacity factor for the dispatchable generators above,

1502 $\underline{\phi}_{y,h,vre} = \underline{G}_{h,vre}/\underline{P}_{vre}$.

1503   Due to the limitations of this paper, we will not present the derivation here. A detailed derivation is available upon request.

1504 **Appendix E: Coupling iteration schematics**

1505 Coupled region: Germany

1506 Coupled REMIND time horizon: 2020-2150 (2010-2015 are not coupled since they are historical years and have mostly hard-

1507 fixed quantities)
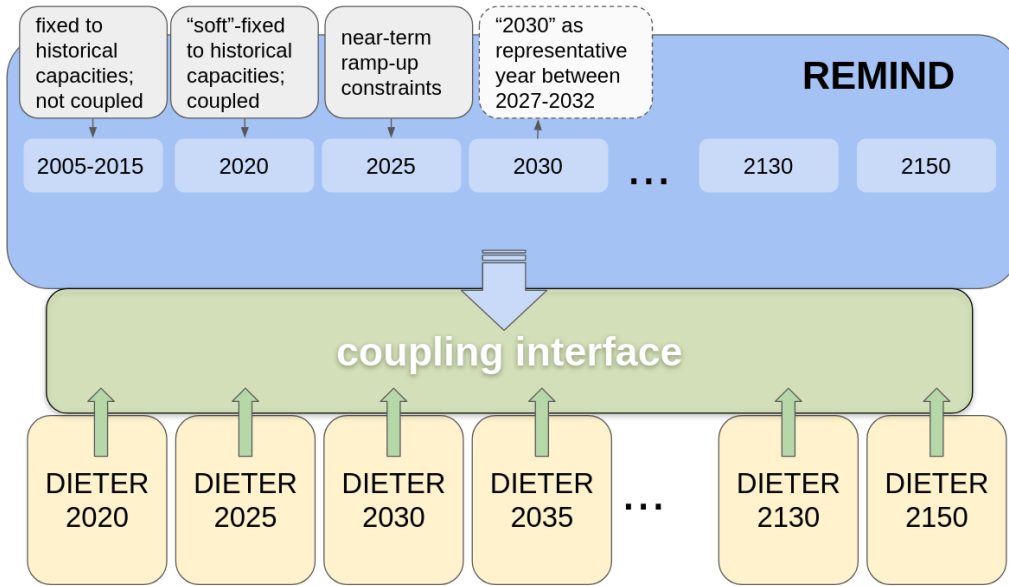
1508
1509 **(a) Graphic illustration of the bi-directional coupling in the temporal dimension.**
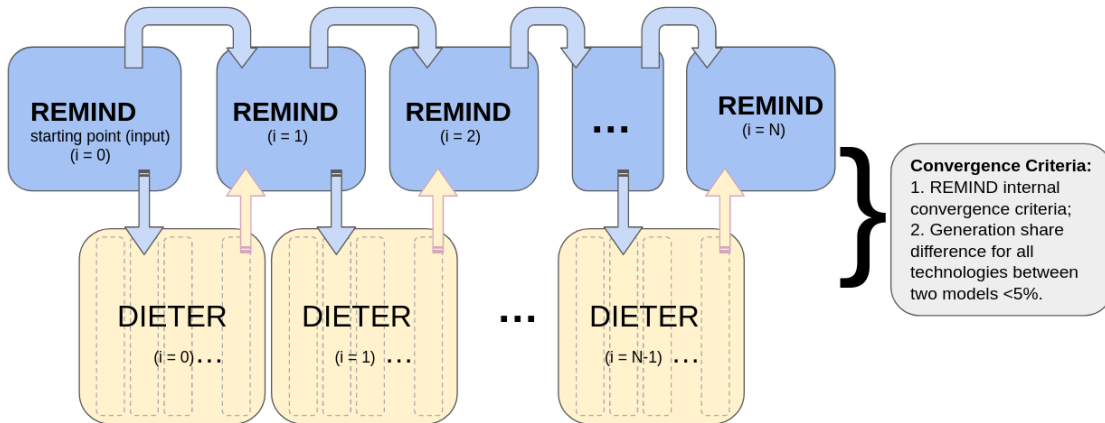
1510
1511 **(b) Graphic illustration of the bi-directional coupling in the iteration dimension.**

1512 **Figure E1: A graphic description of the model iterative coupling. (a) The temporal slices of REMIND which are mapped**

1513 **to multiple parallel year-long DIETER problems are illustrated here. The convergence conditions are iteratively mapped**

1514 **at the interface. (b) Every i-th iteration of REMIND takes the (i-1)-th iteration of REMIND as a starting point for**

1515 **optimization, and the endogenous output of the (i-1)-th DIETER as exogenous input parameters. When the convergence**

1516 **conditions are met, i.e. REMIND satisfies its internal convergence condition, and the coupled models differ in their**

1517 **generation share of each technology at most by a certain percentage (e.g. 5% for baseline run without storage), the**

1518 **coupled run halts.**

1519

1520 Under simple configuration (no storage, no flexible demand), every REMIND run takes around 3 minutes and DIETER run

1521 takes a few seconds to solve. Under more detailed configurations (with storage and flexible demand) and climate policies, every

1522 REMIND run takes around 4 minutes and a DIETER run takes a few minutes to solve. The entire REMIND-DIETER coupled

1523 run for a single region Germany under simple configuration is around 3~4 hours. It is around 6~10 hours for the more detailed

1524 configurations under climate policies.

Appendix F: Derivation of the equilibrium conditions for uncoupled REMIND and DIETER

1526 In this appendix, we discuss the equilibrium conditions of the uncoupled models, resulting in a rigorous formulation of the so-

1527 called "zero-profit rules" (ZPRs). We first construct the Lagrangians and compute KKT conditions, then derive the ZPRs for the

1528 standalone versions of REMIND reduced power-sector model and DIETER model.

1529 Using the objective functions and constraints in Sect. 3.1, we can construct Lagrangians for the two standalone models. Using

1530 the KKT conditions derived from the Lagrangians, we can show that if the historical and resource constraint are non-binding,

1531 i.e. shadow prices ω, σ and γ are zero, then each generator would have recovered their fixed, variable cost and curtailment cost

1532 through their total market revenue, i.e. each producer of electricity gets "zero profit", given that the profits are defined as the

1533 difference between revenue and cost. When the capacity constraints exist and are binding, we arrive at a modified version of the

1534 original ZPR, which describes the relation between cost, revenue and the capacity shadow prices.

1535 Here we first construct the Lagrangians and derive the KKT conditions from them (Sect. F.1) for both models. Then both

1536 models' ZPRs are derived, two for each model, namely, the technology-specific ZPR and the system ZPR (Sect. F.2).

F.1 Lagrangians and KKT conditions

1538 The Lagrangians of the uncoupled model have been constructed in Appendix D (Eqs. (D1)-(D2)). From the KKT conditions for

1539 minimization, we can ascertain the following first-order conditions at stationarity for each model.

1540 For REMIND,

1541   1) Stationary conditions:

1542 $$\frac{\partial \mathcal{L}}{\partial P_{y,s}} = 0 \Rightarrow c_{y,s} + \omega_{y,s} - 8760 * \mu_{y,s}\phi_{y,s} - \sigma_{y,s} + \gamma_{y,s} = 0 \ , \tag{F1}$$

1543 $$\frac{\partial \mathcal{L}}{\partial G_{y,s}} = 0 \Rightarrow o_{y,s} - \lambda_y\big(1 - \alpha_{y,s}\big) - \xi_{y,s} + \mu_{y,s} = 0 \ . \tag{F2}$$

1544   2) Complementary slackness:

1545 $$\omega_{y,s}\big(P_{y,s} - \psi_s\big) = 0, \tag{F3}$$

1546 $$\xi_{y,s}G_{y,s} = 0 \ , \tag{F4}$$

1547 $$\mu_{y,s}(G_{y,s} - 8760 * \phi_{y,s}P_{y,s}) = 0, \tag{F5}$$

1548 $$\sigma_{y,s}\big(p_{y,s} - P_{y,s}\big) = 0, \qquad (y \leq 2020) \ , \tag{F6}$$

1549 $$\gamma_{y,s}\big(P_{y,s} - P_{y-\Delta y,s} - q_{y,s}\big) = 0, \qquad (y = 2025) \ . \tag{F7}$$

1550   3) Primal feasibility:

1551 $$d_y - \sum_s G_{y,s}\big(1 - \alpha_{y,s}\big) = 0 \ , \tag{F8}$$

1552 $$G_{y,s} - 8760 * \phi_{y,s}P_{y,s} = 0, \tag{F9}$$

1553   4) Dual feasibility:

1554 $$\xi_{y,s} \geq 0, \omega_{y,s} \geq 0, \sigma_{y,s} \geq 0 , \gamma_{y,s} \geq 0. \tag{F10}$$

1555 For DIETER,

1556   1) Stationary conditions:

1557 $\quad \frac{\partial \mathcal{L}}{\partial \underline{P}_s} = 0 \Rightarrow \underline{c}_s + \underline{\omega}_s - \sum_h \underline{\phi}_{h,s} \underline{\mu}_{h,s} = 0$, $\underline{\phi}_{h,s} = 1$ for dispatchables, $0 < \underline{\phi}_{h,s} < 1$ for renewables $\hspace{2em}$ (F11)

1558 $\quad \frac{\partial \mathcal{L}}{\partial \underline{G}_{h,s}} = 0 \Rightarrow \underline{o}_s - \underline{\lambda}_h - \underline{\xi}_{h,s} + \underline{\mu}_{h,s} = 0$, $\hspace{16em}$ (F12)

1559 $\quad \frac{\partial \mathcal{L}}{\partial \underline{\Gamma}_{h,vre}} = 0 \Rightarrow \underline{o}_{vre} + \underline{\mu}_{h,vre} = 0$. $\hspace{16em}$ (F13)

1560 $\quad$ 2) Complementary slackness:

1561 $\quad \underline{\omega}_s \left(\underline{P}_s - \underline{\psi}_s \right) = 0,$ $\hspace{20em}$ (F14)

1562 $\quad \underline{\xi}_{h,s} \underline{G}_{h,s} = 0,$ $\hspace{20em}$ (F15)

1563 $\quad \underline{\mu}_{h,dis} \left(\underline{G}_{h,dis} - \underline{P}_{dis} \right) = 0,$ $\hspace{18em}$ (F16)

1564 $\quad$ 3) Primal feasibility:

1565 $\quad \underline{d}_h = \sum_s \underline{G}_{h,s},$ $\hspace{20em}$ (F17)

1566 $\quad \underline{G}_{h,vre} + \underline{\Gamma}_{h,vre} = \underline{\phi}_{h,vre} \underline{P}_{vre}$, $\hspace{17em}$ (F18)

1567 $\quad$ 4) Dual feasibility:

1568 $\quad \underline{\omega}_s \geq 0, \underline{\xi}_{h,s} \geq 0, \underline{\mu}_{h,dis} \geq 0$. $\hspace{18em}$ (F19)

1569 **F.2 Derivation of the zero-profit rules**

1570 **F.2.1 REMIND**

1571 The derivation of ZPRs is very similar to the one in Brown and Reichenberg, 2021. Starting with the total costs for technology s

1572 for all years, and applying various KKT conditions (after " | "),

1573 $\displaystyle\sum_y (c_{y,s} P_{y,s} + o_{y,s} G_{y,s})$

1574 $\quad = \sum_y \{ (-\omega_{y,s} + 8760 * \mu_{y,s} \phi_{y,s} + \sigma_{y,s} - \gamma_{y,s}) P_{y,s} + [\lambda_y (1 - \alpha_{y,s}) + \xi_{y,s} - \mu_{y,s}] G_{y,s} \}$ $\hspace{3em}$ | (F1), (F2)

1575 $\quad = \sum_y \{ (-\omega_{y,s} + 8760 * \mu_{y,s} \phi_{y,s} + \sigma_{y,s} - \gamma_{y,s}) P_{y,s} + [\lambda_y (1 - \alpha_{y,s}) - \mu_{y,s}] G_{y,s} \}$ $\hspace{3em}$ | (F4)

1576 $\quad = \sum_y \{ (-\omega_{y,s} + \sigma_{y,s} - \gamma_{y,s}) P_{y,s} + \lambda_y G_{y,s} (1 - \alpha_{y,s}) \}$ $\hspace{7em}$ | (F5)

1577 Rearranging, we arrive at the ZPR of multi-year uncoupled REMIND for technology cost-revenue balance:

1578 $\underbrace{\sum_y (c_{y,s} P_{y,s} + o_{y,s} G_{y,s})}_{\text{Generation cost}_s} = - \underbrace{\sum_y (\omega_{y,s} - \sigma_{y,s} + \gamma_{y,s}) P_{y,s}}_{\text{Capacity shadow revenue}_s} + \underbrace{\sum_y \lambda_y G_{y,s} (1 - \alpha_{y,s})}_{\text{Generation revenue}_s}.$ $\hspace{3em}$ (F20)

1579 Normally, when there are no capacity shadow prices, or when the capacity constraints are not binding, the cost exactly equals

1580 revenue. However, when capacity shadow prices are non-zero, i.e. the constraints (c2) and (c5-c6) are binding, the capacity

1581 shadow prices act as a distortion to the equality relation between costs and revenues. As an example, the shadow price $\omega_{y,s}$ from

1582 limited generation resources (e.g. hydroelectric power in Germany) would be positive $\omega_{y,s} > 0$, when the constraint is binding,

1583 and would appear as a "positive cost", or a "negative revenue" in the modeled power market. We can therefore put it either on

1584 the left (cost) or right (revenue) side of the equation. Here we group it together with revenues.

1585 One observes that from the right-hand-side of Eq. (F20), there is no differentiation between the annual market values of variable

1586 and dispatchable generations such as gas and solar – they are both equal to the annual electricity price λ_y.

1587 From Eq. (F20), we can derive a ZPR between levelized cost of electricity (LCOE), capacity shadow price and market value

1588 (MV), for each generator type. Taking Eq. (F20), we separate the pre-curtailment LCOE from the LCOE due to curtailment,

1589 then divide by total post-curtailment generation $\sum_y G_{y,s}(1-\alpha_{y,s})$ for the generator type s, to obtain the technology-specific

1590 ZPR:

1594
$$\underbrace{\frac{\sum_y(c_{y,s}P_{y,s}+o_{y,s}G_{y,s})}{\sum_y G_{y,s}}}_{\text{Pre-curtailment LCOE}_s}+\underbrace{\frac{\sum_y(c_{y,s}P_{y,s}+o_{y,s}G_{y,s})\alpha_{y,s}}{\sum_y G_{y,s}(1-\alpha_{y,s})}}_{\text{Curtailment LCOE}_s}=-\underbrace{\frac{\sum_y(\omega_{y,s}-\sigma_{y,s}+\gamma_{y,s})P_{y,s}}{\sum_y G_{y,s}(1-\alpha_{y,s})}}_{\text{Capacity shadow price}_s}+\underbrace{\frac{\sum_y\lambda_y G_{y,s}(1-\alpha_{y,s})}{\sum_y G_{y,s}(1-\alpha_{y,s})}}_{\text{Market Value}_s}. \tag{F21}$$

1591 The pre-curtailment LCOE is the cost of one unit of generated electricity – regardless whether it is curtailed or being used to

1592 meet demand, whereas the curtailment LCOE is the cost of one unit of curtailed electricity. Together they add up to post-

1593 curtailment LCOE, i.e. the cost of one unit of usable electricity.

1595 To obtain the ZPR for the whole power system in REMIND, we first sum Eq. (F20) over all generator types s, and obtain the

1596 ZPR for system cost and revenue. Then dividing by total post-curtailment system generation, and split the LCOE into pre-

1597 curtailment and curtailment components, we get

1598
$$\underbrace{\frac{\sum_{y,s}(c_{y,s}P_{y,s}+o_{y,s}G_{y,s})}{\sum_{y,s} G_{y,s}}}_{\text{Pre-curtailment LCOE}_{\text{system}}}+\underbrace{\frac{\sum_{y,s}(c_{y,s}P_{y,s}+o_{y,s}G_{y,s})\alpha_{y,s}}{\sum_{y,s} G_{y,s}(1-\alpha_{y,s})}}_{\text{Curtailment LCOE}_{\text{system}}}=-\underbrace{\frac{\sum_{y,s}(\omega_{y,s}-\sigma_{y,s}+\gamma_{y,s})P_{y,s}}{\sum_{y,s} G_{y,s}(1-\alpha_{y,s})}}_{\text{Capacity shadow price}_{\text{system}}}+\underbrace{\frac{\sum_{y,s}\lambda_y G_{y,s}(1-\alpha_{y,s})}{\sum_{y,s} G_{y,s}(1-\alpha_{y,s})}}_{\text{Electricity Price}_{\text{system}}}, \tag{F22}$$

1599 i.e. the LCOE of the system for usable (pre-curtailment) power, which is equal to the sum of the system LCOE for total power

1600 generated and the curtailment cost, can be recovered by the average electricity price of the system minus system-wide capacity

1601 constraint shadow price per energy unit.

1602 The ZPRs of REMIND hold for the aggregate over multiple years.

1603 From Eqs. (F21)-(F22), we learn that when a market equilibrium can be found, i.e. when the optimization problem can be

1604 successfully solved, there is an equality relation between the generation cost and market value for each generator type, and

1605 similarly between generation cost and price of electricity for the entire system. Capacity shadow prices due to various extra

1606 capacity constraints imposed on the models, distort the equality relation between costs and prices by a linear term, making the

1607 prices be either higher or lower than the costs at the market equilibrium.

1608 **F.2.2 DIETER**

1609 Similar to uncoupled REMIND, from KKT conditions, at stationarity, we can obtain the cost-revenue ZPR for a single

1610 technology s for standalone DIETER. We take the total costs for technology s for all years, and applying various KKT

1611 conditions (after " | "),

1612 $$\underline{c_s}\underline{P_s}+\sum_h\left[\underline{o_s}\left(\underline{G_{h,s}}+\underline{\Gamma_{h,vre}}\right)\right]$$

1613 $$=\left(-\underline{\omega_s}+\sum_h\underline{\phi_{h,s}}\underline{\mu_{h,s}}\right)\underline{P_s}+\sum_h\left(\underline{\lambda_h}-\underline{\mu_{h,s}}+\underline{\xi_{h,s}}\right)\left(\underline{G_{h,s}}+\underline{\Gamma_{h,vre}}\right) \qquad\qquad\mid\text{(F11),(F12)}$$

1614 $$=-\underline{\omega_s}\,\underline{P_s}\ +\sum_h\underline{\phi_{h,vre}}\underline{\mu_{h,vre}}\underline{P_{vre}}+\sum_h\left(\underline{\lambda_h}-\underline{\mu_{h,vre}}+\underline{\xi_{h,vre}}\right)\left(\underline{G_{h,vre}}+\underline{\Gamma_{h,vre}}\right)+\sum_h\underline{\mu_{h,dis}}\underline{P_{dis}}+\sum_h\left(\underline{\lambda_h}-\underline{\mu_{h,dis}}\right)\underline{G_{h,dis}}$$

1615 $\mid$ split $\sum_h\underline{\phi_{h,s}}\underline{\mu_{h,s}}$ into vre and dis, apply (F15) for dispatchable, i.e. $\underline{\xi_{h,dis}}\underline{G_{h,dis}}=0$

1616 $$=-\underline{\omega_s}\,\underline{P_s}\ +\sum_h\underline{\phi_{h,vre}}\underline{\mu_{h,vre}}\underline{P_{vre}}+\sum_h\left(\underline{\lambda_h}-\underline{\mu_{h,vre}}+\underline{\xi_{h,vre}}\right)\left(\underline{G_{h,vre}}+\underline{\Gamma_{h,vre}}\right)+\sum_h\underline{\lambda_h}\underline{G_{h,dis}} \qquad\qquad\mid\text{(F16)}$$

1617 $$=-\underline{\omega_s}\,\underline{P_s}\ +\sum_h\underline{\lambda_h}\underline{G_{h,vre}}+\ \sum_h\left(\underline{\lambda_h}+\underline{\xi_{h,vre}}\right)\underline{\Gamma_{h,vre}}+\sum_h\underline{\lambda_h}\underline{G_{h,dis}} \qquad\mid\text{(F18), apply (F15) for VRE, i.e. }\underline{\xi_{h,vre}}\underline{G_{h,vre}}=0$$

1618 $$=-\underline{\omega_s}\,\underline{P_s}\ +\sum_h\underline{\lambda_h}\underline{G_{h,vre}}+\sum_h\underline{\lambda_h}\underline{G_{h,dis}} \qquad\qquad\mid\text{(F12) \& (F13)}\Rightarrow\underline{\lambda_h}+\underline{\xi_{h,vre}}=0$$

1619 Rearranging, we arrive at the ZPR of single-year uncoupled DIETER for technology-specific cost-revenue balance:

1620 $$\underbrace{c_s P_s + o_s \sum_h \left(G_{h,s} + \Gamma_{h,vre}\right)}_{\text{Annual generation cost}_s} = - \underbrace{\omega_s P_s}_{\text{Annual capacity shadow revenue}_s} + \underbrace{\sum_h \lambda_h G_{h,s}}_{\text{Annual generation revenue}_s} . \qquad (F23)$$

1621 Dividing Eq. (F23) by annual aggregated generation of technology s, we obtain the technology-specific ZPR for DIETER,

1622 $$\underbrace{\frac{c_s P_s + o_s \sum_h \left(G_{h,s} + \Gamma_{h,vre}\right)}{\sum_h G_{h,s}}}_{\text{LCOE}_s} = - \underbrace{\frac{\omega_s P_s}{\sum_h G_{h,s}}}_{\text{Annual capacity shadow price}_s} + \underbrace{\frac{\sum_h \lambda_h G_{h,s}}{\sum_h G_{h,s}}}_{\text{Market value}_s} . \qquad (F24)$$

1623 One observes that from the term of $\underline{Market\ Value_s}$, compared to the REMIND case (right-hand-side of Eq. (F21)), DIETER

1624 has differentiated annual market values of gas and solar generators.

1625 Summing Eq. (F24) over s, dividing both sides by total annual generation $\sum_{h,s} G_{h,s}$, using identity $\underline{d_h} = \sum_s G_{h,s}$ for

1626 simplification, we obtain the ZPR for the whole power system in DIETER,

1627 $$\underbrace{\frac{\sum_s [c_s P_s + o_s \sum_h (G_{h,s} + \Gamma_{h,vre})]}{\sum_{h,s} G_{h,s}}}_{\text{LCOE}_{\text{system}}} = - \underbrace{\frac{\sum_s \omega_s P_s}{\sum_{h,s} G_{h,s}}}_{\text{Annual capacity shadow price}_{\text{system}}} + \underbrace{\frac{\sum_h \lambda_h d_h}{\sum_h d_h}}_{\text{Annual average electricity price}_{\text{system}}} . \qquad (F25)$$

1628 Similar to the case of REMIND, Eqs. (F24)-(F25) show us the equality relations between cost and value (or price) for each

1629 generator type and for the system hold also for DIETER at its market equilibrium. Compared to REMIND, there are no brown-

1630 field or near-term capacity shadow price contributions in DIETER in the standalone versions. The DIETER ZPRs hold for one

1631 year instead of the aggregate of multiple years like in REMIND. For simplicity, even though it is possible to write the LCOE in

1632 pre-curtailment and curtailment terms, but because for DIETER it is relatively cumbersome to do, we do not do it here.

1633 In summary, at REMIND and DIETER power market equilibriums, each generator exactly recovers its cost of one unit of

1634 generation through market value, and obtains "zero profit" under a completely competitive market over its modeling time. In the

1635 aggregate, the entire power sector obtains its cost of one unit of generation through the price of electricity that the consumer

1636 pays. Both types of relations can be distorted by the existence of capacity shadow prices.

1637 **Appendix G: Derivation of the equilibrium conditions for the coupled models**

1638 Here in this Appendix, we gradually build up the derivation for the ZPRs of the coupled REMIND and DIETER, which will be

1639 used later for validating numerical results. The derivation consists of three steps:

1640   1) ZPRs for the uncoupled model REMIND and DIETER;

1641   2) ZPRs for coupled model REMIND and DIETER (simplified version, only considering convergence condition (h1-h7));

1642   3) ZPRs for coupled model REMIND and DIETER (full version, also considering (c7 and c8)).

1643 Step (1) is entirely derived in Appendix F.

1644 For step (2), based on the uncoupled ZPRs, we recognize that from convergence condition (h1-h7), the only condition which

1645 impacts the form of the ZPR is (h3), because the markup terms modify the objective function of the (simplified) coupled version

1646 of REMIND (Eq. (6)). Following similar procedure as in Appendix F, we can derive the technology-specific ZPR for the

1647 coupled REMIND (simplified version) as follows:

1648 $$\underbrace{\frac{\sum_y (c_{y,s} P_{y,s} + o_{y,s} G_{y,s})}{\sum_y G_{y,s}}}_{\text{Pre-curtailment LCOE}_s} + \underbrace{\frac{\sum_y (c_{y,s} P_{y,s} + o_{y,s} G_{y,s}) \alpha_{y,s}}{\sum_y G_{y,s}(1 - \alpha_{y,s})}}_{\text{Curtailment cost}_s} = - \underbrace{\frac{\sum_y (\omega_{y,s} - \sigma_{y,s} + \gamma_{y,s}) P_{y,s}}{\sum_y G_{y,s}(1 - \alpha_{y,s})}}_{\text{Capacity shadow price}_s} + \underbrace{\frac{\sum_y (\lambda_y + \underline{\eta}_{y,s}) G_{y,s}(1 - \alpha_{y,s})}{\sum_y G_{y,s}(1 - \alpha_{y,s})}}_{\text{Market Value}_s} . \qquad (G1)$$

1649 Compared with the ZPR of the uncoupled version (F24), the only difference is that we replace the market value in the uncoupled

1650 REMIND λ_y with the DIETER-markup corrected market value $\lambda_y + \underline{\eta}_{y,s}$. DIETER's ZPR is unchanged at this step.

1651   Step (3) involves two extra capacity constraints, one in each model, the first of which, (c7), is discussed in detail in Appendix H.

1652   The implementation of (c7) further modifies Eq. (G1) and results in the ZPRs of the coupled REMIND. The other constraint

1653   (c8) will be the focus of discussion here. It only modifies the ZPRs for the coupled DIETER and not for the coupled REMIND.

1654   Constraint (c8) is a brown-field capacity constraint implemented in DIETER to address the fact that DIETER is a green-field

1655   model, which is otherwise ignorant about standing-capacities in the real world. There are many ways we can implement this

1656   standing capacity constraint in DIETER. The most straight-forward way is to implement the "standing capacity" at the

1657   beginning of each REMIND period, which REMIND sees before it invests additional capacities, as a lower bound on

1658   endogenous capacities in DIETER. This helps put DIETER and REMIND on equal footing before the 5- or 10-year investment

1659   period starts, allowing us to compare their investment intentions.

1660   c8) "standing capacity constraint" in DIETER, i.e. DIETER capacities at time y need to be larger or equal to the REMIND

1661   standing capacities at the beginning of the time period:

1662 $\underline{P}_s \geq P_{y-\Delta y/2,s}/(1-ER) \quad \perp \underline{\varsigma}_s \, ,$

1663   where the time-step Δy is divided by 2 because the representative year in REMIND is in the middle of the time step, ER is

1664   the endogenous early retirement rate in REMIND.

1665   The reason we implement the standing capacity in this way, is in part because as a proof-of-concept, we want to give DIETER

1666   endogenous freedom to invest in all model years, so we use only the pre-investment capacities as "soft" corridors to bound the

1667   DIETER capacities from below. If we were to transfer precisely the brown-field and near-term constraints from REMIND to

1668   DIETER, it requires a complete list of constraints for each technology, and an identical implementation of all of them in

1669   DIETER. This may raise the precision of convergence in some years for some technologies, but in practice it can be more

1670   complicated to implement than a generic lower bound for all technologies.

1671   To obtain the ZPRs of coupled DIETER, we simply modify the capacity shadow price term of the uncoupled DIETER ZPRs

1672   (Eqs. (F24)-(F25)) by the additional capacity shadow price $\underline{\varsigma}_s$ from (c8):

1673 $\underline{Capacity\ shadowprice}'_s = \frac{\left(\omega_s + \underline{\varsigma}_S\right)\underline{P}_s}{\sum_h \underline{G}_{h,s}},$ (G2)

1674 $\underline{Capacity\ shadowprice}'_{system} = \frac{\sum_s\left(\omega_s + \underline{\varsigma}_S\right)\underline{P}_s}{\sum_{h,s} \underline{G}_{h,s}} \, .$ (G3)

1675   **Appendix H: Additional methods for numerical stability in coupled runs**

1676   Here, we introduce the two methods we employed to improve numerical stability of the coupled runs: 1) the dispatchable

1677   capacity constraint by peak demand to avoid high markups being exchanged (Sect. H.1); 2), endogenous prefactors for all

1678   quantities from last-iteration DIETER to current-iteration REMIND (Sect. H.2).

1679   **H.1 Dispatchable capacity constraints by peak demand**

1680   **H.1.1 Description of the capacity constraint and price manipulation in DIETER post-processing**

1681   Scarcity hour price can occur in a PSM run, which is the highest hourly price in a year, and it is usually equal to the annuitized

1682   fixed cost of Open Cycle Gas Turbine (OCGT) (capital investment cost and fixed O&M costs) (Hirth and Ueckerdt, 2013). In

1683   our simulations, the scarcity prices are usually above 50\$/KWh. If we include the scarcity price into the markups, OCGT will

1684   receive an annual markup usually more than 5 times higher than the annual average electricity price. The high markup results in

1685   OCGT plants receiving too high an incentive in the next iteration REMIND, and the model overshoots (overinvests) in

1686   capacities. Over iterations, this causes oscillations in the quantity and prices in the coupled model. For better numerical stability,

1687   instead of passing on the full markups from DIETER, we only pass on the portion of the annual markups unrelated to scarcity

1688   hour prices, and replace the exchange of the part of the markup due to scarcity hours from DIETER to REMIND with

1689   implementing an additional capacity constraint in REMIND for coupled runs. The two actions can be later shown to be

1690   mathematically equivalent. Generators other than OCGT which produce at the scarcity hours also get paid in the hour at this

1691   high price. However, because they also produce at other hours with lower prices, their average market values are only

1692   moderately impacted by the scarcity hour price, and do not in general lead to instability issues.

1693   Below, we first introduce the aforementioned capacity constraint implemented on the side of REMIND, then discuss the

1694   corresponding manipulation of the markups in DIETER. Lastly, we show their mathematical equivalence, and state the modified

1695   ZPR of coupled REMIND due to these actions.

1696   The extra capacity constraint states that the sum of all dispatchable capacities needs to be at least as large as the peak residual

1697   demand:

1698   c7) $\sum_{dis} P_{y,dis} > d_{y,residual} \quad \perp v_{y,dis}$,

1699   where $d_{y,residual}$ is peak residual demand in REMIND and is semi-endogenous. $d_{y,residual}$ is a function of the peak hourly

1700   residual demand in the last iteration of DIETER $\underline{d}_{residual}(y, i-1)$. The peak hourly residual demand in DIETER is in turn

1701   defined as the maximum hourly amount of inflexible demand not met by wind, solar or hydro generations, and hence must

1702   be met by dispatchable generations (under no storage conditions):

1703 $\underline{d}_{residual} = max_h\left(\underline{d}_h - \underline{G}_{h,Solar} - \underline{G}_{h,Wind} - \underline{G}_{h,Hydro}\right).$ (H1)

1704 $v_{y,dis}$ is the shadow price of the capacity constraint for dispatchable technology dis.

1705   For the exact implementation of (c7) in coupled run, see Sect. 3.3.2, 2. Under storage implementation, in addition to the

1706   variable renewable contribution, the hourly storage discharge is also subtracted from the residual demand.

1707   Simultaneous to implementing this capacity constraint, we remove the surplus scarcity prices in post-processing of DIETER

1708   before passing it onto REMIND. In DIETER, we define the scarcity price as the maximum hourly price in a year:

1709 $\underline{\lambda}_{y,h_{scar}} = max_h(\underline{\lambda}_{y,h})$,   (H2)

1710   and the surplus scarcity hour price is the difference between the scarcity price and the second highest price:

1711 $\underline{\lambda}_{y,surplus} = \underline{\lambda}_{y,h_{scar}} - max(\underline{\lambda}_{y,h|h\neq h_{scar}}) = max_h(\underline{\lambda}_{y,h}) - max(\underline{\lambda}_{y,h|h\neq h_{scar}}),$ (H3)

1712   where h_{scar} is the scarcity hour when scarcity price occurs, corresponding to the peak residual demand hour.

1713   Using this, we manipulate the market value and annual average electricity price in DIETER ex post, excluding the surplus

1714   scarcity hour price:

1715 $\underline{MV}'_s = \dfrac{\sum_{h| h\neq h_{scar}} G_{h,s}\underline{\lambda}_h + \sum_{h| h_{scar}} G_{h,s} * max(\underline{\lambda}_{h|h\neq h_{scar}})}{\sum_{h=1}^{8760} G_{h,s}},$ (H4)

1716 $\underline{J}' = \dfrac{\sum_{h| h\neq h_{scar}} \underline{d}_h\underline{\lambda}_h + \sum_{h| h_{scar}} \underline{d}_h * max(\underline{\lambda}_{h|h\neq h_{scar}})}{\sum_{h=1}^{8760} \underline{d}_h}.$ (H5)

1717   where $\underline{MV}'_s$ is the annual average market value without the surplus scarcity hour price, and $\underline{J}'$ is the annual average electricity

1718   price without the surplus scarcity hour price. Thus, the corresponding modified markup term without the surplus scarcity hour

1719   price is:

1720 $\underline{\eta}'_s = \underline{MV}'_s - \underline{J}'.$ (H6)

1721   Note that since the above manipulation is done in a post-processing step, the LCOE in DIETER is still fully covered by MV, as

1722   the KKT conditions and ZPRs still hold by default in an optimized DIETER model.

1723   With the implementation of (c7), the coupled ZPR (Eq. (G1)) is then further modified to include the new shadow price $v_{y,s}$ as

1724   well as the modified markup $\underline{\eta}'_{y,s}$ (without surplus scarcity price). (We write from now on $v_{y,dis}$ simply as $v_{y,s}$.) Then,

1725   technology-specific ZPR of coupled REMIND is:

1726
$$\underbrace{\frac{\sum_y (c_{y,s}P_{y,s}+o_{y,s}G_{y,s})}{\sum_y G_{y,s}}}_{\text{Pre-curtailment LCOE}_s} + \underbrace{\frac{\sum_y (c_{y,s}P_{y,s}+o_{y,s}G_{y,s})\alpha_{y,s}}{\sum_y G_{y,s}(1-\alpha_{y,s})}}_{\text{Curtailment LCOE}_s} = -\underbrace{\frac{\sum_y (\omega_{y,s}-\sigma_{y,s}+\gamma_{y,s}+v_{y,s})P_{y,s}}{\sum_y G_{y,s}(1-\alpha_{y,s})}}_{\text{Capacity shadow price}'_s} + \underbrace{\frac{\sum_y (\lambda_y+\underline{\eta}'_{y,s})G_{y,s}(1-\alpha_{y,s})}{\sum_y G_{y,s}(1-\alpha_{y,s})}}_{\text{Market Value}'_s}$$
(H7)

1727   System ZPR of coupled REMIND is:

1728
$$\underbrace{\frac{\sum_{y,s} (c_{y,s}P_{y,s}+o_{y,s}G_{y,s})}{\sum_{y,s} G_{y,s}}}_{\text{Pre-curtailment LCOE}_{system}} + \underbrace{\frac{\sum_{y,s} (c_{y,s}P_{y,s}+o_{y,s}G_{y,s})\alpha_{y,s}}{\sum_{y,s} G_{y,s}(1-\alpha_{y,s})}}_{\text{Curtailment cost}_{system}} = -\underbrace{\frac{\sum_{y,s} (\omega_{y,s}-\sigma_{y,s}+\gamma_{y,s}+v_{y,s})P_{y,s}}{\sum_{y,s} G_{y,s}(1-\alpha_{y,s})}}_{\text{Capacity shadow price}'_{system}} + \underbrace{\frac{\sum_{y,s} (\lambda_y+\underline{\eta}'_{y,s})G_{y,s}(1-\alpha_{y,s})}{\sum_{y,s} G_{y,s}(1-\alpha_{y,s})}}_{\text{Electricity Price}'_{system}}$$
(H8)

1729   These are the ZPRs of the coupled REMIND for the full version.

1730   **H.1.2 Equivalence between surplus scarcity price in DIETER and capacity shadow price due to peak residual demand in**
1731   **REMIND**

1732   Because of the intuitive relation between the scarcity price and the peak residual demand – i.e., that scarcity price occurs in the

1733   hour with peak hourly residual demand due to the pricing power of the peaker gas turbines in the hour where VRE is most

1734   scarce, we can draw a quantitative equivalence between the scarcity price contribution to the markup and the capacity constraint

1735   shadow price v_y. This means that the revenue the plant receives in scarcity hour in capacity terms (i.e. capacity credit), can be

1736   transformed directly to a revenue in energy terms (i.e. a part of the annual market value). At convergence, for any given year y,

1737   the negative shadow price, $-v_{y,dis}$, when translated into annual generation terms via capacity factor $\phi_{y,s}$ of dispatchable

1738   technology s, should be equal to the scarcity hour surplus revenue divided by annual generation by s in DIETER:

1739
$$\frac{-v_{y,dis}}{\phi_{y,dis}*8760} = \frac{\lambda_{y,surplus}\,\underline{G}_{h_{scar},dis}}{\sum_h \underline{G}_{y,h,dis}} \,.$$
(H9)

1740   In practice, this equivalence is confirmed by numerical results (e.g. Fig. 8 subplot for OCGT).

1741   Using this equivalence, we can show as follows, that at convergence, λ_y should be equal to DIETER power price without

1742   surplus scarcity price $\underline{J}'$ (Eq. (H5)), and $\lambda_y + \underline{\eta}'_{y,s}$ should be equal to DIETER market value without scarcity price $\underline{MV}'$ (Eq.

1743   (H4)).

1744   At convergence, the annual generations have identical solutions in the two models, i.e. $\sum_h \underline{G}_{y,h,s} = G_{y,s}(1-\alpha_{y,s})$. We plug this

1745   and REMIND capacity factor $\phi_{y,s} = \frac{G_{y,s}(1-\alpha_{y,s})}{P_{y,s}*8760}$ into Eq. (H9) to obtain

1746 $v_y P_{y,s} = \underline{\lambda}_{y,surplus}\,\underline{G}_{y,h_{scar},s}.$ (H10)

1747   Take Eq. (H7), and only consider REMIND annual revenue by multiplying generation $\sum_y G_{y,s}(1-\alpha_{y,s})$ then on the right-

1748   hand-side, take both revenue and the capacity shadow revenue contribution from $v_{y,s}$ for a single year, which is equal to the total

1749   single-year REMIND revenue:

1750
$$\Theta_{y,s} = -\underbrace{v_{y,s}P_{y,s}}_{\text{Capacity shadow revenue from c(7)}_s} + \underbrace{\left(\lambda_y + \underline{\eta}'_{y,s}\right)G_{y,s}\left(1-\alpha_{y,s}\right)}_{\text{Generation revenue}'_s}$$

1751   and plug in (H10), (H6),

1752
$$\Theta_{y,s} = \underbrace{\lambda_{y,surplus}\underline{G}_{y,h_{scar},s}}_{\text{surplus scarcity revenue in scarcity hour}_s} + \underbrace{\left(\underline{MV}'_{y,s} - \underline{J}'_y + \lambda_y\right)G_{y,s}\left(1-\alpha_{y,s}\right)}_{\text{Generation revenue}'_s}.$$

1753   Plugging in (H4),

1754 $\Theta_{y,s} = \underline{\lambda}_{y,surplus}\underline{G}_{y,h_{scar},s} + \sum\limits_{h \neq h_{scar}} \underline{G}_{y,h,s}\underline{\lambda}_{y,h} + \underline{G}_{y,h_{scar},s} * \max(\underline{\lambda}_{y,h|h \neq h_{scar}}) - \underline{J}'_y G_{y,s}(1 - \alpha_{y,s}) + \lambda_y G_{y,s}(1 - \alpha_{y,s})$

1755 Lastly, plug in the definition for $\underline{\lambda}_{y,surplus}$ (Eq. (H3)),

1756 $\Theta_{y,s} = \sum_h \underline{\lambda}_{y,h}\underline{G}_{y,h,s} - \underline{J}'_y G_{y,s}(1 - \alpha_{y,s}) + \lambda_y G_{y,s}(1 - \alpha_{y,s})$. (H11)

1757 Since the single-year revenue $\Theta_{y,s}$ in REMIND should be aligned with DIETER due to harmonization condition (h3), and the

1758 DIETER revenue is $\underline{\Theta}_{y,s} = \sum_h \underline{\lambda}_{y,h} \underline{G}_{y,h,s}$, that means the last two terms in (H11) should sum to 0. Therefore REMIND

1759 electricity price λ_y should be equal to $\underline{J}'_y$.

H.2 Stabilization techniques using prefactors

1761 In this Appendix, we describe the detailed implementations of prefactors for information exchanged from DIETER to REMIND.

1762 1. Markup prefactor:

1763 In order to facilitate convergence in REMIND, we implement an endogenous prefactor $f^{\eta}_{y,s}$ for MV in the REMIND

1764 markup equation Eq. (5):

1765 $\eta_{y,s}(i) = f^{\eta}_{y,s}(i) * \underline{MV}'_{y,s}(i-1) - \underline{J}'_y(i-1)$. (H12)

1766 The endogenous prefactor $f^{\eta}_{y,s}$ is dependent on the difference between in-iteration endogenous generation share and last-

1767 iteration DIETER generation share:

1768 $f^{\eta}_{y,s}(i) = 1 - \underline{b}_{y,s}(i-1)\Delta S_{y,s}$, (H13)

1769 where $\underline{b}_{y,s}$ is a positive parameter, equal to the ratio between market values and average price depending on their

1770 relationship in the last iteration DIETER,

1771 $\underline{b}_{y,s} = \frac{\underline{MV}'_{y,s}}{\underline{J}'_y}$ if $\underline{MV}'_{y,s} > \underline{J}'_y$,

1772 $\underline{b}_{y,s} = \frac{\underline{J}'_y}{\underline{MV}'_{y,s}}$ if $\underline{MV}'_{y,s} < \underline{J}'_y$,

1773 and where the generation share difference across models and consecutive iteration $\Delta S_{y,s}$ is,

1774 $\Delta S_{y,s} = \frac{G_{y,s}(i)(1 - \alpha_{y,s}(i))}{\sum_s[G_{y,s}(i)(1 - \alpha_{y,s}(i))]} - \frac{\sum_h \underline{G}_{y,s}(i-1)}{\sum_{h,s} \underline{G}_{y,s}(i-1)}$.

1775 The values of $\underline{b}_{y,s}$ are heuristically determined (see Sect. 6.2).

1776 When in-iteration REMIND solar generation share increases due to the price signal from the last-iteration DIETER market

1777 value, such that the REMIND share is larger than in the last DIETER iteration, the formula Eq. (H13) results in a prefactor

1778 smaller than one, decreasing in-iteration markup $\eta_{y,s}(i)$.

1779 2. Peak demand prefactor:

1780 The peak demand in REMIND $d_{residual,y}$ depends on the last iteration DIETER peak hourly residual demand

1781 $\underline{d}_{residual}(y, i-1)$. Implementing it in constraint (c7),

1782 $\sum_{dis} P_{y,dis} < d_{residual,y} * f^{d_{residual}}_y(i)$,

1783 for iteration i, we use $f^{d_{residual}}_y(i)$ as a prefactor for stabilization,

1784 $f^{d_{residual}}_y(i) = 1 - b_{y,peak} * \Delta S_{y,wind}$.

1785 $b_{y,peak}$ is a heuristic constant dependent on y, $\Delta S_{y,wind}$ is the wind generation share. We use the wind generation share in

1786 the current iteration of REMIND for stabilization, because in the peak residual demand hour, there usually is some wind

1787 production for the historical year we chose (but no solar). In general, $b_{y,peak}$ is 0.5 for earlier years, and increasing to 1 for

1788   later years, under a baseline scenario. For climate scenarios, $b_{y,peak}$ is around 1.5 for less stringent scenarios, and for more

1789   stringent scenarios, it is 0.5 for earlier years, and increasing to 3 for later years.

1790   3. Capacity factor prefactor:

1791   We set REMIND capacity factor $\phi_{y,dis}$ to be equal to the DIETER annual average capacity factor from the last iteration

1792   multiplied by a prefactor:

1793 $\phi_{y,dis}(i) = \underline{\phi}_{dis}(y, i-1) * f_{y,s}^{\phi_{dis}}(i),$

1794   where DIETER annual average capacity factor is $\underline{\phi}_{dis} = \frac{\Sigma_h \underline{G}_{h,dis}}{\underline{P}_{dis}* 8760}$ for each year y. In order to facilitate convergence, a

1795   similar prefactor $f_{y,s}^{\phi_{dis}}$ as in Eq. (H13) is implemented:

1796 $f_{y,s}^{\phi_{dis}}(i) = 1 - 0.5\Delta S_{y,s}$ if $\underline{\phi}_{dis}(y,i-1) < 0.5$ (i.e. the plant is "peaker" or "mid-load" type in the last iteration),

1797 $f_{y,s}^{\phi_{dis}}(i) = 1 + 0.5\Delta S_{y,s}$ if $\underline{\phi}_{dis}(y,i-1) \geq 0.5$ (i.e. the plant is "base-load" type in the last iteration),

1798   where 0.5 is a heuristic factor.

1799   The sign in the prefactor formula is determined based on the observation that under a system with variable renewable

1800   generations, for generator plants that have relatively high running cost and low investment cost, i.e. they are most

1801   economically operated as "peaker" plants or as "mid-load" plants of lower capacity factor, so when their generation share

1802   incrementally increases, their capacity factor decreases. Conversely, for generators with relatively low running cost and

1803   high investment cost, i.e. they are most economically operated as "base-load" plants, when their generation share

1804   incrementally increases, their capacity factor increases.

1805   4. Curtailment prefactor:

1806   The curtailment ratio in REMIND $\alpha_{y,vre}$ is equal to last iteration DIETER curtailment ratio, multiplied by prefactor $f_{y,vre}^{\alpha}$:

1807 $\alpha_{y,vre}(i) = \frac{\Sigma_h \underline{\gamma}_{h,vre}(y,i-1)}{\Sigma_{h,s} \underline{G}_{h,vre}(y,i-1)} * f_{y,vre}^{\alpha}(i)$,

1808   where the prefactor is $f_{y,vre}^{\alpha}(i) = 1 + \Delta S_{y,vre}$.

1809   5. Capture price prefactor:

1810   Similar to the case of markup from the demand side, the markup for any demand-side technology given to REMIND is:

1811 $\eta_{y,s_d}(i) = f_{y,s_d}^{\eta}(i) * \underline{CP}_{y,s_d}(i-1) - \underline{J}_y(i-1)$,

1812   where $\underline{J}_y$ is the annual average electricity price of all demand types s_d for period y,

1813 $\underline{J} = \frac{\Sigma_h \left(\Sigma_{s_d} \underline{d}_{h,s_d}\right)*\underline{\lambda}_h}{\Sigma_{h,s_d} \underline{d}_{h,s_d}}$,

1814   and $f_{y,s_d}^{\eta}(i)$ is an endogenous stabilization prefactor for the flexible-demand markup based on shares of demand by s_d in

1815   total demand for each year.

1816   **Appendix I: Derivation for equilibrium condition for REMIND in the case of additional adjustment cost**

1817   Adjustment cost – an additional linear term in the objective function, acts as an inertia against fast or slow capacity additions or

1818   retirement. The implementation of positive adjustment costs mimics the challenges of scaling up the supply chains and of

1819   training new workers to do installation and construction. Adjustment costs are applied to all model time periods, so it is by

1820   nature intertemporal. The objective function for power sector including the adjustment cost $\Xi_{y,s}$ is

1821 $Z = \sum_{y,s}(c_{y,s}P_{y,s} + o_{y,s}G_{y,s} + \Xi_{y,s})$,

1822   where $\Xi_{y,s}$ is a quadratic function of the difference between capacity additions of subsequent time periods $y - \Delta y$ and y:

1823 $\Xi_{y,s} = c_{y,s} k_s \left(\frac{\Delta P_{y,s} - \Delta P_{y-\Delta y,s}}{\Delta y^2}\right)^2 / \left(\frac{\Delta P_{y-\Delta y,s}}{\Delta y} + \beta_{y,s}\right),$

1824 where $\Delta P_{y,s}$ is as before the capacity addition during time period y of technology s, $\beta_{y,s}$ is an offset parameter to offset additions

1825 in initial time periods, k_s is a regional technological coefficient, $c_{y,s}$ is the capital expenditure cost per capacity unit as before.

1826 Because the adjustment cost is a quadratic function of the endogenous variable $P_{y,s}$, it turns the power sector cost minimization

1827 in REMIND into a nonlinear problem.

1828 Similar to the case without adjustment costs in Sect. 3.2.3, the first stationary condition becomes:

1829 $\frac{\partial \mathcal{L}}{\partial P_{y,s}} = 0, \Rightarrow c_{y,s} + \omega_{y,s} - \mu_{y,s}\phi_{y,s} - \sigma_{y,s} + \gamma_{y,s} + 2c_{y,s}k_s \frac{\Delta P_{y,s} - \Delta P_{y-\Delta y,s}}{(\Delta P_{y-\Delta y,s} + \beta_{y,s})\Delta y^2} = 0 ,$

1830 simplifying,

1831 $c_{y,s} = -\omega_{y,s} + \mu_{y,s}\phi_{y,s} + \sigma_{y,s} - \gamma_{y,s} - a_{y,s}\,c_{y,s} ,$

1832 where $a_{y,s} = 2k_s \frac{\Delta P_{y,s} - \Delta P_{y-\Delta y,s}}{(\Delta P_{y-\Delta y,s} + \beta_{y,s})\Delta y^2}$ is the endogenous adjustment factor of investment, and is a function of capacity.

1833 The new ZPR including the adjustment cost in terms of cost and revenue for technology s, can be derived

1834 $\sum_y \left[(c_{y,s} + a_{y,s}c_{y,s})P_{y,s} + o_{y,s}G_{y,s} + \lambda_y\,\alpha_{y,s}G_{y,s} + (\omega_{y,s} - \sigma_{y,s} + \gamma_{y,s})P_{y,s}\right] = \sum_y(\lambda_y G_{y,s}) .$

1835 The adjustment cost $a_{y,s}\,c_{y,s}$ can act as a disincentive or an incentive to capacity additions. If capacity addition in the current

1836 period is higher than in the last period $\Delta P_{y,s} > \Delta P_{y-\Delta y,s}$, i.e. a ramp-up case of capacity addition, the adjustment cost is positive

1837 and acts as a disincentive, so the ramp-up speed is slower. When added capacities are decreasing with time, i.e. a ramp-down

1838 case of capacity addition, adjustment cost is negative and acts as an incentive, and as a result, the ramp-down speed is slower.

1839 In the coupled run we see only a moderate adjustment cost which drops down fast as a function of time (see e.g. Fig.6).

Appendix J: Comparing the coupled and uncoupled run
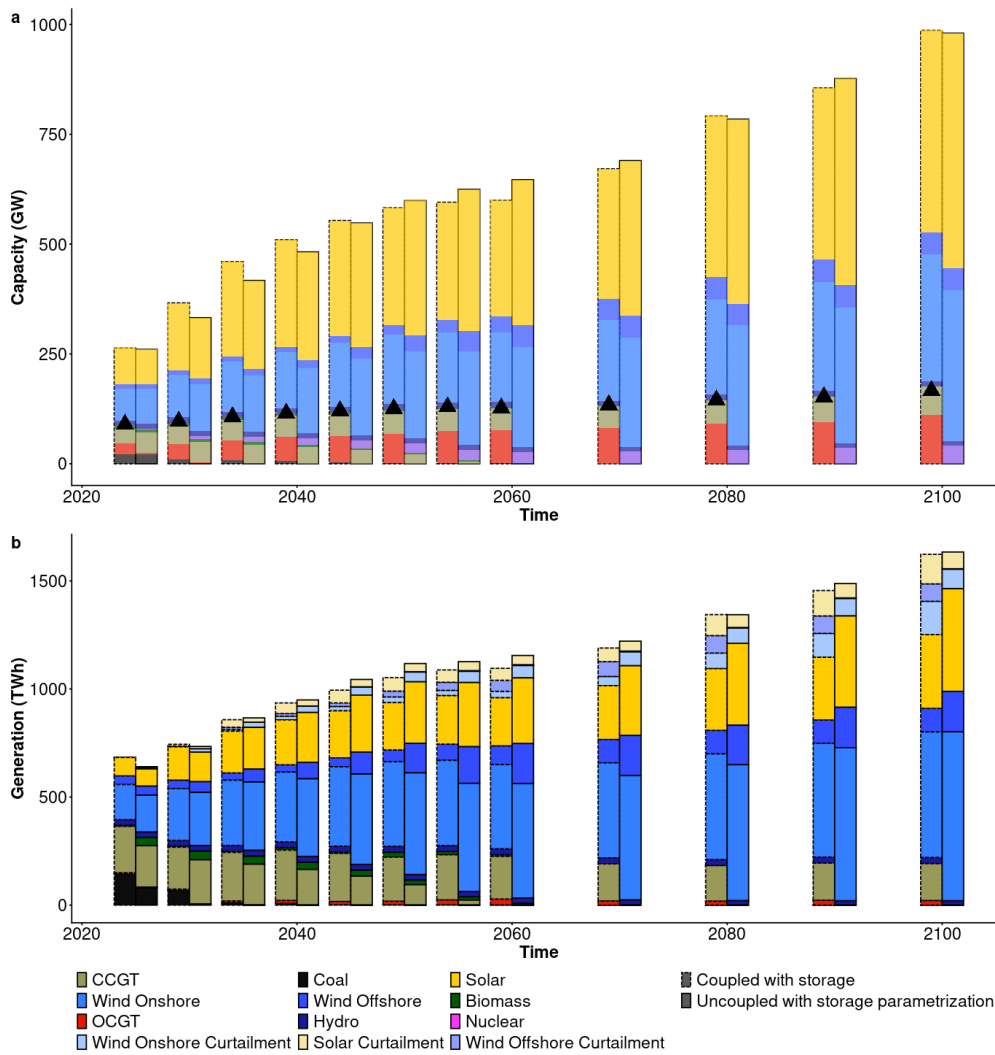
Figure J1: Under the 2C global scenario (no German net-zero goal), we compare (a) the capacity mix and (b) the generation mix of Germany for the DIETER-coupled version of REMIND with endogenous storage (dashed bar) and for the uncoupled version of REMIND with parametrized storage (solid bar). In (a), triangle dots indicate the peak residual demand of the year as determined in DIETER.

Appendix K: Complete list of mathematical symbols

The units used in the two models are usually different. Here we uniformly use MWh for energy units, and MW for capacity units. In the main text, underscore $\_$ is used to denote DIETER parameters and variables. An apostrophe is used to indicate a modified version of the variable. An asterisk is used to indicate the values of variables at the optimum of objective functions.

Symbol	Description	Unit	Symbol	Description	Unit
$y, \Delta y$	REMIND time period, REMIND time step	-	h	Hour	-
s	Supply-side technology type	-	dis, vre	Dispatchable generators, Variable	-

				Renewable	
s_d	Demand-side technology type	-	i	Iteration	-
reg	Region	-	$\mathcal{L}$	Lagrangian	$
Z	Objective function	$	G	Generation	MWh
c	Fixed cost	$/MW	ψ	Total annual renewable potential	MWh
o	Variable cost	$/MWh	ϕ	Capacity factor	1
α	Annual curtailment to pre-curtailment generation ratio in REMIND model	1	d	Exogenous demand	MWh
P	Capacity	MW	p	Standing capacity in REMIND	MW
Γ	Curtailment	MWh	η	Markup	$/MWh
λ	Shadow price of power supply-demand balance equation / power price	$/MWh	MV	Market value	$/MWh
q	Near-term ramp up constraint for capacities in REMIND	MW	Θ	revenue	$
M	Difference in total revenues in the two models	$	ξ	Shadow price due to positive generation	$/MWh
ω	Shadow price due to limited renewable potential	$/MW	γ	Shadow price due to near-term ramp up constraint	$/MW
μ	Shadow price due to limit on generation from capacity	$/MWh	ς	DIETER shadow price due to standing capacity constraint from REMIND	$/MW
σ	Shadow price due to standing capacities in REMIND	$/MW	CP	Capture price of demand-side technologies	$/MWh
υ	Shadow price due to peak residual demand constraint	$/MWh	ΔS	Difference in generation shares between models	1
f	Prefactor for numeric stabilization	1	W	Economic welfare	-
b, b_{peak}	Multiplicative prefactors parameter	1	ϱ	Pure rate of time preference	1

$\varXi$	Adjustment cost	$	β	Offset parameters in adjustment cost	$
χ	Consumption	$	a	Adjustment factor of investment	1
V	Population	1	k	Regional technological coefficient for adjustment cost	1
ER	Early retirement rate in REMIND	1	J	Annual average DIETER electricity price	$/MWh

Table K1: Complete list of mathematical symbols. For simplicity, in general, we only list the symbols, not their indices or in which model they are used.

Appendix L: Complete list of abbreviations

Abbreviation	Description	Abbreviation	Description
IAM	Integrated assessment model	LCOE	Levelized cost of electricity
PSM	Power sector model	MV	Market value
VRE	Variable renewable	O&M	Operation and maintenance
GHG	Greenhouse gas	OMF	Operation and maintenance fixed cost
NLP	Nonlinear programming	OMV	Operation and maintenance variable cost
LP	Linear programming	OCGT	Open cycle gas turbine
CES	Constant elasticity of substitution	CCGT	Combined cycle gas turbine
IPCC	Intergovernmental Panel on Climate Change	CP	Capture price
RLDC	Residual load duration curve	PtG	Power-to-Gas
ZPR	Zero-profit rule	PDC	Price duration curves
KKT	Karush–Kuhn–Tucker	CCS	Carbon capture and storage
EV	Electric Vehicles	GAMS	General Algebraic Modeling System

Table L1: Complete list of abbreviations.

Code and data availability: The coupled and uncoupled REMIND code are implemented in GAMS, and the code and data management is done using R. The coupled and the uncoupled DIETER are entirely implemented in GAMS. The default

uncoupled REMIND v3.0.0 code is available from the GitHub website: https://github.com/remindmodel/remind (last access: 1 September 2022), and is archived on Zenodo under the GNU Affero General Public License, version 3 (AGPLv3) (Luderer et al., 2022b). The technical model documentation is available under https://rse.pik-potsdam.de/doc/remind/3.0.0/ (last access: 1 September 2022). The coupled version of REMIND is available from https://github.com/cchrisgong/remind-coupling-dieter/tree/couple (last access: 2 September 2022); coupled DIETER is available from: https://github.com/cchrisgong/dieter-coupling-remind (last access: 2 September 2022). The two sets of coupling codes are archived at Zenodo under Creative Commons Attribution 4.0 International License (Luderer et al., 2022c). The GAMS code, results, and scripts to produce the figures shown in this paper are archived at Zenodo (Gong, 2022).

Author contribution: Methodology development was done by CG, FU, and RP. CG designed and carried out the numerical implementation, and performed theoretical analysis of the methodology. The methodology was first conceptualized by GL. Supervision and funding acquisition were carried out by FU and GL. OA participated in development of model post-processing and the overall structuring of the manuscript. MK and WPS performed theoretical and conceptual validation of the manuscript. CG prepared the manuscript with contributions from all co-authors.

Competing interests: The authors declare that they have no conflict of interest.

Acknowledgement: The authors thank Professor Dr. Tom Brown at The Technical University of Berlin, and Dr. Marian Leimbach, Dr. Renato Rodrigues, Dr. Nico Bauer at the Potsdam Institute for Climate Impact Research for discussion. We gratefully received financial support by the German Federal Ministry of Education and Research (BMBF) via the project Kopernikus-Ariadne (FKZ 03SFK5N0, FKZ 03SFK5A) and via the INTEGRATE project (FKZ 01LP1928A). We also received financial support from the German Federal Environmental Foundation (Deutsche Bundesstiftung Umwelt).

References

Alimou, Y., Maïzi, N., Bourmaud, J.-Y., and Li, M.: Assessing the security of electricity supply through multi-scale modeling: The TIMES-ANTARES linking approach, Appl. Energy, 279, 115717, https://doi.org/10.1016/j.apenergy.2020.115717, 2020.

Data Platform – Open Power System Data: https://data.open-power-system-data.org/renewable_power_plants/2017-02-16, last access: 22 January 2022.

openmod - Open Energy Modelling Initiative: https://openmod-initiative.org/, last access: 21 January 2022.

Release REMIND v3.0.0 · remindmodel/remind: https://github.com/remindmodel/remind/releases/tag/v3.0.0, last access: 11 August 2022.

Aryanpur, V., O'Gallachoir, B., Dai, H., Chen, W., and Glynn, J.: A review of spatial resolution and regionalisation in national-scale energy systems optimisation models, Energy Strategy Rev., 37, 100702, https://doi.org/10.1016/j.esr.2021.100702, 2021.

Azevedo, I., Bataille, C., Bistline, J., Clarke, L., and Davis, S.: Net-zero emissions energy systems: What we know and do not know, Energy Clim. Change, 2, 100049, https://doi.org/10.1016/j.egycc.2021.100049, 2021.

Bauer, N., Calvin, K., Emmerling, J., Fricko, O., Fujimori, S., Hilaire, J., Eom, J., Krey, V., Kriegler, E., Mouratiadou, I., Sytze de Boer, H., van den Berg, M., Carrara, S., Daioglou, V., Drouet, L., Edmonds, J. E., Gernaat, D., Havlik, P., Johnson, N., Klein, D., Kyle, P., Marangoni, G., Masui, T., Pietzcker, R. C., Strubegger, M., Wise, M., Riahi, K., and van Vuuren, D. P.: Shared Socio-Economic Pathways of the Energy Sector – Quantifying the Narratives, Glob. Environ. Change, 42, 316–330, https://doi.org/10.1016/j.gloenvcha.2016.07.006, 2017.

Baumstark, L., Bauer, N., Benke, F., Bertram, C., Bi, S., Gong, C. C., Dietrich, J. P., Dirnaichner, A., Giannousakis, A., Hilaire,

1894   J., Klein, D., Koch, J., Leimbach, M., Levesque, A., Madeddu, S., Malik, A., Merfort, A., Merfort, L., Odenweller, A., Pehl, M.,

1895   Pietzcker, R. C., Piontek, F., Rauner, S., Rodrigues, R., Rottoli, M., Schreyer, F., Schultes, A., Soergel, B., Soergel, D., Strefler,

1896   J., Ueckerdt, F., Kriegler, E., and Luderer, G.: REMIND2.1: Transformation and innovation dynamics of the energy-economic

1897   system within climate and sustainability limits, Geosci. Model Dev. Discuss., 1–50, https://doi.org/10.5194/gmd-2021-85, 2021.

1898   Bhaskar, A., Assadi, M., and Nikpey Somehsaraei, H.: Decarbonization of the Iron and Steel Industry with Direct Reduction of

1899   Iron Ore with Green Hydrogen, Energies, 13, 758, https://doi.org/10.3390/en13030758, 2020.

1900   Bistline, J. E. T.: The importance of temporal resolution in modeling deep decarbonization of the electric power sector, Environ.

1901   Res. Lett., 16, 084005, https://doi.org/10.1088/1748-9326/ac10df, 2021.

1902   Blanford, G. J. and Weissbart, C.: A Framework for Modeling the Dynamics of Power Markets – The EU-REGEN Model, ifo

1903   Working Paper Series, ifo Institute - Leibniz Institute for Economic Research at the University of Munich, 2019.

1904   Böttger, D. and Härtel, P.: On wholesale electricity prices and market values in a carbon-neutral energy system, Energy Econ.,

1905   106, 105709, https://doi.org/10.1016/j.eneco.2021.105709, 2022.

1906   Brinkerink, M.: Assessing 1.5-2°C scenarios of integrated assessment models from a power system perspective - Linkage with a

1907   detailed hourly global electricity model, Monograph, IIASA, Laxenburg, Austria, 2020.

1908   Brinkerink, M., Zakeri, B., Huppmann, D., Glynn, J., Ó Gallachóir, B. and Deane, P.: Assessing global climate change

1909   mitigation scenarios from a power system perspective using a novel multi-model framework, Environ. Model Softw., 150,

1910   105336, https://doi.org/10.1016/j.envsoft.2022.105336, 2022.

1911   Brown, T. and Reichenberg, L.: Decreasing market value of variable renewables can be avoided by policy action, Energy Econ.,

1912   100, 105354, https://doi.org/10.1016/j.eneco.2021.105354, 2021.

1913   Brown, T., Hörsch, J., and Schlachtberger, D.: PyPSA: Python for Power System Analysis, J. Open Res. Softw., 6, 4,

1914   https://doi.org/10.5334/jors.188, 2018a.

1915   Brown, T., Schlachtberger, D., Kies, A., Schramm, S., and Greiner, M.: Synergies of sector coupling and transmission

1916   reinforcement in a cost-optimised, highly renewable European energy system, Energy, 160, 720–739,

1917   https://doi.org/10.1016/j.energy.2018.06.222, 2018b.

1918   Brunner, C., Deac, G., Braun, S., and Zöphel, C.: The future need for flexibility and the impact of fluctuating renewable power

1919   generation, Renew. Energy, 149, 1314–1324, https://doi.org/10.1016/j.renene.2019.10.128, 2020.Butnar, I., Li, P.-H., Strachan,

1920   N., Portugal Pereira, J., Gambhir, A., and Smith, P.: A deep dive into the modelling assumptions for biomass with carbon

1921   capture and storage (BECCS): A transparency exercise., Environ. Res. Lett., https://doi.org/10.1088/1748-9326/ab5c3e, 2019.

1922   Calvin, K., Bond-Lamberty, B., Clarke, L., Edmonds, J., Eom, J., Hartin, C., Kim, S., Kyle, P., Link, R., Moss, R., McJeon, H.,

1923   Patel, P., Smith, S., Waldhoff, S., and Wise, M.: The SSP4: A world of deepening inequality, Glob. Environ. Change, 42, 284–

1924   296, https://doi.org/10.1016/j.gloenvcha.2016.06.010, 2017.

1925   Chang, M., Thellufsen, J. Z., Zakeri, B., Pickering, B., Pfenninger, S., Lund, H., and Østergaard, P. A.: Trends in tools and

1926   approaches for modelling the energy transition, Appl. Energy, 290, 116731, https://doi.org/10.1016/j.apenergy.2021.116731,

1927   2021.

1928   Cherp, A., Vinichenko, V., Tosun, J., Gordon, J. A., and Jewell, J.: National growth dynamics of wind and solar power

1929   compared to the growth required for global climate targets, Nat. Energy, 6, 742–754, https://doi.org/10.1038/s41560-021-00863-

1930   0, 2021.

1931   Clarke, L., Wei, Y.-M., De La Vega Navarro, A., Garg, A., Hahmann, A. N., Khennas, S., Azevedo, I. M. L., Löschel, A.,

1932   Singh, A. K., Steg, L., Strbac, G., and Wada, K.: Energy Systems. In IPCC, 2022: Climate Change 2022: Mitigation of Climate

1933   Change. Contribution of Working Group III to the Sixth Assessment Report of the Intergovernmental Panel on Climate Change,

219, https://doi.org/doi: 10.1017/9781009157926.008, 2022.

Conejo, A.J., Castillo, E., Mínguez R. and García-Bertrand, R.: Decomposition techniques in mathematical programming. Springer-Verlag Berlin Heidelberg, 2006.

Creutzig, F., Agoston, P., Goldschmidt, J. C., Luderer, G., Nemet, G., and Pietzcker, R. C.: The underestimated potential of solar energy to mitigate climate change, Nat. Energy, 2, 17140, https://doi.org/10.1038/nenergy.2017.140, 2017.

Deane, J. P., Chiodi, A., Gargiulo, M., and Ó Gallachóir, B. P.: Soft-linking of a power systems model to an energy systems model, Energy, 42, 303–312, https://doi.org/10.1016/j.energy.2012.03.052, 2012.National long-term strategies: https://ec.europa.eu/info/energy-climate-change-environment/implementation-eu-countries/energy-and-climate-governance-and-reporting/national-long-term-strategies_en, last access: 15 January 2022.

E3MLab, PRIMES Model Version 2018 - detailed model description, http://www.e3mlab.ntua.gr/e3mlab/PRIMES, last access: 4 May 2023, 2018.

Ellenbeck, S. and Lilliestam, J.: How modelers construct energy costs: Discursive elements in Energy System and Integrated Assessment Models, Energy Res. Soc. Sci., 47, 69-770, https://doi.org/10.1016/j.erss.2018.08.021, 2019.

Figueiredo, N. C. and Silva, P. P. da: The price of wind power generation in Iberia and the merit-order effect, Int. J. Sustain. Energy Plan. Manag., 15, 21–30, https://doi.org/10.5278/ijsepm.2018.15.4, 2018.

Frysztacki, M. M., Hörsch, J., Hagenmeyer, V., and Brown, T.: The strong effect of network resolution on electricity system models with high shares of wind and solar, Appl. Energy, 291, 116726, https://doi.org/10.1016/j.apenergy.2021.116726, 2021.

Fuso Nerini, F., Keppo, I., Strachan, N.: Myopic decision making in energy system decarbonisation pathways. A UK case study. Energy Strategy Rev., 17, 19–26, https://doi.org/10.1016/j.esr.2017.06.001, 2017.

Gaete-Morales, C., Kittel, M., Roth, A., and Schill, W.-P.: DIETERpy: A Python framework for the Dispatch and Investment Evaluation Tool with Endogenous Renewables, SoftwareX, 15, 100784, https://doi.org/10.1016/j.softx.2021.100784, 2021.

Gan, D., Feng, D., and Xie, J.: Electricity Markets and Power System Economics, CRC Press, Boca Raton, 220 pp., https://doi.org/10.1201/b15550, 2013.

Geels, F., Berkhout, F. and van Vuuren, D.: Bridging analytical approaches for low-carbon transitions, Nat. Clim. Change, 6, 576–583, https://doi.org/10.1038/nclimate2980, 2016.

Giarola, S., Mittal, S., Vielle, M., Perdana, S., Campagnolo, L., Delpiazzo, E., Bui, H., Kraavi, A. A., Kolpakov, A., Sognnaes, I., Peters, G., Hawkes, A., Köberle, A. C., Grant, N., Gambhir, A., Nikas, A., Doukas, H., Moreno, J., and van de Ven, D.-J.: Challenges in the harmonisation of global integrated assessment models: A comprehensive methodology to reduce model response heterogeneity, Sci. Total Environ., 783, 146861, https://doi.org/10.1016/j.scitotenv.2021.146861, 2021.

Gils, H. C., Gardian, H., Kittel, M., Schill, W.-P., Zerrahn, A., Murmann, A., Launer, J., Fehler, A., Gaumnitz, F., van Ouwerkerk, J., Bußar, C., Mikurda, J., Torralba-Díaz, L., Janßen, T., and Krüger, C.: Modeling flexibility in energy systems — comparison of power sector models based on simplified test cases, Renew. Sustain. Energy Rev., 158, 111995, https://doi.org/10.1016/j.rser.2021.111995, 2022a.

Gils, H. C., Gardian, H., Kittel, M., Schill, W.-P., Murmann, A., Launer, J., Gaumnitz, F., van Ouwerkerk, J., Mikurda, J., and Torralba-Díaz, L.: Model-related outcome differences in power system models with sector coupling—Quantification and drivers, Renew. Sustain. Energy Rev., 159, 112177, https://doi.org/10.1016/j.rser.2022.112177, 2022b.

Gong, C. C.: REMIND-DIETER - code, reportings, scripts, https://doi.org/10.5281/zenodo.7072625, 2022.

Griffiths, S., Sovacool, B. K., Kim, J., Bazilian, M., and Uratani, J. M.: Industrial decarbonization via hydrogen: A critical and systematic review of developments, socio-technical systems and policy options, Energy Res. Soc. Sci., 80, 102208, https://doi.org/10.1016/j.erss.2021.102208, 2021.

1974 Guivarch, C., Kriegler, E., Portugal-Pereira, J., and Bosetti, V.: IPCC, 2022: Annex III: Scenarios and modelling methods, In

1975 IPCC, 2022:, in: Climate Change 2022: Mitigation of Climate Change. Contribution of Working Group III to the Sixth

1976 Assessment Report of the Intergovernmental Panel on Climate Change, Cambridge University Press, Cambridge, United

1977 Kingdom and New York, NY, USA, https://doi.org/10.1017/9781009157926.022, 2022.

1978 Günther, C., Schill, W.-P., and Zerrahn, A.: Prosumage of solar electricity: Tariff design, capacity investments, and power

1979 sector effects, Energy Policy, 152, 112168, https://doi.org/10.1016/j.enpol.2021.112168, 2021.

1980 Guo, F., van Ruijven, B.J., Zakeri, B., Zhang, S., Chen, X., Liu, C., Yang, F., Krey, V., Riahi, K., Huang, H. and Zhou, Y.:

1981 Implications of intercontinental renewable electricity trade for energy systems and emissions, Nat. Energy, **7**, 1144–1156,

1982 https://doi.org/10.1038/s41560-022-01136-0, 2022.

1983 Haydt, G., Leal, V., Pina, A., and Silva, C. A.: The relevance of the energy resource dynamics in the mid/long-term energy

1984 planning models, Renew. Energy, 36, 3068–3074, 2011.

1985 Hildmann, M., Ulbig, A., and Andersson, G.: Empirical Analysis of the Merit-Order Effect and the Missing Money Problem in

1986 Power Markets With High RES Shares, IEEE Trans. Power Syst., 30, 1560–1570,

1987 https://doi.org/10.1109/TPWRS.2015.2412376, 2015.

1988 Hirth, L.: The market value of variable renewables: The effect of solar wind power variability on their relative price, Energy

1989 Econ., 38, 218–236, https://doi.org/10.1016/j.eneco.2013.02.004, 2013.

1990 Hirth, L.: What caused the drop in European electricity prices? A factor decomposition analysis, Energy J., 39,

1991 https://doi.org/10.5547/01956574.39.1.lhir, 2018.

1992 Hirth, L. and Ueckerdt, F.: Redistribution effects of energy and climate policy: The electricity market, Energy Policy, 62, 934–

1993 947, https://doi.org/10.1016/j.enpol.2013.07.055, 2013.

1994 Huppmann, D., Gidden, M., Fricko, O., Kolp, P., Orthofer, C., Pimmer, M., Kushin, N., Vinca, A., Mastrucci, A., Riahi, K., and

1995 Krey, V.: The MESSAGEix Integrated Assessment Model and the ix modeling platform (ixmp): An open framework for

1996 integrated and cross-cutting analysis of energy, climate, the environment, and sustainable development, Environ. Model. Softw.,

1997 112, 143–156, https://doi.org/10.1016/j.envsoft.2018.11.012, 2019.

1998 ICCSD Tsinghua University: Power Sector, in: China's Long-Term Low-Carbon Development Strategies and Pathways:

1999 Comprehensive Report, edited by: Institute of Climate Change and Sustainable Development of Tsinghua University et al.,

2000 Springer, Singapore, 109–130, https://doi.org/10.1007/978-981-16-2524-4_4, 2022.

2001 IEA: World Energy Outlook 2021, https://www.iea.org/reports/world-energy-outlook-2021, 2021.

2002 IPCC: Climate change 2014: mitigation of climate change : Working Group III contribution to the Fifth assessment report of the

2003 Intergovernmental Panel on Climate Change, edited by: Edenhofer, O., Pichs-Madruga, R., Sokona, Y., Farahani, E., Kadner, S.,

2004 Seyboth, K., Alder, A., Baum, I., Brunner, S., Eikemeier, P., Kriemann, B., Salolainen, J., Schlömer, S., Stechow, C. von,

2005 Zwickel, T., and Minx, J. C., Cambridge University Press, Cambridge, United Kingdom and New York, NY, USA, 2014.

2006 IRENA: Renewable power generation costs in 2019, International Renewable Energy Agency, 2020.

2007 Kannan, R. and Turton, H.: A Long-Term Electricity Dispatch Model with the TIMES Framework, Environ. Model. Assess., 18,

2008 325–343, https://doi.org/10.1007/s10666-012-9346-y, 2013.

2009 Karush, W.: Minima of functions of several variables with inequalities as side conditions., 1939.

2010 Keppo, I., Butnar, I., Bauer, N., Caspani, M., Edelenbosch, O., Emmerling, J., Fragkos, P., Guivarch, C., Harmsen, M., Lefèvre,

2011 J., Le Gallic, T., Leimbach, M., McDowall, W., Mercure, J.-F., Schaeffer, R., Trutnevyte, E., and Wagner, F.: Exploring the

2012 possibility space: taking stock of the diverse capabilities and gaps in integrated assessment models, Environ. Res. Lett., 16,

2013 053006, https://doi.org/10.1088/1748-9326/abe5d8, 2021.

Koch, J. and Leimbach, M.: Update of Ssp GDP Projections: Capturing Recent Changes in National Accounting, PPP Conversion and Covid 19 Impacts, https://doi.org/10.2139/ssrn.4011838, 2022.

Koutstaal, P. R. and va. Hout, M.: Integration costs and market value of variable renewables: A study for the Dutch power market, 2017.

Kuhn, H. W. and Tucker, A. W.: Nonlinear Programming, Proc. Second Berkeley Symp. Math. Stat. Probab., 2, 481–493, 1951.

Lazard: Lazard's Levelized Cost of Energy Analysis - Version 15.0., 2021.

Levesque, A., Pietzcker, R. C., Baumstark, L., De Stercke, S., Grübler, A., Luderer, G.: How much energy will buildings consume in 2100? A global perspective within a scenario framework, Energy, 148, 514-527, https://doi.org/10.1016/j.energy.2018.01.139, 2018.

Leimbach, M., Bauer, N., Baumstark, L., Luken, M., and Edenhofer, O.: Technological Change and International Trade - Insights from REMIND-R, Energy J., 31, 109–136, https://doi.org/10.5547/ISSN0195-6574-EJ-Vol31-NoSI-5, 2010.

Li, P.-H. and Pye, S.: Assessing the benefits of demand-side flexibility in residential and transport sectors from an integrated energy systems perspective, Appl. Energy, 228, 965–979, https://doi.org/10.1016/j.apenergy.2018.06.153, 2018.

López Prol, J. and Schill, W.-P.: The Economics of Variable Renewable Energy and Electricity Storage, Annu. Rev. Resour. Econ., 13, 443–467, https://doi.org/10.1146/annurev-resource-101620-081246, 2021.

Luderer, G., Pietzcker, R. C., Carrara, S., de Boer, H. S., Fujimori, S., Johnson, N., Mima, S., and Arent, D.: Assessment of wind and solar power in global low-carbon energy scenarios: An introduction, Energy Econ., 64, 542–551, https://doi.org/10.1016/j.eneco.2017.03.027, 2017.

Luderer, G., Vrontisi, Z., Bertram, C., Edelenbosch, O., Pietzcker, R. C., Rogelj, J., De Boer, H. S., Drouet, L., Emmerling, J., Fricko, O., Fujimori, S., Havlik, P., Iyer, G., Keramidas, K., Kitous, A., Pehl, M., Krey, V., Riahi, K., Saveyn, B., Tavoni, M., Van Vuuren, D. P., and Kriegler, E.: Residual fossil CO_2 emissions in 1.5–2°C pathways, Nat. Clim. Change, 8, 626–633, https://doi.org/10.1038/s41558-018-0198-6, 2018.

Luderer, G., Madeddu, S., Merfort, L., Ueckerdt, F., Pehl, M., Pietzcker, R., Rottoli, M., Schreyer, F., Bauer, N., Baumstark, L., Bertram, C., Dirnaichner, A., Humpenöder, F., Levesque, A., Popp, A., Rodrigues, R., Strefler, J., and Kriegler, E.: Impact of declining renewable energy costs on electrification in low-emission scenarios, Nat. Energy, 7, 32–42, https://doi.org/10.1038/s41560-021-00937-z, 2022a.

Luderer, G., Bauer, N., Baumstark, L., Bertram, C., Leimbach, M., Pietzcker, R., Strefler, J., Aboumahboub, T., Abrahão, G., Auer, C., Benke, F., Bi, S., Dietrich, J., Dirnaichner, A., Giannousakis, A., Gong, C. C., Haller, M., Hasse, R., Hilaire, J., Hoppe, J., Klein, D., Koch, J., Körner, A., Kowalczyk, K., Kriegler, E., Levesque, A., Lorenz, A., Ludig, S., Lüken, M., Malik, A., Manger, S., Merfort, A., Merfort, L., Moreno-Leiva, S., Mouratiadou, I., Odenweller, A., Pehl, M., Piontek, F., Popin, L., Rauner, S., Richters, O., Rodrigues, R., Roming, N., Rottoli, M., Schmidt, E., Schötz, C., Schreyer, F., Schultes, A., Sörgel, B., Ueckerdt, F., Verpoort, P., and Weigmann, P.: REMIND - REgional Model of INvestments and Development, Zenodo, https://doi.org/10.5281/zenodo.6794920, 2022b.

Luderer, G., Bauer, N., Gong, C. C., Odenweller, A., Baumstark, L., Bertram, C., Leimbach, M., Pietzcker, R., Strefler, J., Aboumahboub, T., Abrahão, G., Auer, C., Benke, F., Bi, S., Dietrich, J., Dirnaichner, A., Giannousakis, A., Haller, M., Hasse, R., Hilaire, J., Hoppe, J., Klein, D., Koch, J., Kowalczyk, K., Kriegler, E., Levesque, A., Ludig, S., Malik, A., Merfort, A., Merfort, L., Moreno, S., Mouratiadou, I., Pehl, M., Piontek, F., Popin, L., Rauner, S., Richters, O., Schötz, C., Rodrigues, R., Ueckerdt, F., Zerrahn, A., Schreyer, F., Sörgel, B., Weigmann, P., Schill, W.-P., Verpoort, P., and Rottoli, M.: REMIND - DIETER coupling, Zenodo, https://doi.org/10.5281/zenodo.7053246, 2022c.

Ludig, S., Haller, M., Schmid, E., and Bauer, N.: Fluctuating renewables in a long-term climate change mitigation strategy,

Energy, 36, 6674–6685, https://doi.org/10.1016/j.energy.2011.08.021, 2011.

Martínez-Gordón, R., Morales-España, G., Sijm, J., and Faaij, A. P. C.: A review of the role of spatial resolution in energy systems modelling: Lessons learned and applicability to the North Sea region, Renew. Sustain. Energy Rev., 141, 110857, https://doi.org/10.1016/j.rser.2021.110857, 2021.

Mills, A. D. and Wiser, R. H.: Strategies to mitigate declines in the economic value of wind and solar at high penetration in California, Appl. Energy, 147, 269–278, https://doi.org/10.1016/j.apenergy.2015.03.014, 2015.

Mowers, M., Mignone, B. K. and Steinberg, D. C.: Quantifying value and representing competitiveness of electricity system technologies in economic models, Applied Energy, 329, 120132, https://doi.org/10.1016/j.apenergy.2022.120132, 2023.

NGFS: NGFS Climate Scenarios for central banks and supervisors, Network for Greening the Financial System, 2020.

van Ouwerkerk, J., Gils, H. C., Gardian, H., Kittel, M., Schill, W.-P., Zerrahn, A., Murmann, A., Launer, J., Torralba-Díaz, L., and Bußar, C.: Impacts of power sector model features on optimal capacity expansion: A comparative study, Renew. Sustain. Energy Rev., 157, 112004, https://doi.org/10.1016/j.rser.2021.112004, 2022.

Padhy, N. P.: Unit commitment-a bibliographical survey, IEEE Trans. Power Syst., 19, 1196–1205, https://doi.org/10.1109/TPWRS.2003.821611, 2004.

Pahle, M., Tietjen, O., Osorio, S., Egli, F., Steffen, B., Schmidt, T. S. and Edenhofer O.: Safeguarding the energy transition against political backlash to carbon markets, Nat. Energy, 7, 290–296, https://doi.org/10.1038/s41560-022-00984-0, 2022.

Palzer, A. and Henning, H.-M.: A Future German Energy System with a Dominating Contribution from Renewable Energies: A Holistic Model Based on Hourly Simulation, Energy Technol., 2, 13–28, https://doi.org/10.1002/ente.201300083, 2014.

Parra, D., Valverde, L., Pino, F. J., and Patel, M. K.: A review on the role, cost and value of hydrogen energy systems for deep decarbonisation, Renew. Sustain. Energy Rev., 101, 279–294, https://doi.org/10.1016/j.rser.2018.11.010, 2019.

Pietzcker, R. C., Ueckerdt, F., Carrara, S., de Boer, H. S., Després, J., Fujimori, S., Johnson, N., Kitous, A., Scholz, Y., Sullivan, P., and Luderer, G.: System integration of wind and solar power in integrated assessment models: A cross-model evaluation of new approaches, Energy Econ., 64, 583–599, https://doi.org/10.1016/j.eneco.2016.11.018, 2017.

Pina, A., Silva, C., and Ferrão, P.: Modeling hourly electricity dynamics for policy making in long-term scenarios, Energy Policy, 39, 4692–4702, https://doi.org/10.1016/j.enpol.2011.06.062, 2011.

Prina, M.G., Manzolini, G., Moser, D., Nastasi, B., and Sparber, W.: Classification and challenges of bottom-up energy system models - A review, Renewable and Sustainable Energy Reviews, 129, 109917, https://doi.org/10.1016/j.rser.2020.109917, 2020.

P.R. Shukla et al.: Climate Change 2022: Mitigation of Climate Change. Contribution of Working Group III to the Sixth Assessment Report of the Intergovernmental Panel on Climate Change, https://doi.org/10.1017/9781009157926, 2022.

Prol, J. L. and Schill, W.-P.: The Economics of Variable Renewables and Electricity Storage, ArXiv201215371 Econ Q-Fin, 2020.

Ram, M., Bogdanov, D., Aghahosseini, A., Gulagi, A., Oyewo, S., Child, M., Caldera, U., Sadovskaia, K., Farfan Orozco, F., Noel, L., Fasihi, M., Maybodi, S., and Fell, H.-J.: Global Energy System based on 100% Renewable Energy: Energy Transition in Europe Across Power, Heat, Transport and Desalination Sectors, https://doi.org/10.13140/RG.2.2.10143.00160, 2018.

Ramsebner, J., Haas, R., Ajanovic, A., and Wietschel, M.: The sector coupling concept: A critical review, WIREs Energy Environ., 10, e396, https://doi.org/10.1002/wene.396, 2021.

Rechsteiner, R.: German energy transition (Energiewende) and what politicians can learn for environmental and climate policy, Clean Technol. Environ. Policy, 23, 305–342, https://doi.org/10.1007/s10098-020-01939-3, 2021.

Ringkjøb, H.-K., Haugan, P. M. and Solbrekke, I. M.: A review of modelling tools for energy and electricity systems with large shares of variable renewables, Renewable and Sustainable Energy Reviews, 96, 440-459,

https://doi.org/10.1016/j.rser.2018.08.002, 2018.

Rodrigues, R., Pietzcker, R., Fragkos, P., Price, J., McDowall, W., Siskos, P., Fotiou, T., Luderer, G., and Capros, P.: Narrative-driven alternative roads to achieve mid-century CO_2 net neutrality in Europe, Energy, 239, 121908, https://doi.org/10.1016/j.energy.2021.121908, 2022.

Rogelj, J., Shindell, D., Jiang, K., Fifita, S., Forster, P., Ginzburg, V., Handa, C., Kheshgi, H., Kobayashi, S., Kriegler, E., Mundaca, L., Séférian, R., and Vilariño, M. V.: Mitigation pathways compatible with 1.5°C in the context of sustainable development, in: Special Report on the impacts of global warming of 1.5 °C, Intergovernmental Panel on Climate Change, Geneva, 2018.

Rotmans, J. and van Asselt, M. B. A.: Uncertainty in Integrated Assessment Modelling: A Labyrinthic Path, Integr. Assess., 2, 43–55, https://doi.org/10.1023/A:1011588816469, 2001.

Ruhnau, O.: How flexible electricity demand stabilizes wind and solar market values: The case of hydrogen electrolyzers, Appl. Energy, 307, 118194, https://doi.org/10.1016/j.apenergy.2021.118194, 2022.

Say, K., Schill, W.-P., and John, M.: Degrees of displacement: The impact of household PV battery prosumage on utility generation and storage, Appl. Energy, 276, 115466, https://doi.org/10.1016/j.apenergy.2020.115466, 2020.

Schill, W.-P., Roth, A., Guéret, A.: Ampel-Monitor Energiewende Shows the Pace of the Energy Transition Must Be Accelerated Significantly. https://doi.org/10.18723/diw_dwr:2022-26-1, 2022.

Schill, W.-P. and Zerrahn, A.: Long-run power storage requirements for high shares of renewables: Results and sensitivities, Renew. Sustain. Energy Rev., 83, 156–171, https://doi.org/10.1016/j.rser.2017.05.205, 2018.

Schill, W.-P. and Zerrahn, A.: Flexible electricity use for heating in markets with renewable energy, Appl. Energy, 266, 114571, https://doi.org/10.1016/j.apenergy.2020.114571, 2020.

Schill, W.-P., Pahle, M., and Gambardella, C.: Start-up costs of thermal power plants in markets with increasing shares of variable renewable generation, Nat. Energy, 2, 1–6, https://doi.org/10.1038/nenergy.2017.50, 2017.

Seljom, P., Rosenberg, E., Schäffer, L. E., and Fodstad, M.: Bidirectional linkage between a long-term energy system and a short-term power market model, Energy, 198, 117311, https://doi.org/10.1016/j.energy.2020.117311, 2020.

Sensfuß, F.: Assessment of the impact of renewable electricity generation on the German electricity sector: An agent-based simulation approach, https://doi.org/10.5445/IR/1000007777, 2007.

Sensfuß, F., Ragwitz, M., and Genoese, M.: The merit-order effect: A detailed analysis of the price effect of renewable electricity generation on spot market prices in Germany, Energy Policy, 36, 3076–3084, 2008.

Sepulveda, N. A., Jenkins, J. D., de Sisternes, F. J., and Lester, R. K.: The Role of Firm Low-Carbon Electricity Resources in Deep Decarbonization of Power Generation, Joule, 2, 2403–2420, https://doi.org/10.1016/j.joule.2018.08.006, 2018.

Sitarz, J., Pahle, M., Osorio, S., Luderer, G. and Pietzcker, R.: EU carbon prices signal high policy credibility and farsighted actors, preprint, https://doi.org/10.21203/rs.3.rs-2761645/v1, 2023.

Staub-Kaminski, I., Zimmer, A., Jakob, M. and Marschinski, R.: Climate policy in practice: a typology of obstacles and implications for integrated assessment modeling, Clim. Change Econ., 05, 1440004, https://doi.org/10.1142/S2010007814400041, 2014.

Stehfest, E., van Vuuren, D., Bouwman, L., and Kram, T.: Integrated assessment of global environmental change with IMAGE 3.0: Model description and policy applications, Netherlands Environmental Assessment Agency (PBL), 2014.

Stöckl, F., Schill, W.-P., and Zerrahn, A.: Optimal supply chains and power sector benefits of green hydrogen, Sci. Rep., 11, 14191, https://doi.org/10.1038/s41598-021-92511-6, 2021.

Sullivan, P., Krey, V., and Riahi, K.: Impacts of considering electric sector variability and reliability in the MESSAGE model,

Energy Strategy Rev., 1, 157–163, https://doi.org/10.1016/j.esr.2013.01.001, 2013.

The White House: The Long-Term Strategy of the United States: Pathways to Net-Zero Greenhouse Gas Emissions by 2050, United States Department of State and the United States Executive Office of the President, Washington DC., 2021.

Ueckerdt, F., Brecha, R., Luderer, G., Sullivan, P., Schmid, E., Bauer, N., Böttger, D., and Pietzcker, R.: Representing power sector variability and the integration of variable renewables in long-term energy-economy models using residual load duration curves, Energy, 90, Part 2, 1799–1814, https://doi.org/10.1016/j.energy.2015.07.006, 2015.

Ueckerdt, F., Pietzcker, R., Scholz, Y., Stetter, D., Giannousakis, A., and Luderer, G.: Decarbonizing global power supply under region-specific consideration of challenges and options of integrating variable renewables in the REMIND model, Energy Econ., 64, 665–684, https://doi.org/10.1016/j.eneco.2016.05.012, 2017.

UNEP: The Emissions Gap Report 2019, UNEP, Nairobi, Kenya, 2019.

Welsch, M., Mentis, D., and Howells, M.: Chapter 17 - Long-Term Energy Systems Planning: Accounting for Short-Term Variability and Flexibility, in: Renewable Energy Integration, edited by: Jones, L. E., Academic Press, Boston, 215–225, https://doi.org/10.1016/B978-0-12-407910-6.00017-X, 2014.

Weyant, J.: Some Contributions of Integrated Assessment Models of Global Climate Change, Rev. Environ. Econ. Policy, 11, 115–137, https://doi.org/10.1093/reep/rew018, 2017.

Wiese, F., Schlecht, I., Bunke, W.-D., Gerbaulet, C., Hirth, L., Jahn, M., Kunz, F., Lorenz, C., Mühlenpfordt, J., Reimann, J., and Schill, W.-P.: Open Power System Data – Frictionless data for electricity system modelling, Appl. Energy, 236, 401–409, https://doi.org/10.1016/j.apenergy.2018.11.097, 2019.

Wilson, C., Guivarch, C., Kriegler, E., van Ruijven, B., van Vuuren, D. P., Krey, V., Schwanitz, V. J., and Thompson, E. L.: Evaluating process-based integrated assessment models of climate change mitigation, Clim. Change, 166, 3, https://doi.org/10.1007/s10584-021-03099-9, 2021.

Younis, A., Benders, R., Ramírez, J., de Wolf, M. and Faaij, A.: Scrutinizing the Intermittency of Renewable Energy in a Long-Term Planning Model via Combining Direct Integration and Soft-Linking Methods for Colombia's Power System, Energies, 15, 7604, https://doi.org/10.3390/en15207604, 2022.

Zerrahn, A. and Schill, W.-P.: Long-run power storage requirements for high shares of renewables: review and a new model, Renew. Sustain. Energy Rev., 79, 1518–1534, https://doi.org/10.1016/j.rser.2016.11.098, 2017.

Zerrahn, A., Schill, W.-P., and Kemfert, C.: On the economics of electrical storage for variable renewable energy sources, Eur. Econ. Rev., 108, 259–279, https://doi.org/10.1016/j.euroecorev.2018.07.004, 2018.